

CORROSION PROTECTION OF COPPER IN OILY MEDIA:  
MICROSCOPIC MECHANISMS

By

AVIDIPTO BISWAS

Submitted in partial fulfillment of the requirements

For the degree of Doctor of Philosophy

Adviser: Prof. Frank Ernst

Department of Materials Science and Engineering

CASE WESTERN RESERVE UNIVERSITY

May, 2013

***CORROSION PROTECTION OF COPPER IN OILY MEDIA:  
MICROSCOPIC MECHANISMS***

CASE WESTERN RESERVE UNIVERSITY  
SCHOOL OF GRADUATE STUDIES

We hereby approve the dissertation\* of

***Avidipto Biswas***

candidate for the degree of

**Doctor of Philosophy**

**Prof. Frank Ernst**  
Committee Chair, Adviser  
Department of Materials Science and Engineering

**Prof. Arthur Heuer**  
Committee Member  
Department of Materials Science and Engineering

**Prof. James D. McGuffin-Cawley**  
Committee Member, Department Chair  
Department of Materials Science and Engineering

**Prof. J. Adin Mann**  
Committee Member  
Department of Chemical Engineering

Date: January 23, 2013

---

<sup>1</sup> We certify that written approval has been obtained for any proprietary materials contained therein.

© 2013 AVIDIPTO BISWAS

Dedicated to

My Parents

*Mitali Biswas & Banshi Dhari Biswas*

## ACKNOWLEDGEMENT

I would like to express my deepest gratitude to Prof. Frank Ernst, my thesis adviser, for contributing with his invaluable ideas and giving the right direction towards the successful completion of this project, and also for the timely discussions which helped me to sharpen my analytical skills. The helpful inputs from Prof. Arthur Heuer, Prof. Jay Mann, and Prof. Gary Michal are highly appreciated as well. I would like to especially thank Dr. Wayne Jennings, and Dr. David Hovis, from Swagelok Center for Surface Analysis of Materials (SCSAM) for their priceless help and support in technical matters related to XPS-, and ToF-SIMS-handling at all times during the course of this project work.

I am highly grateful to Ohio Department of Development and SCSAM for funding the project throughout the course of my thesis work. I am also indebted to Dr. Douglas Jayne and Dr. Yanshi Zhang from Lubrizol Corporation for their highly valuable advice with an industrial perspective. I also thank them for making raw materials, used in this project, available to me. I am also thankful to Dr. Craig Bishop of The Best Mode Company, for his incessant enthusiasm, and inspiring discussions.

Finally, I would like to take this opportunity to thank my friends Dr. Sonalika Goyel and Rahul Neulkar for being pillars of support in my personal life through all ups and downs during my PhD. I would also like to express my pleasure in working with all my friends at the department. Apart from this, I would like to heartily thank my sister Dr. Sudeshna Ghosh for being a continuous source of motivation throughout my PhD. I also thank my

room-mates, Anandaroop Ghosh, Dhrubajyoti Saha, and Apoorva Chandar, for making my stay in Cleveland a cherished experience. Along with already mentioned friends, I would also like to thank my friends Dr. Mahesh Tanniru, Dr. Jason Wang, Min-Kyung Chung, Harsha Choday, Chihoon Lee, Chen-tsan Tsai, Chei-wen Chen, and Bhupendra Mishra, for unconditionally helping me during the turbulent times of hospitalization and bed-rest owing to my auto-accident.

At last, but not the least, I would like to acknowledge my uncle, Dr. Ahindra Ghosh and my aunt, Dr. Radha Ghosh, along with my parents, who instilled in me, the ambition of pursuing PhD program, for their unwavering support and encouragement without which, I would not have been able to achieve this degree.

Avidipto Biswas

January 2013

## TABLE OF CONTENTS

	Page
ACKNOWLEDGEMENT .....	5
TABLE OF CONTENTS .....	7
LIST OF TABLES .....	9
LIST OF FIGURES .....	10
LIST OF SYMBOLS .....	15
ABSTRACT .....	16
 CHAPTER	
1. INTRODUCTION .....	18
1.1 Materials System .....	18
1.2 Copper Corrosion in Automotive Oils .....	18
1.3 Corrosion Inhibitors .....	20
1.4 Corrosive Medium .....	21
1.5 Corrosion Inhibition Mechanism .....	23
1.6 Surface Characterization .....	24
1.7 Project Objective and Thesis Organization .....	26
2. LITERATURE REVIEW .....	28
2.1 Adsorption Mechanism .....	29
2.2 Molecular Bonding and Orientation .....	32
2.3 Adsorption Isotherm .....	36
2.4 Inhibitor Efficiency .....	39
2.5 Synergistic Effects of other Inhibitors and certain Ions .....	40
2.6 Film Thickness .....	41
2.7 Rate of Inhibitive Film Formation .....	43
2.8 Desorption Study .....	45
2.9 Effect of Corrosive Medium .....	46
2.10 Performance in Real Oil .....	47
2.11 Effect of Surface Roughness and Poly-Crystal .....	49
2.12 Effect of Temperature .....	50
2.13 Effect of Inhibitor Concentration .....	50
2.14 Effect of Presence of Oxide on Surface .....	51
2.15 Effect of Oxygen Purging .....	53

2.16 Comparison of Adsorbed Layer Formation on Cu Strip vs. Powdered Cu .....	53
2.17 Effect of Stress.....	54
2.18 Corrosion Product Analysis.....	54
2.19 Effect of Primary Ion Dose Density.....	56
2.20 Effect of Primary Ion Gun Source in ToF-SIMS.....	57
2.21 General Comments.....	58
3. EXPERIMENTAL DESIGN AND PROCEDURES .....	62
3.1 Raw Materials.....	63
3.2 Sample Preparation.....	66
3.3 Instrumental Conditions and Procedures .....	68
3.4 Experimental Logistics.....	70
4. RESULTS .....	79
4.1 Process Control.....	79
4.2 Characterization of TTAH Adsorption Film on Cu.....	94
4.3 Temporal Evolution of the TTAH Adsorption Film Structure on Cu.....	114
4.4 Corrosion of Cu in Sulfide Solution .....	119
4.5 O <sup>18</sup> Isotope Tracer Study in ToF-SIMS .....	136
5. DISCUSSION .....	142
5.1 TTAH Adsorption Film Formation Mechanism .....	142
5.2 Mechanism for Protection against Corrosion of Cu in Sulfide Solution .....	150
5.3 Validation of the Proposed Mechanism against Observations Reported in the Literature .....	153
6. CONCLUSIONS .....	156
APPENDIX I .....	159
BIBLIOGRAPHY .....	167

## LIST OF TABLES

Table		Page
4.1	Negative SI fragments acquired by Au <sup>+</sup> PI beam on 8.64 x 10 <sup>4</sup> s (24 h) immersed TTAH adsorption film on Cu .....	96
4.2	Surface composition for TTAH adsorption film on Cu formed upon 8.64 x 10 <sup>4</sup> s (24 h) immersion in oil .....	103
4.3	Surface composition of Cu surface upon 8.64 x 10 <sup>4</sup> s (24 h) immersion in oil containing 0.36 wt. % S.....	121

## LIST OF FIGURES

Figure	Page
1.1 (a) Imidazole (b) Secondary amine (c) Amino acid (d) Thiol group (e) Triphenylmethane .....	20
1.2 (a) BTAH (b) TTAH .....	21
2.1 Molecular orientation of TTAH in chemisorbed state on Cu (111) <sup>[Kok10]</sup> .	35
2.2 Adsorption orientation of BTAH on Cu <sub>2</sub> O in aerated HCl solutions obtained from Monte Carlo simulations <sup>[Kha09]</sup> .....	36
2.3 Ellipsometry data showing CI film growth in PAO at 25°C <sup>[Lev07]</sup> .....	42
2.4 Effect of primary-ion dose density on fragmentation behavior <sup>[Tro08]</sup> .....	56
3.1 (a) 5-methyl-1 <i>H</i> -benzotriazole (b) 4-methyl-1 <i>H</i> -benzotriazole methane ..	64
3.2 Bis(2-ethylhexyl) phthalate .....	65
3.3 sec-Butyl disulfide .....	65
3.4 Schematic flow-diagram for sample processing .....	68
4.1 XPS survey spectrum of as-received Cu foil .....	80
4.2 XPS survey spectra of 2M HNO <sub>3</sub> treated Cu coupon. (a) Analyzed immediately (b) Analyzed after 5 days .....	81
4.3 XPS survey spectrum of 2M NPA-treated Cu coupon .....	82
4.4 XPS survey spectrum of CuO .....	83
4.5 Comparison of (a) Cu 2p (b) Cu L <sub>3</sub> M <sub>4,5</sub> M <sub>4,5</sub> peaks acquired on Cu surfaces treated in different ways .....	85
4.6 Comparison of O 1s peak acquired on Cu surfaces treated in different ways.....	85
4.7 Bar-graphs showing characteristic secondary-ion yield from Cu, Cu <sub>2</sub> O, and CuO for (a) Au <sub>3</sub> <sup>+</sup> (b) Au <sup>+</sup> (c) C <sub>60</sub> <sup>+</sup> primary ion beams .....	87

Figure	Page
4.8 (a) Positive ion mass spectrum for bis(2-ethylhexyl) phthalate acquired by Au <sup>+</sup> PI beam (b) Comparison of secondary ion yield distribution acquired by Au <sup>+</sup> and C <sub>60</sub> <sup>+</sup> PI beams normalized to C <sub>3</sub> H <sub>5</sub> O <sub>3</sub> <sup>+</sup> yield in respective cases .	89
4.9 (a) Positive secondary ion mass spectrum for PAO-2 oil acquired by Au <sup>+</sup> PI beam (b) Comparison of secondary ion yield distribution acquired by Au <sup>+</sup> and C <sub>60</sub> <sup>+</sup> PI beams normalized to C <sub>3</sub> H <sub>7</sub> <sup>+</sup> yield in respective cases.....	90
4.10 XPS survey spectrum of Cu surface after being immersed in PAO-2 oil for 3600 s (1 h).....	92
4.11 XPS survey spectrum of Cu surface after being immersed in bis(2-ethylhexyl) phthalate for 3600 s (1 h) .....	92
4.12 (a) Cu 2p (b) O 1s (c) Cu L <sub>3</sub> M <sub>4,5</sub> M <sub>4,5</sub> peaks for Cu samples immersed in PAO-2 oil and bis(2-ethylhexyl) phthalate.....	93
4.13 Negative SI mass spectrum for a TTAH adsorption film on Cu formed upon immersion in oil solution for 8.64 x 10 <sup>4</sup> s (24 h) acquired by (a) Au <sup>+</sup> (b) C <sub>60</sub> <sup>+</sup> PI beam .....	95
4.14 Positive SI mass spectrum of TTAH adsorption film on Cu formed upon 8.64 x 10 <sup>4</sup> s (24 h) immersion in oil showing the presence of PAO-2 oil and bis(2-ethylhexyl) phthalate in the film .....	96
4.15 Spatial mapping of (a) [TTA] <sup>-</sup> (b) [(TTA) <sub>2</sub> Cu] <sup>-</sup> (c) [Cu(CN) <sub>2</sub> ] <sup>-</sup> (d) [TTACu(CN)] <sup>-</sup> .....	97
4.16 Sputter depth-profiles for SI fragments relevant to TTAH adsorption film formed upon 8.64 x 10 <sup>4</sup> s (24 h) immersion .....	98
4.17 Surface acquired images for [(TTA) <sub>2</sub> Cu] <sup>-</sup> , [TTA] <sup>-</sup> , and [Cu(CN) <sub>2</sub> ] <sup>-</sup> after sputtering for (a) t = 0 s (b) t = 120 s (c) t = 360 s (d) t = 600 s (e) t = 810 s (f) t = 1080 s. All micron markers are for 100 μm .....	101
4.18 Sputter depth-profiles for SI fragments relevant to TTAH adsorption film formed upon 1.08 x 10 <sup>4</sup> s (3 h) immersion .....	102
4.19 XPS survey spectrum for TTAH adsorption film on Cu formed upon 8.64 x 10 <sup>4</sup> s (24 h) immersion in oil.....	103

Figure	Page
4.20 XPS multiplex scans for (a) Cu 2p (b) O 1s (c) Cu L <sub>3</sub> M <sub>4,5</sub> M <sub>4,5</sub> (d) N 1s (e) C 1s peaks for TTAH adsorption film on Cu formed upon 8.64 x 10 <sup>4</sup> s (24 h) immersion in oil .....	105
4.21 Tougaard background curve fitting in the vicinity of Cu 2p peak for a 8.64 x 10 <sup>4</sup> s (24 h) immersed sample with 2.5 nm uniform organic over-layer .....	108
4.22 Cu L <sub>3</sub> M <sub>4,5</sub> M <sub>4,5</sub> peak acquired at TOA (a) 5° (b) 20° (c) 45° (d) 90° .....	109
4.23 O 1s peak acquired at TOA (a) 5° (b) 20° (c) 45° (d) 90° .....	110
4.24 N 1s peak acquired at TOA (a) 5° (b) 20° (c) 45° (d) 90° .....	111
4.25 Plots of peak-integral ratio vs. TOA for various elemental peaks .....	113
4.26 Proposed structure for the surface film .....	114
4.27 Immersion time dependent variations for N/Cu, and N/Cu <sub>2</sub> O in (a) 1 s to 2700 s (45 min) (b) 5400 s (90 min) to 6.05 x 10 <sup>5</sup> s (1 week) .....	116
4.28 Immersion time dependent variations for Cu <sub>(-N)</sub> /Cu <sub>Cu2O</sub> , and Cu <sub>Cu2O</sub> /Cu <sub>M</sub> in (a) 1 s to 2700 s (45 min) (b) 5400 s (90 min) to 6.05 x 10 <sup>5</sup> s (1 week).....	117
4.29 Immersion time dependent variation for O <sub>Cu2O</sub> /Cu in (a) 1 s to 2700 s (45 min) (b) 5400 s (90 min) to 6.05 x 10 <sup>5</sup> s (1 week) .....	118
4.30 Immersion time dependent variation for ratios (a) [TTA <sub>2</sub> Cu] <sup>-</sup> /[Cu(CN) <sub>2</sub> ] <sup>-</sup> (b) [TTA] <sup>-</sup> /[TTA <sub>2</sub> Cu] <sup>-</sup> .....	119
4.31 XPS survey spectrum for Cu surface upon 8.64 x 10 <sup>4</sup> s (24 h) immersion in oil containing 0.36 wt. % S.....	121
4.32 XPS multiplex scans for (a) O 1s (b) S 2p peaks acquired on Cu surface film formed upon 8.64 x 10 <sup>4</sup> s (24 h) immersion in oil containing 0.36 wt. % S.....	122
4.33 Comparative plots of (a) Cu 2p (b) Cu L <sub>3</sub> M <sub>4,5</sub> M <sub>4,5</sub> (c) O 1s (d) S 2p peaks acquired on Cu surface films formed under different conditions .....	124
4.34 Quantitative comparison of O (in Cu <sub>2</sub> O), S (in Cu <sub>2</sub> S), and S (in Cu <sub>2</sub> SO <sub>4</sub> ) content in the surface film formed under different conditions .....	125

Figure	Page
4.35	Normalized N content in the Cu surface film formed under different conditions..... 128
4.36	Normalized $O_{Cu_2O}$ , $S_{Cu_2S}$ , and $S_{Cu_2SO_4}$ content in the Cu surface film formed under different conditions..... 129
4.37	Comparative plots of (a) Cu 2p (b) Cu $L_{3M_{4,5}M_{4,5}}$ (c) O 1s (d) S 2p peaks acquired on Cu surface films formed under different conditions ..... 132
4.38	O 1s peak acquired at TOA (a) $5^\circ$ (b) $20^\circ$ (c) $45^\circ$ (d) $90^\circ$ on a Cu sample surface corroded upon sulfide attack..... 133
4.39	Sulfate component of the S 2p peaks upon normalizing the respective sulfide components acquired at TOA $5^\circ$ , $20^\circ$ , $45^\circ$ , and $90^\circ$ on a Cu sample surface corroded upon sulfide attack ..... 134
4.40	Peak-integral ratio vs. TOA plots for various elemental peaks acquired on a Cu sample surface corroded upon sulfide attack..... 135
4.41	Proposed morphology for the corrosion surface film formed on Cu in presence of TTAH ..... 135
4.42	Sputter depth-profiles for SI fragments relevant to TTAH adsorption film formed upon 1 week immersion in TTAH, and S containing oil at $80^\circ C$ .. 138
4.43	Sputter depth-profiles for SI fragments relevant to Cu sulfide corrosion products formed upon 1 week immersion in TTAH, and S containing oil at $80^\circ C$ ..... 140
4.44	Sputter depth-profiles for SI fragments characteristic to $Cu_2O$ layer formed upon 1 week immersion in TTAH, and S containing oil at $80^\circ C$ ..... 141
5.1	Schema of the surface film formation mechanism. (a) Pristine Cu surface immersed in oil. (b) Initial formation $Cu_2O$ and TTAH-Cu complex on the surface. (c) Interaction of TTAH with $Cu_2O$ . (d) Continued formation of $Cu_2O$ under-layer and simultaneous growth of TTAH-Cu at the expense of $Cu_2O$ . (e) Development of uniform TTAH adsorption layer and $Cu_2O$ under-layer. (e) Polymerization of top layer of the TTAH-Cu complex. (f) Diffusion current of O and $Cu^+$ through various layers of surface film sustaining the formation of $Cu_2O$ and TTAH-Cu complex ..... 144
5.2	BTAAH-Cu polymeric film structure suggested by Xue <i>et al.</i> <sup>[Xue91]</sup> ..... 148

Figure	Page
AI.1 Comparison of (a) Cu L <sub>3</sub> M <sub>4,5</sub> M <sub>4,5</sub> (b) O 1s peaks acquired on Cu <sub>2</sub> O specimen with increasing neutralization time.....	161
AI.2 Comparison of relative fractions of (a) Cu and O at. % (b) Cu metallic to Cu <sub>2</sub> O component in Cu L <sub>3</sub> M <sub>4,5</sub> M <sub>4,5</sub> peak acquired on Cu <sub>2</sub> O specimen with increasing neutralization time .....	161
AI.3 Comparison of (a) Cu 2p (b) Cu L <sub>3</sub> M <sub>4,5</sub> M <sub>4,5</sub> (c) O 1s (d) Ar 2p peaks acquired on CuO specimen with increasing neutralization time .....	163
AI.4 Comparison of relative fractions of Cu and O at. % acquired on CuO specimen with increasing neutralization time.....	164
AI.5 Comparison of (a) Cu L <sub>3</sub> M <sub>4,5</sub> M <sub>4,5</sub> (b) O 1s peaks acquired on native-oxide of Cu with increasing neutralization time.....	165
AI.6 Comparison of relative fractions of Cu and O at. % acquired on native-oxide of Cu with increasing neutralization time.....	166

## LIST OF SYMBOLS

Symbol	Definition
ARXPS	Angle-Resolved X-Ray Photo-Electron Spectrometry
BE	Binding Energy
BTA	De-Hydrogenated Benzotriazole
BTAH	Benzotriazole
CI	Corrosion Inhibitor
Cu <sub>M</sub>	Metallic Cu
Cu <sub>Cu2O</sub>	Cu Associated with Cu <sub>2</sub> O
Cu <sub>(-N)</sub>	Cu Associated with TTAH
<i>D</i>	Depth of Analysis
FWHM	Full-Width-Half-Max
IMFP	Inelastic-Mean-Free-Path
KE	Kinetic Energy
NPA	Mixture of 2M HNO <sub>3</sub> , H <sub>3</sub> PO <sub>4</sub> , and CH <sub>3</sub> COOH
O <sub>Cu2O</sub>	O Associated with Cu <sub>2</sub> O
O <sub>H2O</sub>	O Associated with H <sub>2</sub> O
PAO	Poly-Alpha-Olefin
PI	Primary Ions
PIDD	Primary-Ion Dose Density
SI	Secondary Ions
⊖	Surface Coverage
⊖	Take-Off Angle
TOA	Take-Off Angle
ToF-SIMS	Time-of-Flight Secondary-Ion Spectrometry
TTA	De-Hydrogenated Tolyltriazole
TTAH	Tolyltriazole
UHV	Ultra-High Vacuum
XPS	X-Ray Photo-Electron Spectrometry

## **Corrosion Protection of Copper in Oily Media: Microscopic Mechanisms**

### ***Abstract***

By

Avidipto Biswas

Tolyltriazole (TTAH) is an extensively used industrial-grade corrosion inhibitor (CI) for Cu. This PhD project developed an understanding on the microscopic mechanisms for the TTAAH adsorption on Cu, and the effective protection against sulfide-attack in oily medium analogous to automotive lubricants.

XPS and ToF-SIMS characterization were carried out on TTAAH adsorption films formed on pristine Cu surfaces immersed in 0.01 wt. % TTAAH oil solution at room temperature for immersion times ranging from 1 s to 0.6 Ms. Instantaneous complete coverage of the Cu surface by TTAAH is revealed by ToF-SIMS. In Tougaard analysis of XPS spectra, the adsorption film morphology is best described by a uniform-layer model assuming a film thickness of 2.5 nm after 86.4 Ks. Depth-profiling in ToF-SIMS and ARXPS provide evidence for two distinct adsorption configurations for TTAAH on Cu – polymerized layer, and monomer layer. TTAAH adsorption is found to take place on  $\text{Cu}_2\text{O}$ . Studying the time-dependent evolution of the surface film suggests a kinetics-controlled mechanism involving two competing reactions: oxidation of Cu to  $\text{Cu}_2\text{O}$ , and TTAAH-Cu complex formation. The TTAAH-Cu complex formation proceeds at the cost of  $\text{Cu}_2\text{O}$ . The structure and the chemical-composition of the surface film fluctuate with reaction time.

Studying the corrosion of Cu in sulfide solution at 80°C in the absence of TTAH suggests that the oxidation of Cu to Cu<sub>2</sub>O is kinetically favored over Cu corrosion by sulfide attack. The incubation time for the sulfide-attack decreases with increasing S concentration. Two distinct sulfide corrosion products are identified – Cu<sub>2</sub>SO<sub>4</sub>, forming at the oxide interface, and Cu<sub>2</sub>S, forming atop. The presence of TTAH significantly impedes the extent of sulfide-attack. At 80°C, the TTAH adsorption film is substantially thicker than that of room temperature. This suggests that the rate-determining step for the formation of the adsorption film is the outward diffusion of Cu from the substrate. At this temperature, the TTAH adsorption film also reveals a substantially lower degree of polymerization. In the presence of TTAH, both oxidation and sulfide related corrosion of Cu occur underneath the CI adsorption film. The TTAH adsorption film preferentially allows the transport of O through it, leading to the formation of a substantial Cu<sub>2</sub>O underlayer, while blocking the sulfide radicals.

The TTAH adsorption film-forming mechanism proposed in this work explains a number of observations for TTAH- and BTAH-Cu systems reported in the literature, both in oily and aqueous media. The protection of the Cu surface against sulfide attack is attributed to the formation of a physical barrier by TTAH-Cu complex rather than blocking of active sites on the surface. Hence, future research should be focused on finding CI capable of forming better packed Cu-complex structures.

# Chapter 1

## Introduction

### 1.1 Materials System

Copper and its alloys form an important class of metallic materials, which find applications in various fields of engineering industries owing to their suitable thermo-electrical and mechanical properties. The applications of these alloys can be broadly classified into those related to energy sector, transportation sector, construction industry, semiconductor industry, and aesthetics. Some specific applications include heat exchangers, condensers, heating and air conditioning systems, electrical and electronic circuitry, and ornamental parts <sup>[Hay04]</sup>. Depending upon the application, the alloy is subjected to various chemical environments that are often corrosive in nature. Corrosive environments, which are liquid media in most cases, in consideration to the present work, can largely be categorized into two classes: aqueous, chloride and sulfate solutions being most frequently encountered, and oil- or hydrocarbon-based. The present project addresses corrosion problems of Cu and its alloys in oily media. This is of great importance in automobile-related applications.

### 1.2 Copper Corrosion in Automotive Oils

It has been established that corrosion of copper in oily media are more of a chemical phenomenon rather than an electrochemical activity <sup>[ASTxx]</sup>. The biggest concern regarding corrosion of copper in any automotive oil medium is the formation of CuS

upon sulfide ion attack <sup>[Jay02]</sup>. There are a number of sulfur-containing constituents with important functionalities in automotive oils <sup>[Rud03]</sup>, of which the following compounds are worth mentioning: zinc dithiophosphate (ZDP), molydiphosphate, molydithiocarbonates, molybdic acid, amine complexes, and sulfur containing detergents and antioxidants. Decomposition of these compounds, promoted by high temperature and long service time, leads to the formation of reactive sulfur, resulting in corrosion of copper, forming CuS <sup>[Jay02]</sup>. Organic sulfides, especially aliphatic sulfides, are the primary source of this active sulfur <sup>[San84]</sup>. Base oil also decomposes to produce organic acids, which are mildly corrosive <sup>[Cus94]</sup>. Secondary factors affecting Cu corrosion in automotive applications are oxidizing acids, high-velocity-aerated water, oxidizing metal salts, ammonium hydroxide, and other sulfur compounds, such as H<sub>2</sub>S <sup>[Jay02], [Uhl63]</sup>. Oxidation of copper resulting in the formation of passivating Cu<sub>2</sub>O or CuO films on the surface proves beneficial for the protection of the surface against sulfide attack because of its structural integrity and consequent passivity <sup>[All07], [Jay02]</sup>. Depending upon the application, Cu is often alloyed with other metals, such as Ni, with the objective of stabilizing this passivating oxide film, thus, enhancing the corrosion resistance of the alloy. The copper oxide layer incorporates the alloyed metal cations in the lattice sites, such as point defect sites <sup>[Bre98]</sup>. Studies have shown that this results in lowering of the electronic and ionic conductivities of the oxide layer, hence leading to a higher corrosion resistance <sup>[Blu72], [Nor70]</sup>. Sulfide ions, in contrast, accelerate Cu corrosion because they have a detrimental effect on the integrity of the oxide film <sup>[Eis83]</sup>.

### 1.3 Corrosion Inhibitors

Corrosion can be defined as the surface degradation of a material (typically a metal) due to its interaction with its environment. To prevent metals from corrosion, certain chemical compounds, called corrosion inhibitors, are often added to the corrosive environment. Ideally, the inhibitor will rapidly form a self-healing film on the surface of the metal, providing an effective barrier against the corrosive agents in the medium. The choice of corrosion inhibitors depends on the metal to be protected, the chemical nature of the corrosive environment, and related process parameters, such as temperature, pH of medium, e.m.f. of corrosion cell, etc. The inhibitor should be cheap, readily available, environment friendly, and function over a large window of physical conditions. Both organic and inorganic corrosion inhibitors have been used for Cu alloys, depending upon the application <sup>[ASMxx]</sup>. However, in general, heterocyclic organic compounds with  $\pi$  electron orbitals and O, N, P, or S heteroatoms (two or more in number) have proven to be more efficient inhibitors <sup>[Sch84]</sup>. Chromates are the most popular inorganic corrosion inhibitors for Cu alloys. However, chromates may pose serious health hazards, and there are also a large number of less aggressive organic inhibitors: azoles, amines, amino acids and their respective derivatives, triphenylmethane derivatives, thiol group compounds, organic phosphates, etc. The parent molecular structures of these organic compounds are shown in Fig. 1.1.

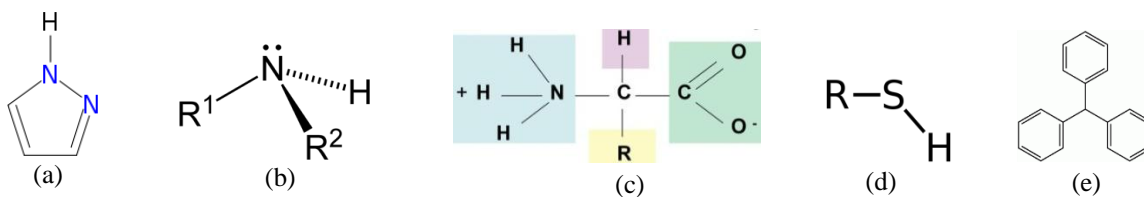


Fig. 1.1: (a) Imidazole (b) Secondary amine (c) Amino acid (d) Thiol group (e) Triphenylmethane.

Of these, organic inhibitors, especially amines, azoles, and their derivatives are more effective in protecting copper from corroding in most practical applications [She06]. In particular, triazoles, members of the azole family, are the most well accepted corrosion inhibitors for Cu alloys in both aqueous based mediums as in water treatment plants and oil based mediums like fuels [Way01], lubricants [Ham90], insulating oils [Rab04], and turbine oils [Ash06]. The solubility of these organic inhibitors in their solvent is often controlled by chain modifications that alter the hydrophobicity of the molecules. The most tried and tested corrosion inhibitors for Cu alloys are benzotriazole (BTAH) and tolyltriazole (TTAH). The former has been used for over 60 years now in all kinds of industries [Pro47]. Their structures, shown in Fig. 1.2, provide bonding sites suitable for a variety of metal atoms. As a result, much research on corrosion inhibition of Cu has been focused on attributes related to the performance and the mechanisms of inhibition provided by BTAH and TTAAH.

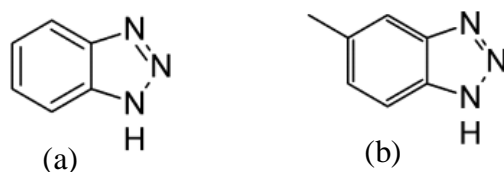


Fig. 1.2: (a) BTAH; (b) TTAAH.

#### 1.4 Corrosive Medium

For both the inhibitors, TTAAH and BTAH, almost all research work has been conducted for copper corrosion in aqueous media. In fact, only two significant studies for Cu corrosion in oily medium [Lev07], [Pol70] are available in the open literature for inhibition by BTAH and one corresponding study for TTAAH [Lev07]. TTAAH is believed to be a better

corrosion inhibitor than BTAH, especially in oil based medium and hence, TTAH finds greater application in most automobile related applications involving oil environment. Yet, most of the research directed towards the scientific understanding of the microscopic mechanism of corrosion inhibition and characterization and the evolution of the passivating film on the copper surface has been limited to BTAH in aqueous systems. The interaction between the corrosion inhibitor, the solvent, and the metal substrate can be represented as:  $Inhibitor (soln.) + n Solvent (ads.) \rightleftharpoons Inhibitor (ads.) + n Solvent (Soln.)$  (1.1). As illustrated by this equation, it is important to study the performance and behavior of these inhibitors in oily media separately from the aqueous systems because water interacts very weakly with the hydrophobic Cu surface <sup>[Hod09]</sup>, <sup>[Mic04]</sup>, hence does not significantly affect the inhibitor–metal surface interactions. However, similar interactions between oil and Cu surface may be significantly stronger, depending upon the chemical nature of the hydrocarbon oil. Thus, for the present PhD thesis project, a detailed study on the adsorption behavior of tolyltriazole on copper surface in oil medium with ToF-SIMS (time-of-flight secondary-ion mass spectrometry) and XPS (X-ray photoelectron spectrometry) as the primary investigation tools was undertaken with the objective of developing an insight into the microscopic mechanism of corrosion inhibition by TTAH in oily environment. The scientific knowledge available regarding the inhibitive mechanism of TTAH, compositional and structural distribution of the inhibitive film formed by TTAH on Cu irrespective of the medium is quite limited. Even in the absence of a unified theory on similar concerns for BTAH, the latter has been much more studied and far better understood, although only for aqueous based systems.

As a result, the literature review presented in Chapter 2 has been substantially built upon the available ideas on BTAH in aqueous based copper systems.

### **1.5 Corrosion Inhibition Mechanism**

The microscopic mechanism of corrosion inhibition is primarily determined by the chemical natures of the inhibitor and the corrosive medium [Sas01]. In the case of electrochemical corrosion, inhibitors once adsorbed are able to arrest, completely or partially, either the anodic and/or the cathodic reactions involved in the process of corrosion, which is often due to the stabilization of a passive film formed on the metal surface. An understanding of the inhibitive mechanism is of utmost importance, as it empowers predictability of the system with variations in process parameters. At present, industries have to rely heavily on empirical testing of Cu corrosion as the inhibition mechanisms for both BTAH and TTAH are poorly understood. The proposed mechanisms for corrosion inhibition of Cu by BTAH, which has been fairly established to be a mixed inhibitor in aqueous systems, i.e. impedes both anodic [Tro98] and cathodic [Yup03] reactions, can broadly be classified into two categories: polymeric film formation on the Cu surface, which acts as a physical barrier, and adsorption of individual inhibitor molecules on the metal surface hence, blocking the active sites [Pap98]. The former is a better accepted postulate, but no consensus has been reached. One of the primary reasons for this unresolved mechanism is the fact that the organic complex film formed in this process is insoluble in common solvents, barring detailed structural and chemical studies. Understandably, there is no unified acceptance on the orientation of the adsorbed inhibitor molecules, either. Alongside experimental approaches, simulation efforts like

DFT <sup>[Kok10], [Jia03]</sup>, molecular dynamics <sup>[Kha08]</sup>, molecular mechanics <sup>[Edw94], [Kha09]</sup>, and quantum chemical calculations <sup>[Kha08]</sup> have been carried out to understand the inhibition mechanism better and to ascertain the adsorption behavior of the inhibitors in terms of molecular orientation and bond strength. Following a thermodynamic approach to understand the adsorption mechanism, adsorption isotherms and their properties have been studied under different corrosive conditions <sup>[Kha10], [Bas06]</sup>. Even though, for rightful reasons, computational work is gaining importance in this field of research, experimental studies remain very important, primarily due to the fact that for the computational studies to be carried out in a reasonable fashion the process conditions have to be oversimplified and it is not yet possible to simulate a real-scale scenario computationally. The need for experimental studies further increases owing to the extreme sensitivity of inhibitor behavior on process conditions. For examples, it has been claimed that the adsorption mode may change drastically from physisorption to chemisorption over a narrow shift in conditions <sup>[Kok10]</sup> whereas in some other studies it has been established that molecules with similar electronic properties and parameters, like that of benzotriazole and 1-hydroxy benzotriazole (BTAOH), can also reveal drastically different inhibitive properties <sup>[Fin08], [Fin10]</sup>.

## **1.6 Surface Characterization**

A combination of ToF-SIMS and XPS was considered to be the ideal set of characterization tool required to probe into the adsorption behavior of TTAH on Cu in oily media. ToF-SIMS is an extremely surface sensitive characterization technique. It provides information on both elemental and molecular species from one or two

monolayers of the surface (depth resolution < 1nm) with some other notable advantages being that practically any surface can be studied, high chemical sensitivity, submicron spatial resolution, and short acquisition time. While the extreme surface sensitivity is the greatest advantage of this technique, it also implies that exceedingly careful considerations are required to interpret the ToF-SIMS spectra in order to obtain meaningful information as slight alterations in the surface condition during sample handling may substantially modify the secondary ion spectra. For example, the spectra may get substantially modified due to undesired surface reactions when exposed to the atmosphere, signals from airborne molecular contamination (AMC), and other kinds of ionic contaminants adsorbed on the specimen surface from the atmosphere <sup>[Tro08]</sup>. All of these are hard to control. In the process of characterization, cautious deliberations are required in choosing characteristic peaks used to identify specific chemical species. The stability of the spectra with variations in acquisition conditions should also be taken into account – especially, the primary ion dose density (PIDD). The ability of ToF-SIMS to provide useful information on the molecular structure of organic compounds, deduced from the fragmentation behavior of the specimen, along with the extreme surface sensitivity, is the key to its effectiveness in studies related to the field of corrosion inhibition of metallic surfaces by film forming organic molecules. In modern ToF-SIMS instruments, a better sensitivity and an increased mass range, as well as enhanced mass resolution at much lower PIDD have resulted in higher sensitivity of the instrument to molecular structure. This has made it an even more powerful tool to characterize complex organic films that are being considered in the present project. Surface analysis techniques like ToF-SIMS complemented with XPS ideally enable complete characterization of the

surface and subsurface film structure and composition, rendering valuable information for understanding the microscopic mechanisms of environment/film/surface interactions and hence, involved molecular interactions. Functionality of the organic molecules can also be investigated by means of XPS, as it also provides information on the chemical states of atoms. XPS also enables quantitative analysis of the surface composition in terms of the constituting elements hence, overcoming one of the biggest limitations posed by ToF-SIMS characterization. Quantitative analysis of the constituent elements by means of XPS can be easily extended to the quantitative analysis of larger molecular ions provided the binding energies for the specific elements can be correctly associated to the respective molecular ions with certainty. Hence, ToF-SIMS and XPS provided the ideal choice of instruments to characterize the TTAH adsorption film on Cu directed towards obtaining extremely precise qualitative and quantitative information.

### **1.7 Project Objective and Thesis Organization**

It was realized that at present, TTAH is the best corrosion inhibitor for copper in most commonly encountered industrial atmospheres, especially in oil-based media used in automobiles. But there is hardly any data in the open literature, neither on the performance of TTAH in oily media nor on the mechanism of inhibition for TTAH – irrespective of the medium. In the present light, this PhD project was an attempt to study the adsorption behavior of TTAH in oil-based media that are typical for automobile lubricants in order to get an insight into the microscopic mechanism of corrosion inhibition specific to the oily media. To meet this purpose, two objectives were laid down for this project: study the *time dependent structural evolution* of the TTAH adsorption

film on Cu in hydrocarbon medium and study the *effect of sulfide corrosive agents* present in the hydrocarbon medium on the formation of the TTAH adsorption film. This understanding will not only help industries to optimize their process performance with changing conditions with greater ease and higher confidence, but also lead to the possibility of designing and developing new and improved corrosion inhibitors for copper by identification of structurally similar compounds worthy of synthesis and subsequent corrosion testing.

In this PhD thesis, the literature review is presented in Chapter 2, discussing the available knowledge and scientific understanding on primarily BTAH systems. However, this mostly concerns aqueous systems, which have been investigated to a much greater depth than TTAH systems, especially with respect to surface analysis and characterization. The details of the experimental design and techniques aimed to meet the project objectives are laid down in Chapter 3. Subsequently, Chapter 4 presents all the experimental results obtained under the current initiative followed by a detailed discussion of the results in Chapter 5 aimed at developing a better scientific understanding of the corrosion inhibitive film forming mechanism. Finally, Chapter 6 summarizes the conclusions that can be drawn from this research project.

## Chapter 2

### Literature Review

This chapter presents a concise review of the findings on the adsorption behavior of corrosion inhibitors benzotriazole (BTAH), and tolyltriazole (TTAH) on copper. A large number of papers have been published on the study of these compounds. However for the present review only those papers have been considered that help to develop an understanding of the organic film formation on Cu surface by these two corrosion inhibitors and discuss their corresponding mechanisms and/or respective characterization methods. Though the project in hand aims to study the adsorption behavior of TTAH on Cu in oily media, yet, the present chapter for the most part deals with BTAH/Cu systems in aqueous media. This is because the BTAH/Cu system in aqueous media has been studied in far greater details as compared to any other system. Note, the adsorption behavior of corrosion inhibitors may significantly depend on the solvent medium for reasons mentioned in section 1.4. Nevertheless, learning the already known facts regarding this system paves a stronger path into the exploration of other similar systems. Note that even for the so well studied BTAH/Cu system in aqueous media, no consensus has been reached on the mechanism of BTAH adsorption on Cu and the effects of most process parameters like time, temperature, pH etc. are not explained unanimously. This chapter has been divided into multiple sections, where each section discusses findings on a specific aspect of the adsorption behavior of the corrosion inhibitor on Cu. In this chapter, the medium by default should be assumed to be aqueous based unless and until mentioned otherwise.

## 2.1 Adsorption Mechanism

This section focuses on the molecular form in which the inhibitor is adsorbed on to the Cu surface and the near-surface structure and composition of the resultant protective film. In case of adsorption of the molecule in a dissociated state, it is important to learn the dissociation reaction and to realize the stage (pre/post adsorption) at which it happens. Present day ideas on molecular adsorption as against complex formation and polymerization have also been considered.

*Known:*

- i. BTAH is a mixed inhibitor reducing both anodic and cathodic reaction rates in aqueous media but often stated particularly to be either a cathodic or an anodic inhibitor <sup>[Tro98]</sup>, <sup>[Yup03]</sup>.
- ii. Two mechanisms are proposed for BTAH adsorption on Cu in aqueous media: adsorption of single inhibitor molecule on metal surface, and formation of protective polymeric film involving complexes of  $\text{Cu}^+$  and  $\text{BTA}^-$  forming  $[\text{Cu-BTA}]_n$  <sup>[Pap98]</sup>. It has been proposed that in neutral aqueous media, BTAH coordinates with copper ions via nitrogen lone pair electrons (less prone to polymerization) whereas in basic media BTAH exists as  $\text{BTA}^-$  forming inner complexes like  $[\text{Cu}^+-\text{BTA}^-]$  or  $[\text{Cu}^{2+}-(\text{BTA})_2^-]$  which usually polymerize <sup>[Xue91]</sup>.  $\text{Cu}(\text{BTAH})_{\text{ads}}$  i.e. BTAH adsorbed on Cu in molecular state has also been proposed to be a reaction intermediate formed either at low concentration of BTAH insufficient to cover the entire surface or conditions leading to low adsorption rate which finally forms a Cu-BTA porous film over-layer as time lapses or

concentration of BTAH increases <sup>[Bas06]</sup>. In chloride media, formation of  $\text{Cu}^+$  is suggested to be the first step which then readily reacts with BTAH to form  $[\text{Cu}^+-\text{BTA}^-]$  complex and release  $\text{H}^+$  <sup>[Ali07]</sup>. However, no consensus has been reached on this matter.

- iii. BTAH treated Cu sample consists of three different layers:  $\text{Cu}^+-\text{BTA}^-$  complex layer,  $\text{Cu}_2\text{O}$  under-layer, and Cu substrate <sup>[Fin10], [Qaf02]</sup>. BTAH is claimed to reinforce the  $\text{Cu}_2\text{O}$  under-layer whereas no such under-layer has been detected for the case of BTAOH. This model is not widely accepted.
- iv. For BTAH treated Cu samples in chloride media, contradictory results have been reported on the presence of chlorine on the surface: in some cases no Cl has been reported to be found on the surface <sup>[Fin10]</sup> whereas in others it has been, which is likely due to entrapment of Cl in the Cu-BTA film. If Cu:Cl:N is found in a stoichiometric ratio, it implies halogen bridging in the film which has also been reported <sup>[Has88]</sup>. Cl entrapment without changing the valence state of Cu is reported for BTAOH treated samples <sup>[Fin10], [Cli66]</sup>.
- v. TTAH and BTAH are adsorbed intact on Cu surface in Poly alpha olefin (PAO-2) medium. In case of N-methylamino substituted triazoles, the amino-methyl tails are lost (likely by retro-Mannich reaction) <sup>[Lev07]</sup>.
- vi. Cu in BTAH + Oil: Low intensity of molecular ion signals in ToF-SIMS. High intensity for  $\text{Cu}_x\text{C}_y\text{N}_z$ , and  $\text{Cu}_n(\text{BTA})_{n\pm 1}$  implying high tendency of complex formation and polymerization <sup>[Lev07]</sup>.

- vii. Cu in TTAH + Oil: Strong signal for intact molecular ion in negative spectrum of ToF-SIMS. No such signal in positive mode. Low signals for  $\text{Cu}_x\text{C}_y\text{N}_z$  implying that TTAH has higher tendency for adsorbing as individual molecule and is less prone to form polymerized film as compared to BTAH <sup>[Lev07]</sup>.
- viii. Cu in I39 + Oil: No signal from intact molecule but strong signal corresponding to  $\text{TTA}^-$  in ToF-SIMS and signals corresponding to TTA-Cu bonding implying dissociation of I39 <sup>[Lev07]</sup>.
- ix. Cu in I30 + Oil: No signal in ToF-SIMS for intact molecule but dominant signals for Cu containing fragments related to Cu-triazole bonding, and fragments related to the triazole part of the molecule <sup>[Lev07]</sup>.
- x. The mechanism of film formation in PAO-2 oil by triazoles with free N-H functional group (BTAH and TTAH) is different from that of N-methylamino substituted functional groups (I30 and I39) due to drastic difference in film thickness <sup>[Lev07]</sup>.
- xi. In ToF-SIMS, most important signature peaks of BTAH on Cu formed in aqueous media are  $\text{Cu}(\text{BTA})_2^-$  ( $m/z = 299$ ),  $\text{BTA}^-$  ( $m/z = 118$ ), and  $\text{Cu}_2(\text{BTA})^+$  ( $m/z = 244$ ) <sup>[Tro08], [Lev07], [Swi95]</sup>. Other important peaks:  $\text{Cu}(\text{BTA})^-$ , and  $\text{CuO}(\text{BTA})^-$ .  $\text{C}_2\text{H}_2\text{N}_3^-$  are also considered to be signature peaks for BTAH on Cu.
- xii. BTAOH likely to prevent corrosion by reducing the cuprous oxide formed on the surface in aqueous media <sup>[Fin10]</sup>.

- xiii. From ARXPS results, two oxygen peaks detected corresponding to  $\text{Cu}_2\text{O}$ , and oxidized carbonaceous contaminant while a third peak reveals that either O or  $\text{H}_2\text{O}$  is involved in Cu-BTAH film structure or the film gets partially oxidized or otherwise the inhibitor adsorption on the Cu surface is patchy leading to oxidation of the uncovered metal surface <sup>[Man06], [Mou92]</sup>. There are multiple studies claiming the presence of water molecules coordinated with the inhibitive film <sup>[Tom97]</sup>.
- xiv. Alteration in environment (from  $\text{Cu}^+$ - $\text{BTA}^-$  environment) of Cu, and N revealed on sputtering through in XPS which has been attributed to the presence of adsorbed molecular BTAH present below the  $[\text{Cu}^+-\text{BTA}^-]_n$  polymerized complex <sup>[Fin10], [Fan86]</sup>. The shift in N 1s peak is typical to that of nitrogen bound with phenyl group/conjugated nitrogen to Cu-hydrocarbon complexes/pyridine like nitrogen <sup>[Man06], [Lah99]</sup>.
- xv.  $\text{Cu}_2\text{O}$  from surface is partly consumed in the formation of Cu-BTAH complex film. In Cu-Ag alloy treated with BTAH in sodium sulfate solution, surface enrichment with Ag is observed which is likely due to dissolution of Cu from surface during formation of  $[\text{Cu}^+-\text{BTA}^-]$  film <sup>[Man06]</sup>.

## 2.2 Molecular Bonding and Orientation

This section deals with the bonding characteristics of the corrosion inhibitor molecules with Cu – physisorption vs. chemisorption, and adsorption orientation – vertical vs.

parallel orientation. In case of chemisorption, it is important to understand which functional group and which atoms in particular bond with the Cu surface.

*Known:*

- i. Commonly proposed ideas: adsorption occurs directly by donor-acceptor interactions through electrons of the triazole ring and vacant d-orbital of copper. Vertical/Perpendicular orientation – bonding through the lone pair orbital of nitrogen with the lone nitrogen atom bonded to two Cu atoms <sup>[Rub83]</sup>. Flat/Parallel orientation – formation of BTA<sup>-</sup> ion by loss of imino-hydrogen leading to a conjugated  $\pi$  structure delocalized over three nitrogen atoms <sup>[Vog97]</sup>. Angular orientation – nitrogen lone pairs bonding to Cu but not in a flat orientation <sup>[Tom89]</sup>. There is a lack of agreement regarding orientation of BTA on Cu surface.
- ii. Primary factors affecting adsorbate orientation: crystal surface orientation of adsorbant, type of medium/environment, pH, electrode potential. Other process parameters, such as temperature may also affect the orientation.
- iii. Most experimental researchers suggested chemisorption in aqueous media even though physisorption is likely to provide a better steric hindrance to corrosive molecules <sup>[Kok10], [Sch00]</sup>.
- iv. BTAH molecule – Cu surface distance: chemisorption: 0.2 nm; physisorption: 0.3 nm <sup>[Kok10]</sup>.
- v. Projected molecular area of BTAH calculated: vertical orientation – 0.2 nm<sup>2</sup>; horizontal orientation – 0.38 nm<sup>2</sup>. Area occupied by water molecule which has

vertical orientation: 0.08-0.12 nm<sup>2</sup>. Interpreted as vertical orientation of BTAH on Cu [Bas06].

- vi. From density functional theory (DFT) calculations performed for ATAH (3-amino-1,2,4-triazole), BTAH, and BTAOH on Cu(111)/vacuum interface, physisorption is stronger than chemisorption for molecules in neutral form on defect free surface [Kok10]. Strength of chemisorption in neutral state: BTAH (-0.4 eV) < BTAOH (-0.53 eV) < ATAH (-0.6 eV). Strength of physisorption in neutral state: ATAH (-0.56 eV) < BTAH (-0.72 eV) < BTAOH (-0.97 eV). Chemisorption in an upright geometry with molecules bonded to Cu surface through triazole N atoms and X-H--Cu (X=N, O) hydrogen bonds whereas physisorption with molecular plane nearly parallel to metal surface in order to maximize contact with surface. Hydrogen bonding plays a role in physisorption as well along with dispersion forces especially in case of BTAOH. Chemisorption bond energies increase substantially for adsorption on uncoordinated surface defects to become almost same as the respective physisorption energies [Kok10], [Kok04]. These calculations are done for very low surface coverage.
- vii. As per DFT studies, for dehydrogenated species chemisorption is stronger than physisorption with chemisorption bond strength order (this order is corresponding to experimentally observed corrosion inhibition effectiveness in near neutral chloride solution): BTAO<sup>-</sup> (-1.65 eV) < ATA<sup>-</sup> (-2.22 eV) < BTA<sup>-</sup> (-2.78 eV) implying a stronger interaction with Cu surface as compared to their respective neutral states [Kok10]. Deprotonated forms are expected to have even higher

chemisorption energies whereas the physisorption energies for molecules in dehydrogenated, and deprotonated forms are expected to be similar to that of their neutral states due to similarity in size. There is again a lack of agreement on this [Jia03]

- viii. Proposed molecular orientations in chemisorbed state are shown in Fig. 2.1 [Kok10]. In all cases of chemisorption, N-Cu bonds are very similar implying that differences in hydrogen bonding is the key factor in differentiating the bonding characteristics and orientation of one molecule from the other.

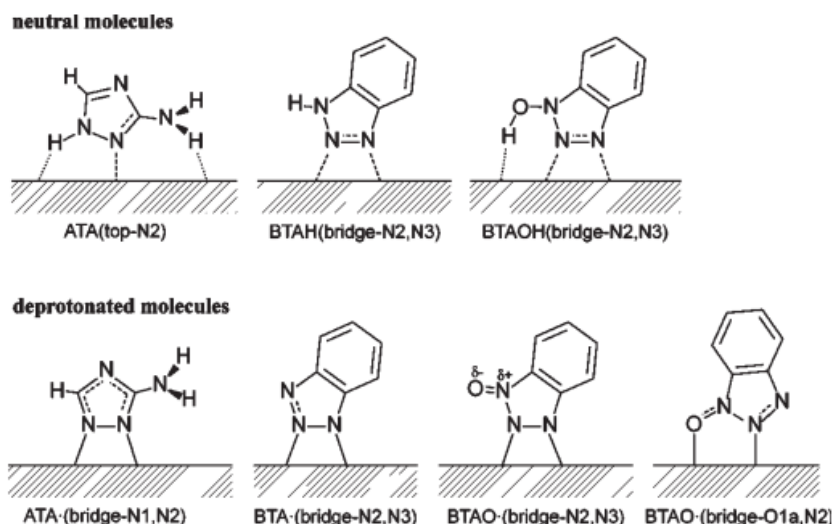


Fig. 2.1: Molecular orientation of TTAH in chemisorbed state on Cu (111) [Kok10].

- ix. DFT calculations show that in chemisorption of  $\text{ATA}^-$ ,  $\text{BTA}^-$ , and  $\text{BTAO}^-$ , the triazole derivatives interact with the Cu surface through the nitrogen lone pair orbitals of the triazole ring. In case of physisorption, lateral dipole-dipole, and dispersion interactions are significant which increasingly stabilize the system with

increasing surface coverage up to a critical point beyond which Pauli repulsion gets into the act. For parallel geometry, no interaction between molecular  $\pi$  orbitals and metal surface are observed [Kok10].

- x. DFT calculations also reveal strong dipole-induced dipole interaction between inhibitor molecule and metal surface, it being strongest for BTAH [Kok10].
- xi. Based on Monte Carlo simulations, BTAH adsorbs in flat/parallel orientation on  $\text{Cu}_2\text{O}$ , as shown in Fig. 2.2

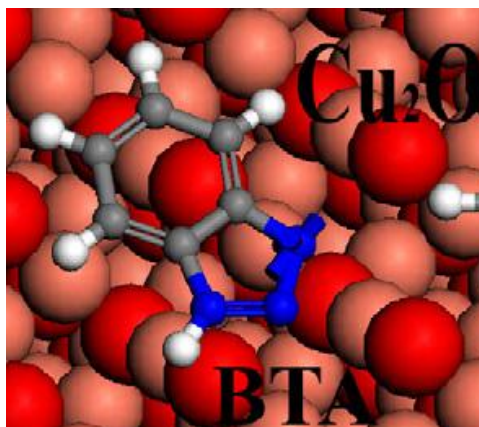


Fig. 2.2: Adsorption orientation of BTAH on  $\text{Cu}_2\text{O}$  in aerated HCl solutions obtained from Monte Carlo simulations [Kha09].

- xii. Medium also plays an important role in the energy balance of the entire process as the medium molecules will be initially adsorbed on the metal surface and hence, for the inhibitor, molecular orientation and mode, and strength of bonding largely depends on the medium as well.
- xiii. In chloride media, BTAH adsorbs on Cu surface such that N atoms are closer to the surface as compared to the C atoms whereas BTAOH adsorbs such that O is closer

to the free surface as compared to N atoms implying that the OH group most likely is not directly involved in the inhibitor-metal interaction <sup>[Fin10]</sup>.

### 2.3 Adsorption Isotherm

Adsorption isotherm is a general thermodynamic concept to express the amount of adsorbate on the adsorbent as a function of concentration for fluids at constant temperature. Adsorption isotherm gives an insight into the process in terms of number of adsorption layers and free energy changes involved in the process. Changes in isotherm model with process parameters like temperature, solvent medium etc. also throws light on mechanistic shifts.

*Known:*

- i. The Langmuir adsorption isotherm models the adsorption process of BTAH on Cu-Ni alloy in 5% HCl aqueous solution quite satisfactorily. Maximum coverage of 0.998 at 35°C and 15g/l inhibitor has been reported <sup>[Kha10]</sup>. Even in aqueous H<sub>2</sub>SO<sub>4</sub> medium, the Langmuir isotherm is followed <sup>[Rav05]</sup>. At lower concentrations of HCl (1 to 5 mM) aqueous solutions, the Frumkin equation has been reported to be the most suitable adsorption model for BTAH on commercially pure Cu <sup>[Bas06]</sup>. In the studies concluding the Langmuir adsorption isotherm as the best fit, determining the highest correlation coefficient between experimental data and mathematical models was the key approach, whereas for the study recommending the Frumkin model, the inflection points in  $dc/d\theta$  vs.  $\theta$  was the key parameter compared.

- ii. The Freundlich adsorption model and the Kinetic-Thermodynamic model are unsuitable in aqueous media <sup>[Kha10]</sup>.
- iii. The Langmuir adsorption isotherm is expressed as:  $\theta = \frac{KC}{1+KC}$  (2.1). Higher K values in (2.1) imply stronger adsorption of BTAH on Cu surface in aqueous HCl medium. K values practically do not change in the temperature range of 35°C to 55°C <sup>[Kha10]</sup>.
- iv. As per the Frumkin model,  $\theta$  vs.  $c$  follows a sigmoidal (S-shaped) curve <sup>[Bas06]</sup>.
- v. Monolayer adsorption suggested in aqueous media <sup>[Kha10]</sup>.
- vi. Calculated  $\Delta G_{ads}$  values for BTAH in 5% HCl solution: -17.37 to -24.76 kJ/mol <sup>[Kha10]</sup>. Calculated  $\Delta G_{ads}$  values for BTAH in 1 to 5 mM HCl solution: -20 to -34 kJ/mol <sup>[Bas06]</sup>. Typically for physisorption,  $\Delta G_{ads} > -20$  kJ/mol and for chemisorption  $\Delta G_{ads} < -40$  kJ/mol but some researchers have suggested that for chemisorption of organic inhibitors on metal surfaces in aqueous media  $\Delta G_{ads}$  lies in the range of -21 to -42 kJ/mol <sup>[Umo08], [Dam71]</sup>. However, Monte Carlo simulations revealed an adsorption energy of -318 kJ/mol for BTA on Cu (110) <sup>[Kha09]</sup>.
- vii. Small in magnitude but positive values for thermodynamic interaction parameter (f) imply weak laterally attractive forces between adsorbed BTAH molecules in aqueous media. This has been associated to vertical orientation <sup>[Bas06], [Bas97]</sup>.
- viii. Electrical interactions between the double layer existing at the phase boundary and the adsorbing BTAH molecules have been reported <sup>[Bas06]</sup>.

- ix. Configuration term or size ratio parameter ( $\chi$ ) which signifies the number of water molecules being replaced by one BTAH molecule has been predicted to be in range of 1-5 by the Frumkin model [Bas06].
- x. Non-uniform surface conditions and effective interaction between adsorbed molecules may lead to significant deviation in adsorption isotherm model.

## 2.4 Inhibitor Efficiency

Inhibitor Efficiency is a general measure of the ability of a corrosion inhibitor to protect the metal surface from being etched out in a corrosive environment. It may vary significantly with process parameters of which the chemical nature of the corrosive medium and the surface condition of the metal are of utmost importance in order to gain insight into the inhibition process.

*Known:*

- i. Typical values ranging from 86% to 99.8% have been reported for BTAH in the literature depending upon the testing conditions, though, all in aqueous media [Kha10].
- ii. CuO/Cu does not change even after 1 week for BTAH treated (in aqueous medium followed by washing and drying) Cu surface. Possibility of Cu<sub>2</sub>O formation has been neglected in this result as Cu<sup>0</sup>, and Cu<sup>+</sup> were considered to represent Cu metal [Nis03].

- iii. In neutral aqueous medium, inhibitive film formed by BTAH on a freshly etched Cu surface ( $\text{Cu}^0$ ) has better anticorrosion properties as compared to that on  $\text{Cu}_2\text{O}$  because BTAH treated  $\text{Cu}_2\text{O}$  surface suffers significant oxidation post treatment as compared to that of fresh Cu surface <sup>[Xue91]</sup>.
- iv. BTAH is a better corrosion inhibitor than BTAOH, the latter having almost no influence on the formation of copper oxide. BTAOH fails to form a preventive polymerized film and to reinforce the  $\text{Cu}_2\text{O}$  under-layer <sup>[Fin08], [Fin10], [Qaf02]</sup>.
- v. Chemically modified BTAH, C6BTA (5-hexyl-1,2,3-benzotriazole) or TBC (N-2-thiazolyl-1H-benzotriazole-1-carbothiamide) provides greater resistance to corrosion than un-substituted BTAH <sup>[Kha09], [Bru92]</sup>.

## **2.5 Synergistic Effects of other Inhibitors and certain Ions**

In a number of applications, synergy effects of secondary corrosion inhibitors or certain other intentionally or unintentionally added ions/chemicals with the primary corrosion inhibitor come into play which considerably determines the ultimate effectiveness in protecting the metal surface from corroding. These effects may be beneficial or adverse. To control these effects to advantage, it is important to understand the interaction mechanisms among the chemical species.

*Known:*

- i. Halogens, especially chlorine, containing chemical species are well known to have a disruptive effect on the protective film formed by BTAH, and TTAH on Cu in aqueous media <sup>[Lu94], [Hol94]</sup>. No understanding of the molecular mechanism has been reported.
- ii. Adding BTAH and TTAH in conjugation shows beneficial effects in protecting Cu metal in most aqueous media, especially in water treatment industries. Also presence of  $\text{MoO}_4^{2-}$ ,  $\text{NO}_2^-$ , organic phosphonates, and Cobratec 939 (a commercial product) are considered to have beneficial effects on the inhibition capability of both BTAH, and TTAH in aqueous media <sup>[Zuk82], [One76]</sup>.

## **2.6 Film Thickness**

Film thickness does not necessarily imply anything directly about the inhibition efficiency or the passivating ability of the corrosion inhibitor and the film respectively but with a thicker film the steric hindrance provided to the corrosive media in reaching the metal surface is known to increase. There is not enough information on the structure of the film to support either of the models – uniform composition homogenous films as against multi-layer structured films with varying film compositions. Further, the possible interfacial reactions at the metal/film/environment interfaces, the chemical nature of the inhibitor, and the effect of process parameters, most importantly the corrosive medium, on the adsorption behavior of the inhibitor need to be studied to a much greater extent.

*Known:*

- i. Inhibitive film thickness in PAO-2 oil: TTAH – 1nm; BTAH – 2 nm; I30, and I39 (N-methylamino substituted triazoles) – 0.5 nm. Slightly thinner films are obtained in dodecyl benzene medium <sup>[Lev07]</sup>.

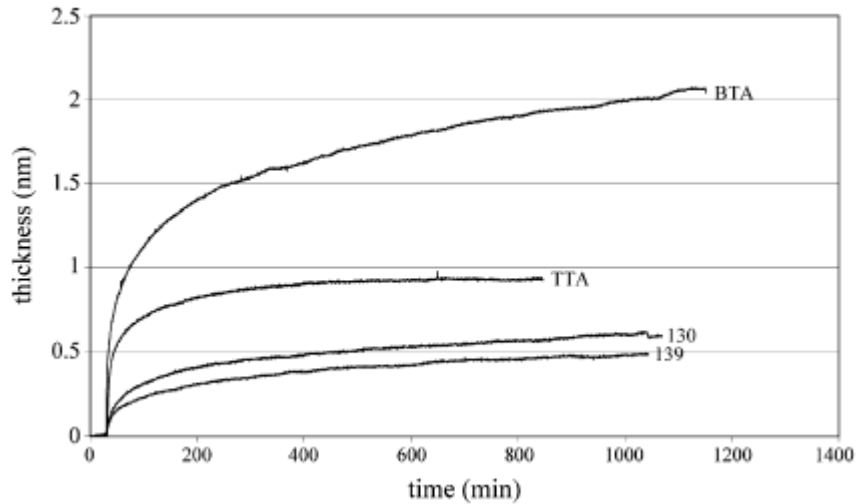


Fig. 2.3: Ellipsometry data showing CI film growth in PAO at 25°C <sup>[Lev07]</sup>.

- ii. Generally, much higher film thickness, values up to 200 nm, are reported in aqueous media, though, in certain cases like in NaCl, a Cu-BTAH film thickness of  $1.5 \pm 0.3$  nm, and that of  $0.5 \pm 0.2$  nm for Cu-BTAOH have been reported after 1h. But, in Na<sub>2</sub>SO<sub>4</sub> medium 20-36 nm thick films have been obtained with BTAH in 4h depending upon the applied potential difference <sup>[Met00], [Man06], [Fin10]</sup>.
- iii. In aqueous media also, TTAH forms thinner layers than BTAH on Cu but with similar passivating abilities <sup>[Hol85]</sup>.

- iv. In comparison of N-, and C- methyl substituted benzotriazole, N- substitution prevents formation of protective layer whereas C- substitution enhances film formation <sup>[Tor89]</sup>.
- v. Cu-BTAOH layer is much thinner and less ordered as compared to Cu-BTAH layer <sup>[Fin10]</sup>.
- vi. In inhibitor free chloride medium (NaCl), immersion of Cu for 1h leads to the formation of Cu<sub>2</sub>O ( $\approx$  1.1 nm) on surface and no chlorine is detected on the surface. In BTAH treated samples in the same solution for the same time, the Cu<sub>2</sub>O film has been reported to grow under the [Cu<sup>+</sup>-BTA<sup>-</sup>] film. It might be an artifact of patchy surface coverage by the [Cu<sup>+</sup>-BTA<sup>-</sup>] film <sup>[Fin10], [Coh90], [Mci81]</sup>.

## 2.7 Rate of Inhibitive Film Formation

The rate of film formation can indirectly provide information on the possible interfacial interaction reactions. It is also a direct parameter to judge reaction mechanism shifts with time for a given case and compare mechanistic differences from one case to the other. It further helps to distinguish the effects of process parameters related to the corrosive medium on the corrosion process.

*Known:*

- i. For both BTAH and TTAH the initial adsorption rate is rapid. Adsorption starts immediately in oily media <sup>[Lev07]</sup>.

- ii. Inhibitive film growth rate in oily media slows down with time but steady state is not reached in 1000 minutes implying complex mechanism requiring at least 2 time constants to develop mathematical model <sup>[Lev07]</sup>.
- iii. Chemisorption of BTAH in neutral aqueous solution on freshly etched Cu ( $\text{Cu}^0$ ) forms  $[\text{Cu}(0)\text{-BTAH}]$  surface layer observed in less than 15 sec that converts to  $[\text{Cu}^+\text{-BTA}^-]$  polymeric film within 2 minutes when exposed to air due to co-adsorption of oxygen <sup>[Xue91]</sup>.
- iv. Film formation with BTAH on Cu follows a parabolic growth law in the initial stages followed by logarithmic rate law whereas for BTAOH, it follows a linear curve suggesting a mechanistic difference <sup>[Fin08]</sup>. BTAOH is expected to prevent corrosion by reducing the cuprous oxide formed on the surface instead of forming a preventive complex film as in the case of BTAH <sup>[Fin10]</sup>.
- v. In aqueous media, the rate of film growth is expected to be higher for less negative potentials with respect to standard electrode. Exceptions are also cited and a number of contradictory results have been published without discussing any possible explanation. As per Youda et al. <sup>[You90]</sup>, negative potentials are required for film formation in acidic solution whereas in neutral range film forms irrespective of the potential with respect to the standard electrode. But Yao <sup>[Yao04]</sup> suggested in his work that in acetonitrile, at negative potential difference, BTAH is adsorbed on Cu in molecular state whereas film formation occurs at positive potential differences with respect to Ag/AgCl electrode. Gao <sup>[Gao02]</sup> suggested that the  $[\text{Cu-BTA}]_n$  complex film changes its composition with potential and at negative potentials

ranging from -0.5 to -1.1 V (against SCE) 'n' assumes a value of 4 in neutral chloride solution as lower potential results in lower pH at electrode surface resulting in film decomposition. As per Chan <sup>[Chan99]</sup>, adsorbed BTAH molecules, deprotonate on Cu surface in sulfate solution for less negative potentials with respect to SCE for pH>2 whereas Schultz <sup>[Sch04]</sup> suggested that BTAH adsorbs in its deprotonated form (BTA<sup>-</sup>) in well-ordered manner for Cu (100) in the whole potential range of -0.65 to -0.2 V against Ag/AgCl electrode while the layer is disordered for Cu(111) under similar conditions. The various studies have provided a varied and, in many cases, contradicting results. However no mechanistic understanding of the corrosion process has been reached that takes into account all the process parameters involved.

## 2.8 Desorption

Desorption behavior illustrates the thermodynamic stability of the adsorbed layer. Knowledge of the reversibility of the adsorption process may be utilized to optimize the inhibitor concentration level to be maintained in a real application.

*Known:*

- i. Both BTAH and TTAH show a largely irreversible adsorption behavior. Only 20% of the adsorbed material desorbs when placed in fresh oil medium <sup>[Lev07]</sup>.
- ii. Desorption kinetics is faster than adsorption in PAO-2 oil and reaches steady state in few hours <sup>[Lev07]</sup>.

- iii. Adsorbed Cu-BTAH film on the surface formed in aqueous media is very easily destroyed by a mild acid wash leading to drastic oxidation of Cu (formation of CuO) <sup>[Nis03]</sup>.
- iv. BTAOH has been proposed to desorb at higher concentrations of the inhibitor due to self-interaction of the adsorbed molecules with the ones in the solution which at first leads to the formation of oligomers and finally desorption <sup>[Mor04]</sup>.

## **2.9 Effect of the Corrosive Medium**

The chemical nature of the corrosive medium including its pH, and its interaction with the inhibitor and the metal surface dictate the entire corrosion process and its inhibition. Change in the medium may drastically affect the corrosion process, and the adsorption behavior at the metal surface and hence, the efficiency of the inhibitor as well. Oil- and water-based media are completely different in nature from each other. Most studies till now have been conducted in aqueous based systems. Independent investigations into oil based systems are thus equally important for certain applications.

*Known:*

- i. Thicker films have been reported for both TTAH and BTAH in aqueous based systems as compared to oil based media. Thinner protective films were obtained with BTAH, and TTAH in dodecyl benzene, another convenient oil based solvent for experiments, as compared to PAO-2 <sup>[Lev07]</sup>.

- ii. Medium plays an important role in the energy balance of the entire process as the medium molecules will be initially adsorbed on the metal surface and hence, for the inhibitor adsorption, molecular orientation and mode, and strength of bonding largely depends on the medium as well.
- iii. Interaction between water molecules and Cu surface is very weak, so it does not affect metal-inhibitor interaction significantly which might not be the case for oily media <sup>[Hod09], [Rou05]</sup>.

## 2.10 Performance in Real Oil

Corrosion inhibition process in real automotive oil is extremely complicated. To develop a comprehensive understanding, a systematic study on performance of inhibitor needs to be undertaken in real oil with all additives at experimental scale starting from simpler to more complex oil formulations in order to identify the effects of individual additives on the corrosion inhibition property. The effects of oil additives, both individually and collectively, on the mechanism of inhibitor adsorption at molecular level also need to be investigated.

*Known:*

- i. Corrosion of copper in oily media is more of a chemical attack rather than an electrochemical activity <sup>[ASTxx]</sup>.
- ii. Decomposition of oil constituents leads to formation of reactive sulfur which further leads to corrosion of Cu and formation of CuS. Active sulfur primarily

comes from organic sulfides. Alkyl sulfides, disulfides, and mercaptans are effective oxidation inhibitors in oily media but corrode copper heavily. Aliphatic sulfides are more corrosive than aromatic sulfides. Typical sulfur containing compounds in oil: zinc dithiophosphate (ZDDP), molybdenum diphosphate especially sulfurized oxymolybdenum organo-phosphoridithioate (Mo-S-P), molybdenum dithiocarbonates, molybdic acids, amine complexes, and sulfur containing detergents and antioxidants [Jay02], [Cus94], [San84], [Rud03].

- iii. CuO/Cu<sub>2</sub>O formed on Cu surface is structurally more passive than CuS. CuS allows corrosion via cation diffusion from Cu metal to sulfide/lubricant interface [Jay02], [All07] [Bre98], [Eis83].
- iv. Secondary factors causing Cu corrosion in real automotive oily media: oxidizing acids like HNO<sub>3</sub>/H<sub>2</sub>SO<sub>4</sub>, aerated non-oxidizing acids, aerated NH<sub>4</sub>OH and substituted amines forming Cu(NH<sub>3</sub>)<sup>4+</sup>, high velocity aerated water containing carbon dioxide and low dose of Ca<sup>2+</sup> and Mg<sup>2+</sup>, oxidizing metal salts like FeCl<sub>3</sub>, and H<sub>2</sub>S or other sulfur compounds [Jay02], [Uhl63].
- v. Presence of magnesium sulfonate in lubricants causes more wear of Cu than calcium sulfonate whereas presence of zinc oxide or sulfide reduces wear [Jay02], [Mcg85].
- vi. Cu alloying with Al, Be, Mg, Sn, Zn reduces the rate of oxidation. Sb, Ca, Fe, Mn, Li, Ti, Ni also help in enhancing the anti-corrosion properties of the metal. In

reactive SO<sub>2</sub> gas atmosphere, 10-12% Al is required to avoid substantial oxidation of Cu alloys <sup>[Lei71]</sup>.

- vii. Heterocyclic compounds like 1-phenyl-5-mercaptotetrazole, and 1-thiocarbamyl-3,5,5-trimethylpyrazone form a shiny protective film on Cu in oily media <sup>[Lei71]</sup>.

## 2.11 Effect of Surface Roughness and Poly-Crystal

Adsorption process is sensitive to crystal orientation. Adsorption behavior on single crystal in a specific direction may substantially differ from that on a poly-crystal. Surface defects are usually more reactive. Effects of surface roughness/scratches and grain boundaries on adsorption behavior may have noteworthy effects.

*Known:*

- i. Most of the ToF-SIMS and XPS studies involving organic films on Cu surfaces are done on highly polished metallic surfaces/mirror-finish <sup>[Fin10], [Man06], [Xue91], [Lev07], [Swi95], [Tro08]</sup>. Non uniform surface leads to non- ideal adsorption.
- ii. Uncoordinated defects on Cu surface are reactive enough to dehydrogenate unsaturated organic molecules <sup>[Kok10], [Kok04]</sup>.
- iii. Chemisorption bond energies for BTAH-Cu (111) increase substantially for adsorption on uncoordinated surface defects to become almost same as the respective physisorption energies <sup>[Kok10]</sup>.

## 2.12 Effect of Temperature

Temperature directly affects the reaction kinetics involved in the adsorption process. Change in temperature may induce shifts in inhibition mechanism. Also, with increase in temperature, there are possibilities of new surface reactions, and intermolecular interactions coming into play as a result of sufficient thermal energy to overcome the activation energy.

*Known:*

- i. Higher temperature and longer exposure time increases the amount of reactive sulfur in lubricating oils <sup>[Jay02], [Cus94]</sup>.
- ii. ZDDP and most molybdenum species decompose at temperatures above 130°C whereas sulfonate detergents do so above 170°C <sup>[Jay02], [Cus94]</sup>.
- iii. No study found on the effect of temperature on the adsorption behavior of either TTAH or BTAH on Cu irrespective of the medium.

## 2.13 Effect of Inhibitor Concentration

Inhibitor concentration is well known to affect the inhibition efficiency. There have been considerations into the possibility of mechanism shifts in the adsorption process with comparatively larger changes in inhibitor concentration and hence, shift in adsorption isotherm.

*Known:*

- i. In CMP process, Cu treated with higher concentration of BTAH in polishing slurry (aqueous based) shows less oxidation as compared to that treated with low concentration BTAH [Nis03].

## 2.14 Effect of Surface Oxide

Adsorption is a highly surface specific and sensitive process. A small change in the surface condition may cause a major change in the adsorption behavior of the adsorbate. Copper surface very often, in most practical cases, is covered with copper oxide (CuO/Cu<sub>2</sub>O). A careful consideration is required to investigate into the differences in the adsorption behavior of the inhibitor molecules with varying oxidation state (0, +1, +2) of copper at the surface.

*Known:*

- i. Furnace-oxidized Cu exposed to TTAH, and I39 in PAO-2 shows similar peaks as that in case of polished Cu but lower film thicknesses is concluded due to lower intensities of signals from TTA<sup>-</sup> [Lev07]. The study lacks in-depth consideration of effect of oxide on formation of surface layer.
- ii. Reaction rate of BTAH in neutral aqueous solution with clean Cu surface is faster than oxidized Cu surface (Cu<sub>2</sub>O) [Xue91]. Exposure of fresh Cu surface to air forms Cu<sub>2</sub>O film first with thickness of 1 to 2 monolayers in the first 30 minutes, and ≈1.2 nm after 2 hours even though oxygen is adsorbed on a fresh Cu surface as soon as it

is exposed to air <sup>[Xue91], [Tom83], [Pra86], [Ram85]</sup>. After 10 minute exposure to atmosphere Cu on surface is partly metallic and partly Cu<sub>2</sub>O.

- iii. Presence of Cu<sub>2</sub>O on surface degrades the effectiveness of the inhibitive film formed by BTAH in neutral aqueous media <sup>[Xue91]</sup>.
- iv. For PVD Cu on Si wafer, O/Cu ratio, as obtained from XPS, increases continuously during the first four days and then stabilizes to 1 implying surface oxidation continues for first few days and finally forms CuO at the end of 4 days <sup>[Tro08]</sup>.
- v. For a fresh Cu surface exposed to air for a few minutes reveals a very high C content on the surface under XPS. Also, a high intensity of CO<sub>3</sub><sup>-</sup> secondary ions in ToF-SIMS is observed due to rapid adsorption of CO<sub>3</sub><sup>-</sup> ions from the atmosphere on a highly reactive Cu surface in a time span insufficient for oxide formation <sup>[Tro08]</sup>. With increasing oxidation the CO<sub>3</sub><sup>-</sup> gets removed hence the C content on the surface drops down (in about 2-3 hours) but with further passage of time it starts increasing slowly but steadily due to airborne molecular contamination (AMC). In ToF-SIMS, peaks from AMC, typically of the type – C<sub>x</sub>H<sub>y</sub>O<sub>z</sub><sup>-</sup>, may interfere with signature peaks and also limit the effective detection limit of those peaks.
- vi. Cu<sub>x</sub>O<sub>y</sub>H<sub>z</sub><sup>-</sup> secondary ion signals in ToF-SIMS are indicators of surface contamination rather than surface oxide the reason being that for CuO<sup>-</sup>, CuO<sub>2</sub><sup>-</sup>, and CuO<sub>2</sub>H<sup>-</sup> the relative normalized intensities exactly match the pattern followed by CO<sub>3</sub><sup>-</sup>, a surface contaminant <sup>[Tro08]</sup>. This implies that the O for Cu<sub>x</sub>O<sub>y</sub>H<sub>z</sub><sup>-</sup> type of peaks comes from CO<sub>3</sub><sup>-</sup> rather than copper oxide.

## 2.15 Effect of Oxygen Purging

For scientific understanding of the inhibitive film forming process, it is important to explore in what ways oxygen may affect the inhibitive film formation process and key related parameters like film thickness, kinetics of film formation, film composition, its passivity or inhibition efficiency, and extent of polymerization.

*Known:*

- i. Oxygen influences the formation of Cu-BTAH film formation <sup>[Xue91], [Man06], [Man73], [Lev07], [Cus94]</sup>. Role of oxygen is debated and not understood.
- ii. Cu corrosion in nitrogen atmosphere is less aggressive than that of air in ZDDP containing oil <sup>[Jay02], [Cus94]</sup>.

## 2.16 Comparison of Adsorbed Layer Formation on Cu strip vs. Powdered Cu

Powder materials have much higher surface area to volume ratio as compared to bulk/strip material thereby accelerating surface reactions for powders. Thus, it is often suitable to study surface specific phenomenon with powder materials depending upon the objective.

*Known:*

- i. Cu powder immersed for 3 days in neutral BTAH aqueous solution leads to formation of blue powder as the reaction product. Isolated product is related to  $\text{Cu}^{2+}$  whereas the BTAH treated Cu surface shows presence of  $\text{Cu}^+$  <sup>[Xue91]</sup>.

## **2.17 Effect of Stress**

Stress can substantially alter the surface condition of the metal which on the other hand may affect the adsorption behavior of the inhibitor molecules on the Cu surface.

*Known:*

- i. Stress induces a high number density of defects in the metallic surface. Adsorption behavior is sensitive to presence of defects. Above a critical magnitude of plastic deformation of the Cu substrate, differences in the adsorption behavior of the inhibitor molecules on the Cu surface may be observed. However no studies are available on this effect so far.
- ii. In case of surface oxidized Cu sample, stress may as well change the metal/surface oxide interface substantially leading to variations in adsorption behavior. This effect has not been explored by researchers and can be very interesting to study.

## **2.18 Corrosion Product Analysis**

Systematic study on the characterization of the corrosion products formed on the surface of the Cu metal having undergone corrosion test in real oil with practical compositions and testing conditions carried out sequentially from simpler to more complex cases is required for a comprehensive understanding of the corrosion process.

*Known:*

- i. Base oil decomposes to produce organic acids <sup>[Cus94]</sup>. High level of O and C are detected on the surface of Cu tested in oily medium due to decomposition of oil, products of which get incorporated throughout the porous CuS layer <sup>[Jay02]</sup>.
- ii. Friction Modifier: molybdenum dithiophosphate, in oily media, is almost twice as corrosive as molybdic acid at the same wt. % of Mo due to enhanced sulfide formation <sup>[Jay02]</sup>.
- iii. Anti-wear additive: primary and aromatic ZDDP are stronger sulfide formers than secondary ZDDP and hence, cause Cu corrosion to greater extent in oily media. In case of mixed ZDDP, sulfide formation on Cu caused by primary and aromatic ZDDP is suppressed <sup>[Jay02]</sup>.
- iv. Dispersant: forms complex with ZDDP to reduce its surface activity and hence, lowering its tendency to form sulfide with Cu. The lower the total base number (TBN) of the dispersant, the higher is the concentration of the dispersant required for neutralization of free ZDDP present in the oil. Borated dispersants enhance Cu corrosion dramatically as boration, instead of forming passive copper borate layer, reduces the interaction between dispersants and ZDDP leaving higher amount of the latter to react with the Cu surface. Succinimide, and amines play satisfactory roles as dispersants <sup>[Jay02]</sup>.

## 2.19 Effect of Primary Ion Dose Density

Primary Ion Dose Density (PIDD) is a critical parameter to be controlled for detection of the intact molecular ions and acquiring a reproducible data set in ToF-SIMS. Some considerations on the PIDD dependent variations in the ToF-SIMS results are listed below.

*Known:*

- i. With increasing PIDD the intensities of larger molecular fragments in the secondary ion signal are diminished whereas the intensities of smaller fragments increase due to progressive fragmentation of clusters. Fig 2.2 shows a typical example that was published by Trouiller *et al.*

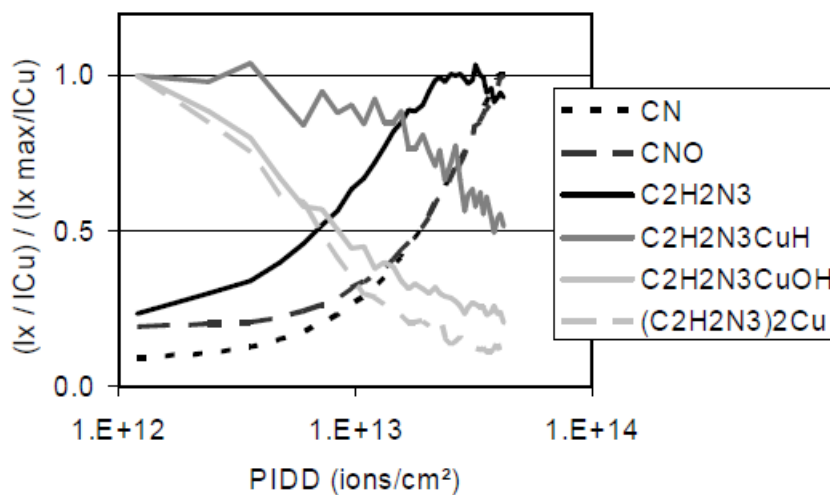


Fig. 2.4: Effect of primary-ion dose density on fragmentation behavior <sup>[Tro08]</sup>.

- ii. For BTAH, BTA<sup>-</sup> signal corresponding to the intact molecular ion is observed for PIDD maximum up to  $3 \times 10^{13}$  ions/cm<sup>2</sup> whereas for C<sub>10</sub>F<sub>21</sub>O<sub>3</sub><sup>-</sup>, the largest fragment

from Per-Fluoro Poly-Ether (PFPE), an often found contaminant on Cu, PIDD of  $2 \times 10^{11}$  ions/cm<sup>2</sup> is already above the static limit [Tro08].

- iii. PIDD for maintaining static conditions with respect to a particular secondary ion can be calculated from the damage cross section which can be determined [Koe98].
- iv. PIDD corresponding to dynamic range acquisition results in lower reproducibility of data. For all other parameters held constant, the smaller the raster area for acquisition, the higher is the PIDD. For small raster areas like  $50 \times 50 \mu\text{m}^2$ , very often PIDD up to 10 times higher than that corresponding to the static limit is applied in order to maintain sufficient counting statistics. In such cases of dynamic acquisition, relative intensities may vary by 20 – 50% from those obtained under static conditions [Tro08].

## **2.20 Effect of Primary Ion Gun Source in ToF-SIMS**

The primary ion stream sputtering off the surface being characterized directly controls the characteristics of the secondary ions. The type of primary ion being used affects the fragmentation process at the surface, and depth of damage which are critical to be optimized depending upon the surface being analyzed and the kind of information being sought.

*Known:*

- i. Clustered primary ion guns are better suited for organic film characterization. They result in secondary ion signals with higher fraction of larger molecular ion

fragments and hence, signature peaks from organic structures are better detected [Kol05]. This facilitates acquiring more information about the surface structure. Available primary ion guns in our instrument:  $C_{60}^+$ ,  $Au_3^+$ ,  $Au^+$ ,  $Bi_3^+$  and  $C_{60}^+$  are usually considered to be more effective.

- ii. Primary ion current is also an important parameter that affects the secondary ion spectrum which is indirectly controlled by optimizing the PIDD by adjusting the raster area.
- iii. Primary ion beam energy again has a direct impact on the sputtering process at the surface which can be controlled by means of the accelerating voltage. It is usually not recommended to alter the accelerating voltage for a given instrument.

### **2.21 General Comments**

- i. For oily medium experimental study, Poly alpha olefin (PAO-2) medium or some other similar hydrocarbon/oil medium should be chosen that is highly refined – uniform molecular size and free from sulfur, and nitrogen.
- ii. TTAH and BTAH have limited solubility in PAO-2. Therefore, they are usually pre-dissolved in bis(2-ethylhexyl)phthalate for lab experiments. In industries, chain modified solvents are used to enhance hydrophobicity/solubility.
- iii. Phthalate related peaks do not interfere with the identification of BTAH and TTAH in ToF-SIMS.

- iv. Adsorption layer thickness and film growth rate are usually studied on PVD Cu as the adsorbed layer is too thin.
- v. Toluene and methanol are typically used solvents to clean the sample before inserting into ToF-SIMS.
- vi. Samples should be stored in glass vials and not plastic bags for cleanliness issues.
- vii. On Si wafer, TTAH, I30 & I39 yield distinct signals for intact molecular ions both in positive and negative secondary ion spectra in ToF-SIMS. BTAH yields very low signals for intact molecular ions likely due to low adsorption on Si <sup>[Lev07]</sup>
- viii. For I30 and I39 adsorbed on Cu in oil-medium, amine tail signals are unspecific and weak <sup>[Lev07]</sup>.
- ix. BTAH exists as  $C_6H_6N_3^+$  in acidic solutions, as  $C_6H_5N_3$  ( $C_6H_5N_3/C_6H_4N_3^- = 96/4$ ) in neutral or near neutral solutions, and as  $C_6H_4N_3^-$  in alkaline solutions.
- x. The only study in oily medium was done with 100 ppm inhibitor <sup>[Lev07]</sup>.
- xi. In XPS,  $Cu^{2+}$  identified by presence of shake up satellite peaks around core transition lines and  $Cu^+$  is differentiated from  $Cu^0$  by auger LMM lines like  $L_3M_{4,5}M_{4,5}$ .
- xii. BTAH practically does not get adsorbed on TaN,  $SiO_2$ , and SiN. BTAH does not form complex  $[Ag^+-BTA^-]$  with Ag strip surface but does react with Ag nanoparticles. <sup>[Man06]</sup>

- xiii. Coverage ( $\theta$ ) being related to inhibitor efficiency (IE) as  $\theta = IE$  is based on three assumptions: adsorption sites on Cu surface are homogenous, monolayer of inhibitor is formed and uniform corrosion with no localized attacks.
- xiv.  $[Cu^+-BTA^-]$  or  $[Cu^{2+}-(BTA)_2^-]$  are usually polymeric and insoluble in water and most organic solvents.
- xv. BTAH has strong intermolecular hydrogen bonding in solid state.
- xvi. Even though BTAH and BTAOH have very similar electronic structure parameters, yet, BTAH is a much better corrosion inhibitor than BTAOH <sup>[Fin10], [Kok10]</sup>.
- xvii. Physisorption is significantly important to be considered in case of organic inhibitors, especially large ones as it scales up with size.
- xviii. During sample preparation and handling, the surface condition can be significantly modified and hence, it is important to be aware of the possible surface phenomenon.
- xix. In XPS, depth of analysis =  $3\lambda\sin\theta$ .
- xx.  $Cu^{2+}$  is not formed on surface after being immersed in NaCl solution for 1h in either presence or absence of inhibitors <sup>[Fin10]</sup>.
- xxi. Carbonaceous contaminants from air always get adsorbed on the surface while transferring/drying sample.

- xxii. Electro-polishing of Cu-Ag alloy leads to surface enrichment with silver which does not allow film formation with BTAH <sup>[Man06]</sup>.
- xxiii. BTA<sup>-</sup> signal in ToF-SIMS after CMP or chemical rinse is 10-100 times higher than the base line signal generated due to AMC whereas after scrubber cleaning it falls below the effective detection limit even though it is 10 times above the instrument detection limit <sup>[Tro08]</sup>.
- xxiv. Cu segregation at surface on oxidation of Cu alloys is a commonly observed feature depending upon the alloying elements.
- xxv. High temperature Cummins bench test (HTCBT) according to the specifications laid down in ASTM D130 is a standard procedure in industries used to test Cu corrosion in oily media.

Note that most conclusions published on the structure of the adsorption film included in this chapter are either speculative or based on indirect experimental evidences. In course of the present PhD project a number of these issues related to the film structure have been better resolved. The next chapter discusses the layout and logistics of the experimental work designed to meet the objectives of this PhD project.

## Chapter 3

### Experimental Design and Procedures

This chapter discusses the experimental framework designed to realize the objectives of this project. Broadly, the objectives were to:

- study the *time dependent structural evolution* of the TTAH adsorption film on Cu in hydrocarbon medium and hence, to resolve the film formation and growth mechanism
- study the *effect of sulfide corrosive agents* present in the hydrocarbon medium on the formation of the TTAH adsorption film and hence, comment on the effectiveness of the corrosion inhibitor

The first objective – time dependent structural evolution of the adsorption film was studied at room temperature whereas the second objective – effect of sulfide corrosive agents was studied at an elevated temperature of 80°C for reasons mentioned in Section 3.2. Immersion test followed by surface analysis was considered as the experimental basis to accomplish these objectives. Cu coupons were immersed in the inhibitor containing oil medium for specific lengths of time in order to study the adsorption behavior of TTAH on Cu. Surface analysis was carried out by means of XPS and ToF-SIMS for reasons outlined in section 1.6. The following sections outline the raw materials, sample preparation methods, instrumentation conditions, and experimental logistics involved in this project.

### 3.1 Raw Materials

The raw material components utilized in the course of this project are listed below:

- Metal Substrate: Cu Foil

A 25  $\mu\text{m}$  thick Cu foil with 99.98 wt.% purity was procured from Sigma Aldrich. Small coupons with face dimensions 8 mm x 8 mm were cut out of the foil for the individual immersion tests.

- Cleaning Reagents: Acid Mixture and Toluene

The Cu foil in as-received condition was mechanically smooth to naked eye but had a surface coating of an unknown carbonaceous material. To get rid of this coating and obtain a fresh Cu surface, an equi-volume aqueous based acid mixture of 2M  $\text{HNO}_3$ ,  $\text{H}_3\text{PO}_4$  and  $\text{CH}_3\text{COOH}$  was used. Toluene was used to rinse off the oil from the sample surfaces at the end of the immersion tests.

- Oil Medium: Poly-alpha-olefin (PAO-2)

PAO-2, a highly refined grade of mineral oil with uniform molecular size, was used as the hydrocarbon oil medium for the corrosion inhibitor adsorption study. In chemical nature, it resembles base oils commonly used in lubrication applications, and insulating oils in electrical power transformers. But for chemically sensitive studies such as this, possibly the biggest advantage of using PAO-2 is that it is free from impurities like sulfur and nitrogen unlike any other grade of commonly

available refined mineral oil. This avoids invoking uncontrolled compositional parameters in the experiments, the chemical effects of which are hard to determine.

- Corrosion Inhibitor: Tolyltriazole (TTAH)

Reagent grade 98 wt.% purity TTAH ( $C_7H_7N_3$ ) was obtained from Sigma-Aldrich. There are a couple of isomers available for this compound – 5-methyl-1*H*-benzotriazole and 4-methyl-1*H*-benzotriazole. The respective structures are shown in Fig. 3.1. In the course of the present project, 5-methyl-1*H*-benzotriazole was used in specific. All experiments were carried out at 100 ppm TTAH concentration level.

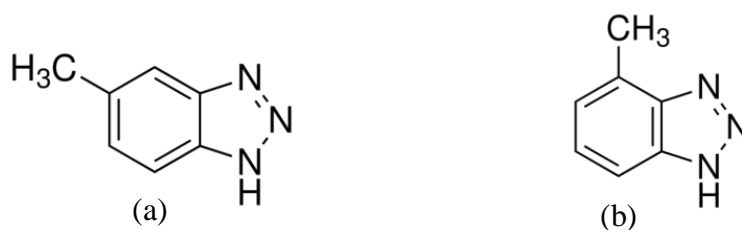


Fig. 3.1: (a) 5-methyl-1*H*-benzotriazole (b) 4-methyl-1*H*-benzotriazole.

- Inhibitor Solvent: Bis(2-ethylhexyl) phthalate

TTAH has limited solubility in PAO-2 oil. Thus, it needs to be pre-dissolved in another solvent which in turn is soluble in the oil medium. Analytical grade bis(2-ethylhexyl) phthalate ( $C_{24}H_{38}O_4$ ) from Sigma Aldrich was used for this purpose, the structure for which is shown in Fig. 3.2. In all experiments, the PAO-2 oil to solvent bis(2-ethylhexyl) phthalate ratio was maintained at 100:1 by weight.

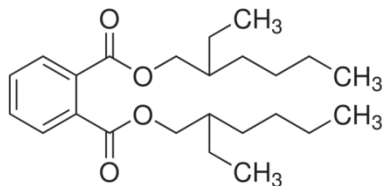


Fig. 3.2: Bis(2-ethylhexyl) phthalate.

- Sulfur Source: sec-Butyl disulfide

For experiments meant to study the sulfide corrosion behavior of Cu in TTAH containing oil, sec-butyl disulfide, molecular formula  $[C_2H_5CH(CH_3)]_2S_2$ , was used as the source of active sulfur. The molecular structure for the same is shown in Fig. 3.3. It was a 90 wt.% purity technical grade reagent as procured from Sigma Aldrich. On heating, the disulfide bonds cleave and ultimately active sulfur is released in the oil medium which is highly prone to chemically attack the Cu surface. The choice for this compound was carefully made so as to make sure that it is readily soluble in the PAO-2 oil and most importantly does not contain any chemical species other than S and hydrocarbon chains in order to avoid uncontrolled parameters.

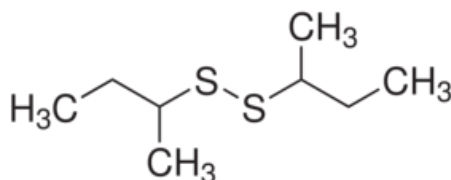


Fig. 3.3: sec-Butyl disulfide.

### 3.2 Sample Preparation

This section outlines the individual steps involved in the processing of the samples for surface characterization. A schematic flow-diagram of the same is shown in Fig. 3.4. Cu coupons (8 mm x 8 mm x 0.025 mm) were cut out from the as-received foil. As mentioned in the prior section, the as-received foil was coated with some unknown carbonaceous material. In order to dissolve any oily substance present on the initial surface, the samples were washed in toluene in an ultra-sonicator for 300 s. This was followed by immersing the samples in an equi-volume aqueous based acid mixture of 2M HNO<sub>3</sub>, H<sub>3</sub>PO<sub>4</sub> and CH<sub>3</sub>COOH for an optimized time of 300 s accompanied by vigorous agitation. Intense bubble formation was noted in this step. The resultant acid roughened Cu surface was in pristine metallic condition, i.e., Cu<sup>0</sup> oxidation state that was chemically stable with respect to oxidation in atmosphere within the time limits of sample preparation. It was observed that a prolonged immersion in the acid up to  $\approx$  500 s led to the formation of a dulled Cu surface along with patchy dark spots which was attributed to the beginning of formation of copper nitrates on the surface as suggested by XPS results.

The acid roughened Cu samples were washed well in distilled water for about 100 s followed by air drying. These samples were then immediately immersed in the PAO-2 oil solution. Two batches of PAO-2 oil solutions were prepared – one with only 0.01 wt.% (100 ppm) TTAH while the other had 0.72 wt.% (7200 ppm) S added by means of sec-butyl disulfide along with the TTAH. The former batch was used to study the time dependent structural evolution of the adsorption film at room

temperature whereas the latter batch was used to study the sulfide corrosion of Cu in presence of TTAH at an elevated temperature of 80°C. There are multiple reasons for conducting the sulfide corrosion tests at 80°C. First of all, thermal energy needs to be provided to the system to break the disulfide bonds in order to release active S in the oil. Secondly, even in the presence of active S, the corrosion process of Cu is extremely slow at room temperature in the presence of TTAH corrosion inhibitor and hence, needs to be thermally accelerated to be studied in a reasonable time-frame. Finally, 80°C is a much more representative temperature for the actual conditions prevailing in certain automobile applications relevant to this study.

On taking the Cu samples out of the oil solution, these were rinsed with toluene again for 600 s in an ultra-sonicator to wash-off the oil from the Cu surface. These samples were then immediately inserted in UHV (ultra-high vacuum) chambers of XPS and ToF-SIMS for respective characterizations.

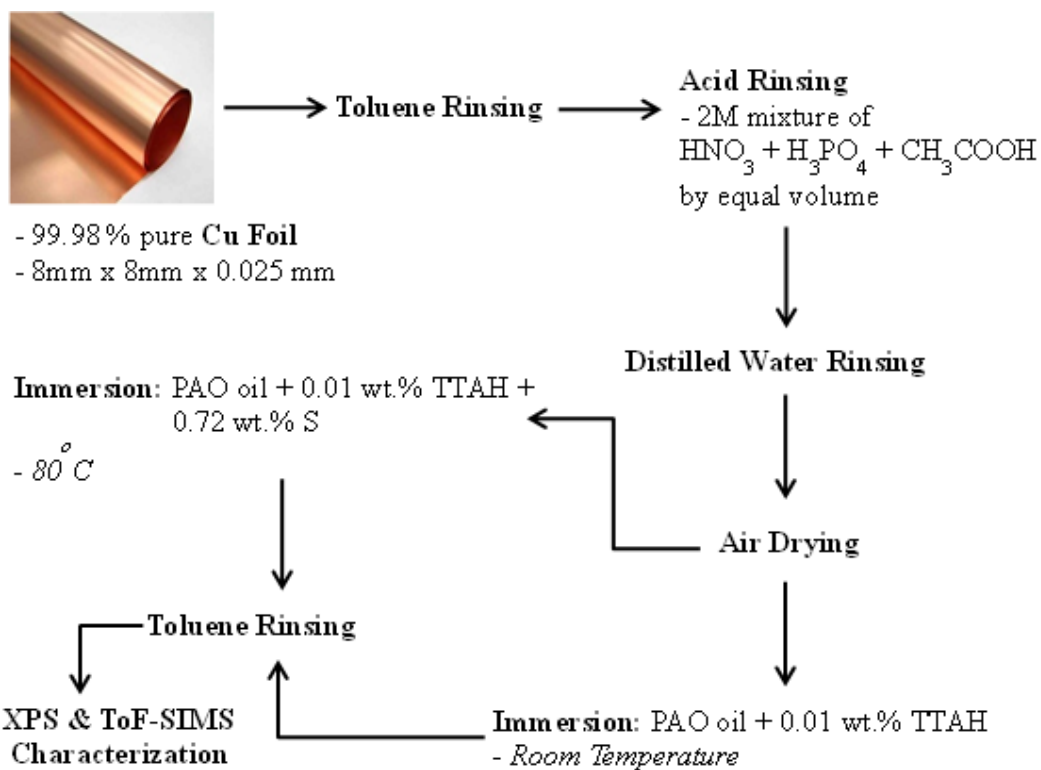


Fig. 3.4: Schematic flow for sample processing.

### 3.3 Instrumental Conditions and Procedures

XPS and ToF-SIMS were considered to be the most judicious choice of instruments to conduct the surface characterization work involved in this project for reasons outlined in section 1.6. The characterization work involving these two instruments was exclusively carried out at Swagelok Center for Surface Analysis of Materials (SCSAM) in Case Western Reserve University. A ToF-SIMS instrument with a TRIFT V nano-TOF analyzer manufactured by PHI was used in consideration to the present project. The instrument is equipped with three ion guns – Au,  $\text{C}_{60}$ , and Ar guns for analytical and sputtering purposes. The XPS work was carried out on a PHI Versa Probe 5000

instrument that is equipped with an Al K $\alpha$  X-ray source producing a monochromatic X-ray beam with energy 1486.6 eV. It is commissioned with a 180° hemispherical electron energy analyzer optimized for energy resolution and PHI's high angular acceptance lens optimized for small area XPS sensitivity. Further details regarding these instruments can be found at SCSAM website: <http://engineering.case.edu/centers/scsam/>.

In course of the present project, all ToF-SIMS experiments were carried out with a 30 kV Au<sup>+</sup> ion beam in bunched mode for analytical purposes and a 20 kV C<sub>60</sub><sup>+</sup> ion beam for depth-profile sputtering. The latter has the advantage of being much less destructive for organic clusters. All ToF-SIMS mass spectra were acquired for negative secondary ions that were collected over 250  $\mu\text{m}$  x 250  $\mu\text{m}$  raster areas. The positive secondary ions did not reveal any relevant information. The data acquisition time was maintained at 600 s and the primary ion dose density (PIDD) was kept under  $6.3 \times 10^{11}$  ions/cm<sup>2</sup> which was well within the static limit as suggested by the fact that the absolute peak intensities in the mass spectrum recorded over a fixed interval of time did not significantly change with prolonged acquisition from the same spot. Moreover, it is well established that the PIDD corresponding to the damage threshold for static SIMS of organic molecules relevant to the present project is of the order of  $1 \times 10^{13}$  ions/cm<sup>2</sup>, i.e., the analyzed surface is effectively undamaged for ToF-SIMS study conducted at a PIDD under this value <sup>[Bri86]</sup>. A typical mass resolution ( $m/\Delta m$ ) of 7500 or greater was obtained at  $m/z = 132$ .

All XPS experiments were performed with a 300  $\mu\text{m}$  spot size incident beam probing the surface at an intensity corresponding to 75 W. The analyzer pass energy was set at 23.5 eV, yielding a FWHM (full-width-half-max) of 0.768 eV for Ag 3d<sub>5/2</sub> peak at the same

incident beam spot size. In all cases, data acquisitions were done at energy steps of 0.4 eV and 0.2 eV for survey spectra and high resolution multiplex spectra, respectively. All experiments were done at a take-off-angle (TOA) of 45° with respect to the sample surface, by default, except for the cases where ARXPS study was carried out at TOA of 5°, 20°, 45°, and 90°. The fact that the analyzed depth increases with increasing TOA as  $d = 3\lambda \sin\theta$  (3.1) serves as the working principle for ARXPS to reveal information on the depth-sensitive distribution of elements. In eqn. 3.1,  $\lambda$  is the IMFP (inelastic mean free path) of photoelectrons through the material medium and  $\theta$  is the TOA. The analyzed depth, defined as the depth from which 90% of the detected photoelectrons are generated, is expected to be in the range of 1.5 nm to 5 nm in the present study for the considered values of TOA. Note that the analyzed depth was greater than the typical thickness values for the corrosion inhibitor adsorption film on Cu. Hence, comparisons on the surface compositions of different samples were made on the basis of the ratios of pure intensities of the XPS peaks rather than the conventional way of reporting atomic percentages which is based on the assumption of a homogeneous distribution of elements in the analyzed volume [Fin10]. All XPS spectra were charge referenced with respect to the LMM Auger transition line for Cu<sup>+</sup> at 570 eV.

### **3.4 Experimental Logistics**

In order to meet the objectives laid down for this project, the following experimental milestones were set. All experiments enlisted in sections 3.4.1 through 3.4.3 were carried out at room temperature whereas those considered in sections 3.4.4 and 3.4.5 were conducted at 80°C.

### 3.4.1 Process Control

- Obtained a reproducible Cu surface
    - a) Optimized the process parameters involved in obtaining a clean Cu surface:
      - i. Concentration and composition of the cleaning acid solution
      - ii. Time of acid cleaning treatment
    - b) Monitored the stability of the acid roughened Cu surface
    - c) Ascertained the reproducibility of the resultant Cu surface
  
  - Determined the characteristic fingerprint for each of the individual components
    - a) Identified the characteristic XPS peak features for
      - i.  $\text{Cu}^0, \text{Cu}^+, \text{and Cu}^{++}$
      - ii. O associated to  $\text{Cu}_2\text{O}, \text{CuO}, \text{and H}_2\text{O}$
    - b) Identified the characteristic mass (m/z) peaks in ToF-SIMS for
      - i. PAO-2
      - ii. Bis(2-ethylhexyl) phthalate
      - iii. TTAH
  
  - Ensured detection of TTAH adsorption film formed on Cu in XPS and ToF-SIMS
- Analyzed the surface of a Cu sample having TTAH adsorbed on it by means of immersing a cleaned Cu coupon in an oil solution – PAO-2 + 0.01 wt.% TTAH

for 3600 s (1 h) and ascertained that the resultant adsorbed layer can be detected in both the instruments. The detection of the same was ensured by means of

- i. N 1s peak in XPS
- ii. TTA<sup>-</sup> (C<sub>7</sub>H<sub>6</sub>N<sub>3</sub><sup>-</sup>) molecular ion mass peak at m/z = 132 in ToF-SIMS negative mode

- Monitored the chemical stability of the TTAH adsorption film

Left the Cu sample with TTAH adsorption layer obtained in the previous step in clean atmosphere for  $\approx$  120 h prior to repeating the XPS and ToF-SIMS characterization on the same sample

- Determined the primary ion beam for the most effective results in ToF-SIMS

There are three different primary ion beams available in the ToF-SIMS installed in our facility – Au<sup>+</sup>, Au<sub>3</sub><sup>+</sup>, and C<sub>60</sub><sup>+</sup> either of which may be employed to characterize sample surfaces. But the consistency and the nature of the resultant secondary ion spectra may vary for these three primary ion beams depending upon the chemical nature of the sample surfaces in consideration. Hence, experiments were done to determine the primary ion beam that maximized the detection of the larger fragments of secondary molecular ions relevant to the TTAH adsorption film formed on Cu.

### 3.4.2 Morphology of the TTAH adsorption film formed on Cu

- Resolved the adsorption film structure: ARXPS study

For this purpose, a Cu sample with TTAH adsorption film formed as a result of immersion in oil solution – PAO-2 + 0.01 wt.% TTAH for 24 h was considered. ARXPS was done with four different take-off-angles (TOA) – 5°, 20°, 45°, and 90°. It revealed depth-sensitive information on the distribution of the involved elements – N, Cu, O, and C in the adsorption film that was interpreted rationally to determine the structure of the adsorption film.

- Determined the adsorption film thickness: Tougaard analysis of XPS spectrum

Thickness of the organic over-layer formed on Cu was determined by means of Tougaard's method for XPS background analysis carried out on the survey spectrum of the same sample as in the previous step. This method takes into account the inelastic scattering of the photoelectrons and Auger electrons originating from the Cu substrate while traveling through the organic over-layer [Tou96], [Tou03]. This phenomenon manifests in the XPS spectra as the background signal on the higher binding energy (BE) sides of the Cu peaks. The survey scan needed to be performed at energy steps of 0.4 eV. This analysis also rendered an insight into the morphological continuity of the film.

- Resolved the adsorption film structure: ToF-SIMS study

This ToF-SIMS experiment, again, was carried out on a sample that was similarly processed as to the one used in the prior XPS experiment. Secondary ion mass spectra from the surface were acquired in the negative mode by means of  $\text{Au}^+$  primary ion beam with alternate sputtering intervals using the  $\text{C}_{60}^+$  ion beam. The ion guns were operated at conditions mentioned earlier in section 3.3. This rendered information on the depth-profile of various secondary molecular ions involved in the adsorption film each of which were characteristically associated with certain chemical component constituting the film. This information could again be interpreted rationally to determine the overall morphology of the adsorption film. This apart, secondary ion mapping in the imaging mode also revealed information on the spatial continuity of the film.

- Integrated results from ToF-SIMS and XPS

Based on the complimentary nature of information revealed by ToF-SIMS and XPS, the hence obtained results from both the instruments under the initiative of section 3.4.2 were integrated together to conclusively comment on the morphology of the TTAH adsorption film formed on Cu in oily medium.

### 3.4.3 Time dependent structural evolution of the TTAH adsorption film

- Prepared multiple time interrupted immersion test samples

To capture the different stages of growth of the TTAH adsorption film on Cu, ten different samples were prepared by immersing initially cleaned Cu coupons in the same oil solution – PAO-2 + 0.01 wt.% TTAH for variable lengths of time ranging from 1 s to  $6.048 \times 10^5$  s (1 week). Ten different immersion times were chosen for this study – 1 s, 60 s (1 min), 600 s (10 min), 1.2 Ks (20 min), 2.7 Ks (45 min), 5.4 Ks (1.5 h), 10.8 Ks (3 h), 21.6 Ks (6 h), 86.4 Ks (24 h), 0.6 Ms (1 week). All these samples were immediately characterized upon preparation.

- Characterized the time interrupted immersion test samples

The surfaces of the above ten samples were characterized using XPS and ToF-SIMS with the objective of investigating the chemical modifications taking place at the surface with changing immersion time. More precisely, the present study aimed to resolve the time-dependent interfacial interactions involved amongst the various structural layers of the surface film. The experimental basis for this study was to compare the compositional changes at the surface with increasing immersion time. In XPS, this was accomplished by monitoring the atomic concentrations and/or peak integrals of different elements – N, and O with respect to Cu. In ToF-SIMS, the same was done by comparing the relative ratios of the peak integrals of various characteristic secondary ion mass peaks normalized to that of Cu ion peak. Integrating the XPS and ToF-SIMS results from all of these

ten samples, a plausible model for the growth mechanism of the TTAH adsorption film on Cu was suggested. ARXPS and ToF-SIMS depth-profiling experiments were carried out for selective samples only so as to ascertain that the structural layout of the adsorption film was consistent with increasing immersion time.

#### *3.4.4 Effect of sulfide corrosive agents*

- Optimized the process parameters:
  - i. Weight % S to be added to the oil solution
  - ii. Time scale for running hot immersion tests
  
- Studied the synergistic effect of active sulfur on TTAH adsorption film formation

In this initiative, surface characterization experiments were exclusively carried out using XPS on a number of different samples prepared under different conditions, respectively. Each of these tests aimed at revealing separate pieces of critical information pertaining to the chemical interactions taking place on the Cu surface at a molecular level. The testing conditions have been enlisted below. In all these cases, the sec-butyl disulfide containing oil solution was preheated at 80°C for 24 h prior to immersing the Cu coupons in order to ascertain that a non-limiting amount of active sulfur was already available in the oil solution to react with the Cu surface immediately upon immersion. Under the present initiative, a freshly cleaned Cu coupon was immediately immersed in

- i. PAO-2 Oil + 0.01 wt. % TTAH + 0.72 wt.% S for 60 s (1 min):  
Revealed information on the relative interaction kinetics of TTAH and active S with the Cu surface in the initial stage
- ii. PAO-2 Oil + 0.01 wt. % TTAH + 0.72 wt. % S for  $6.048 \times 10^5$  s (1 week): Revealed the degree of effectiveness of TTAH in protecting Cu from sulfide corrosion. ARXPS revealed the depth-sensitive distribution of S atoms in the surface film which was interpreted in terms of Cu sulfide corrosion mechanism in the presence of TTAH
- iii. PAO-2 oil + 0.01 wt. % TTAH for 3600 s (1 h) at room temperature and then immediately immersed in PAO-2 oil + 0.72 wt. % S at 80°C for  $6.048 \times 10^5$  s (1 week): Resolved whether the protective TTAH adsorption film formed on Cu is static in nature or otherwise. This piece of information complimented with more optimization experiments in perspective to a particular application can be utilized by industries to minimize the level of corrosion inhibitor concentration to be maintained at all times in the medium.
- iv. PAO-2 oil + 0.01 wt. % TTAH for 3600 s (1 h) at room temperature and then immediately immersed in PAO-2 oil + 0.01 wt. % TTAH + 0.72 wt. % S for  $6.048 \times 10^5$  s (1 week): Justified if a pre-coat of the TTAH adsorption film at room temperature more effective in protecting the Cu surface from sulfide corrosion at elevated

temperatures. More importantly, this experiment also shed light on the rate controlling step in the TTAH film growth mechanism.

#### *3.4.5 O<sup>18</sup> isotope tracer study in ToF-SIMS to understand the role of surface oxide*

- In this piece work, an attempt was made to follow the oxygen present initially in the surface copper oxide and hence, better understand its role in the surface film formation. For this purpose, a freshly cleaned Cu coupon was intentionally oxidized in O<sup>18</sup> atmosphere at 80°C for 1 h. It was then immersed in PAO-2 oil + 0.01 wt. % TTAH + 0.72 wt. % S at 80°C for  $6.048 \times 10^5$  s (1 week). The resultant sample surface was exclusively characterized using ToF-SIMS to obtain a depth-profile of various secondary molecular ions constituting of O<sup>18</sup>. This illustrated the ongoing surface reactions involving the surface oxide.

The results for all the above experiments are presented in the following chapter. From a scientific standpoint, integrating these results allows a comprehensive mechanistic description of TTAH adsorption on Cu in oily medium, its growth with time, and the synergistic effect of active sulfur on the protective film which are discussed in chapter 5.

## Chapter 4

### Results

This chapter presents all the relevant experimental results obtained in the course of this PhD project. The results are laid out in five separate categories based on the logistics of their experimental design, which is discussed in section 3.4. Section 4.1 deals with the process control results, whereas sections 4.2 and 4.3 focus on the results obtained towards determining the structure of the TTAH adsorption film formed on Cu in PAO-2 oil and its temporal growth, respectively. Section 4.4 considers the results on Cu corrosion in sulfide solution and, finally, section 4.5 lists the O<sup>18</sup> isotope tracer study results obtained towards understanding the role of surface oxide in the TTAH adsorption process.

#### 4.1 Process Control

##### *4.1.1 Cu Surface Preparation*

The as-received Cu foil was characterized for its surface composition using XPS, the result for which is shown in Fig. 4.1. As suggested by the survey spectrum, the surface was covered with a thick layer of some unknown carbonaceous material which might be an intentional coating done by Sigma Aldrich to protect the Cu surface or possibly be residual oil on the surface from mechanical processing of the foil. In order to conduct the corrosion inhibitor adsorption study on Cu, it was important to obtain a clean Cu surface with consistent composition. Understanding the adsorption behavior of TTAH on both native oxide (Cu<sub>2</sub>O) and pristine Cu metal (Cu<sup>0</sup>) is of scientific interest. It has practical

significance as well because in applications corrosion inhibitors are used in both mechanically static and dynamic systems. In the former case, the surface usually has a substantial native oxide layer, whereas in the latter case, fresh Cu metal is continuously exposed at the surface. The primary focus of the present work was set at understanding the TTAH adsorption behavior on pristine metallic Cu surface.

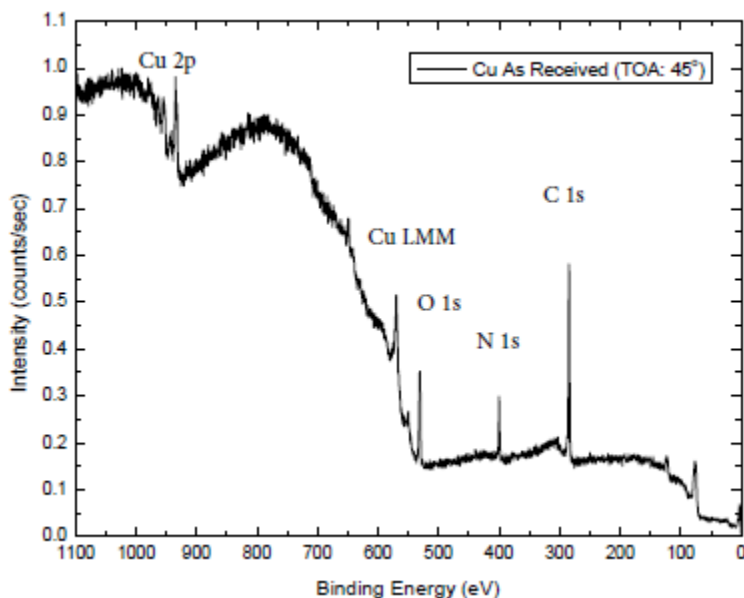


Fig. 4.1: XPS survey spectrum of as-received Cu foil.

Following suggestions from the literature <sup>[Xue91]</sup>, to obtain a chemically stable pristine Cu surface, the as-received coupon was cleaned using a 2M HNO<sub>3</sub> for 300 s (5 min). XPS survey spectrum and the chemical composition of the resultant surface is shown in Fig. 4.2 (a). It suggests the presence of a uniform Cu<sub>2</sub>O layer throughout the analyzed volume based on the Cu to O atomic ratio of 2.1. The carbon present on the surface was associated to airborne molecular contamination (AMC). The surface was chemically stable with time and even after exposure to clean atmosphere for 4.32 x 10<sup>5</sup> s (5 days) the

surface composition was practically unaltered, as shown in Fig. 4.2 (b). The Cu to O atomic ratio had only changed to 2.0. Increasing the acid-treatment time did not help to obtain an oxide free Cu surface and as a matter of fact, it deteriorated the surface condition by forming nitrates on the surface.

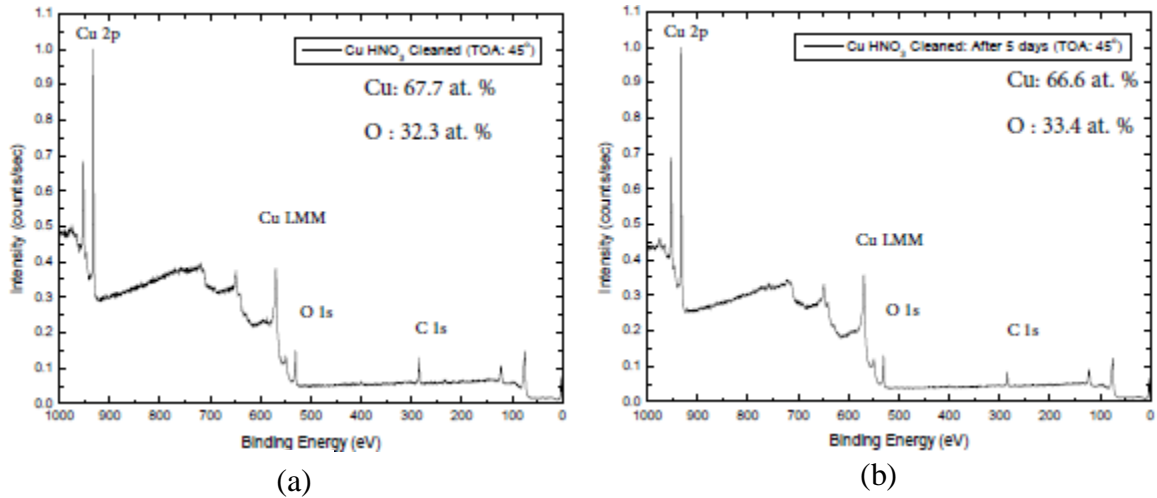


Fig. 4.2: XPS survey spectra of 2M HNO<sub>3</sub>-treated Cu coupon.  
 (a) Analyzed immediately. (b) Analyzed after 5 days.

In further efforts to obtain a pristine Cu surface, the as-received Cu coupon was treated with an equi-volume acid mixture of 2M HNO<sub>3</sub> + H<sub>3</sub>PO<sub>4</sub> + CH<sub>3</sub>COOH (NPA) for 300 s (5 min), which proved to be successful. The XPS survey spectrum and the composition of the hence obtained surface is shown in Fig. 4.3. The O content of the surface was 1 at. %. It is estimated that in XPS, a Cu surface with only the first layer of unit cells converted to Cu<sub>2</sub>O should result in an O content of  $\approx 8$  at. %. Hence, it was concluded that the Cu surface was in pristine condition, i.e., zero oxidation state. This surface was found to be reproducible. In order to study the chemical stability of this surface, an acid-roughened Cu surface in pristine metallic condition was exposed to clean atmosphere for 900 s

(15 min) and then characterized again. The surface composition remained unaltered. This is in accord to the suggestions made in the literature that acid-roughened sample surfaces are chemically more stable than mechanically polished samples.

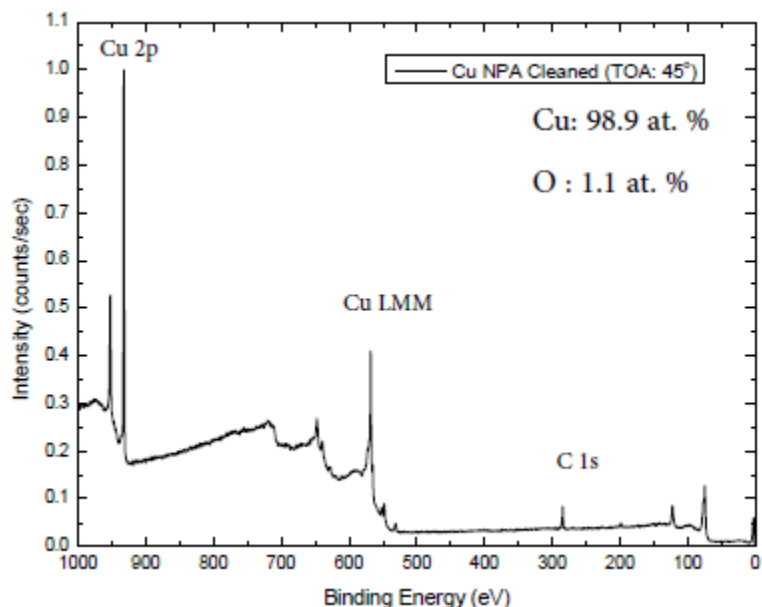


Fig. 4.3: XPS survey spectrum of 2M NPA-treated Cu coupon.

#### 4.1.2 Fingerprints of Individual Components

It was necessary to distinctly identify each of the individual chemical entities that might be present on the surface layer in the course of this project for the effective characterization of the adsorption films formed on Cu surface. In this endeavor, the first assignment was to differentiate between Cu, Cu<sub>2</sub>O, and CuO, more importantly in XPS. Pristine Cu and Cu<sub>2</sub>O were obtained in the same fashion as discussed in the prior section. To obtain CuO, a Cu coupon with pristine surfaces was heated in a tube-furnace at 600°C for 1 h. All the three samples were subsequently characterized in XPS. The survey

spectra for uniform Cu and Cu<sub>2</sub>O are shown in Fig. 4.2 and Fig. 4.3, respectively, whereas the one for homogenous CuO is shown in Fig. 4.4. The Cu to O atomic ratio in each of these cases suggests Cu, Cu<sub>2</sub>O, and CuO, respectively.

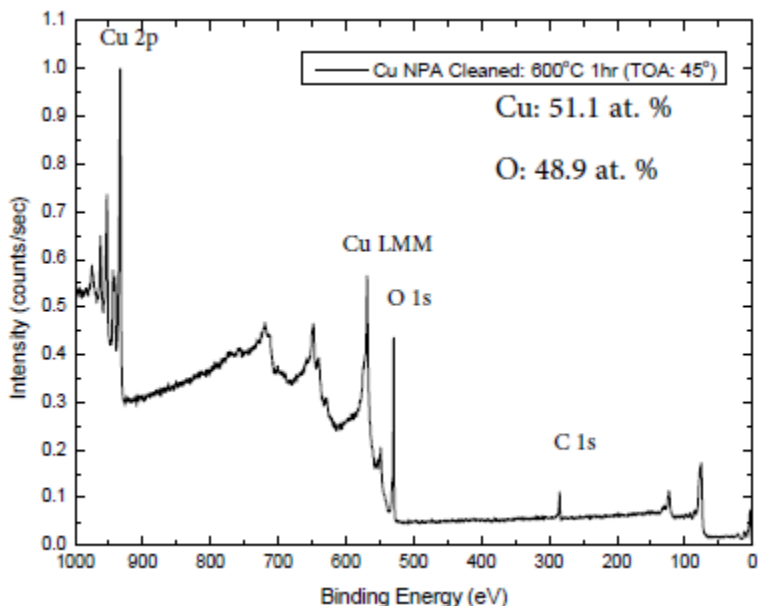
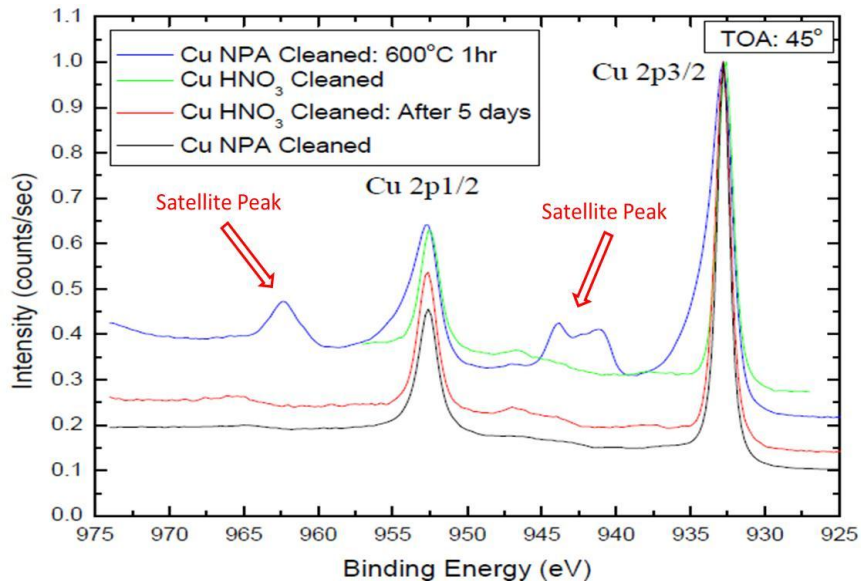


Fig. 4.4: XPS survey spectrum of CuO.

Cu associated with different chemical species – pristine metal, Cu<sub>2</sub>O, and CuO, was differentiated on the basis of Cu 2p and Cu L<sub>3</sub>M<sub>4,5</sub>M<sub>4,5</sub> peak shape and position analysis as illustrated in Fig. 4.5. The former consists of two photo-electron peaks separated by  $\approx$  19.8 eV corresponding to 2p<sub>3/2</sub> and 2p<sub>1/2</sub> non-degenerate orbitals. For pristine Cu, the 2p<sub>3/2</sub> and 2p<sub>1/2</sub> peaks appeared at 932.8 eV and 952.6 eV, respectively. The Cu L<sub>3</sub>M<sub>4,5</sub>M<sub>4,5</sub> peak, often referred to as the Cu L<sub>3</sub>M<sub>4,5</sub>M<sub>4,5</sub> line or simply as the Cu LMM line, is in reality a convolution of four different Auger peaks corresponding to four energetically very closely spaced Auger transitions - L<sub>3</sub>M<sub>4</sub>M<sub>4</sub>, L<sub>3</sub>M<sub>4</sub>M<sub>5</sub>, L<sub>3</sub>M<sub>5</sub>M<sub>4</sub>, and L<sub>3</sub>M<sub>5</sub>M<sub>5</sub>. The binding energy (BE) positions of the Cu 2p peaks were identical for all the three forms of Cu – pristine metal, Cu<sub>2</sub>O, and CuO. In fact, peak width broadening was the only

noticeable difference in those peaks in the increasing order of Cu oxidation state. But as shown in Fig. 4.5 (a), for Cu associated to CuO both Cu 2p<sub>3/2</sub> and 2p<sub>1/2</sub> peaks had smaller satellite peaks at ≈ 10 eV separations to the higher BE side of the main peaks. These satellite peaks are caused by phonon excitation behavior in the CuO crystals and is a crystal-structure sensitive phenomenon. This feature is completely missing in the case of Cu<sub>2</sub>O and Cu. Hence, the presence of CuO was distinctly identified by the satellite pre-peaks to the Cu 2p peaks. Cu associated to Cu<sub>2</sub>O and pristine metal (Cu<sup>0</sup>) were differentiated on the basis of the Cu L<sub>3</sub>M<sub>4,5</sub>M<sub>4,5</sub> peak position. For Cu<sup>0</sup>, the corresponding Auger electrons had predominantly a characteristic kinetic energy (KE) of 918.6 eV, whereas the same for Cu<sub>2</sub>O were detected at KE of 916.6 eV. Converting to the BE scale, the L<sub>3</sub>M<sub>4,5</sub>M<sub>4,5</sub> peaks for Cu in pristine metallic condition and Cu<sub>2</sub>O appeared predominantly at 568 eV and 570 eV, respectively, as shown in Fig. 4.5 (b).



(a)

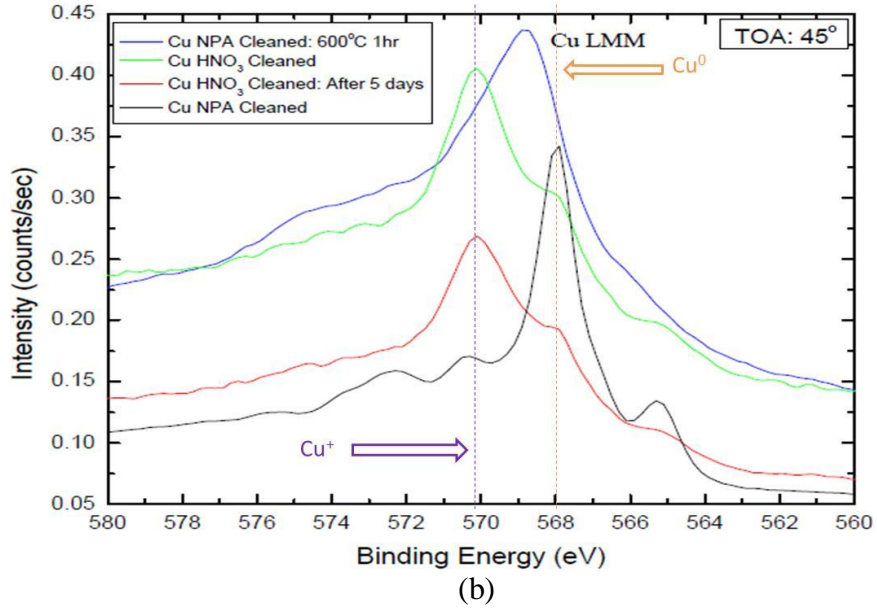


Fig. 4.5: Comparison of (a) Cu 2p (b) Cu L<sub>3</sub>M<sub>4,5</sub>M<sub>4,5</sub> peaks acquired on Cu surfaces treated in different ways.

Oxygen associated to Cu<sub>2</sub>O and CuO were also differentiated based on the BE shift in the O 1s peak. This is illustrated in Fig. 4.6. The O 1s peak for CuO was detected at BE of 529.7 eV, whereas for Cu<sub>2</sub>O the peak shifted by 1 eV to the higher binding energy side to a value of 530.7 eV.

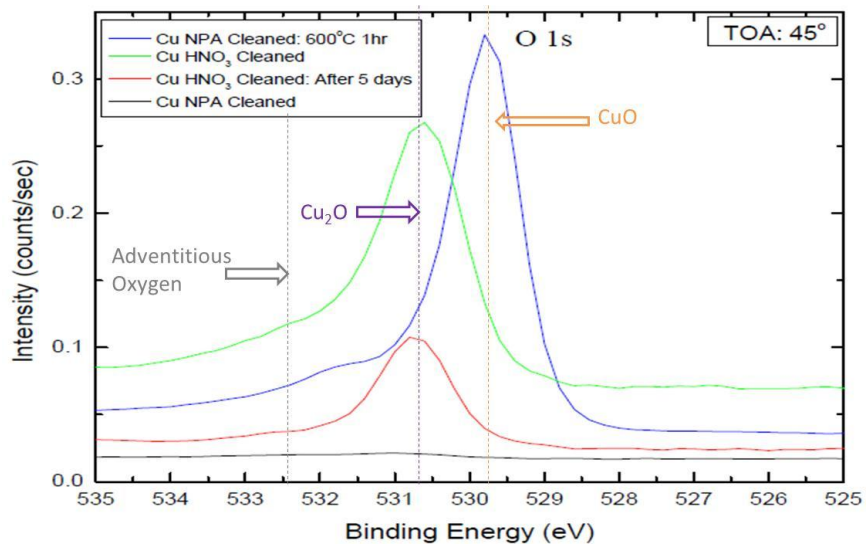


Fig. 4.6: Comparison of O 1s peak acquired on Cu surfaces treated in different ways.

It was of considerable interest to figure out whether ToF-SIMS can differentiate between the three states of Cu that were in consideration above, though not directly useful for the objectives of the present project. For this purpose, all the three reference samples as used for the XPS study were characterized by ToF-SIMS using all the three available primary-ion (PI) beams –  $\text{Au}^+$ ,  $\text{Au}_3^+$ , and  $\text{C}_{60}^+$  in the positive secondary-ion (SI) detection mode. For each case, the peak integrals of certain characteristic SI mass peaks normalized to the  $\text{Cu}^+$  peak were recorded. Comparative bar-graphs showing these results are plotted in Fig. 4.7, where (a), (b), and (c) display the results for  $\text{Au}_3^+$ ,  $\text{Au}^+$ , and  $\text{C}_{60}^+$ , respectively. The results suggested that all the three PI beams were able to differentiate between the three chemical forms of Cu. Irrespective of the PI beam, the differences amongst the three forms of Cu were most visible for larger mass fragments –  $\text{Cu}_2^+$ ,  $\text{Cu}_2\text{H}^+$ ,  $\text{Cu}_3^+$ , and  $\text{Cu}_3\text{H}^+$ , but  $\text{Au}^+$  and  $\text{C}_{60}^+$  were more effective over  $\text{Au}_3^+$ . For an  $\text{Au}^+$  PI beam, the SI yields of these larger fragments were significantly higher for  $\text{Cu}_2\text{O}$  followed by Cu and CuO in that order. On the other hand, for a  $\text{C}_{60}^+$  PI beam, the SI yields for the same fragments were appreciably higher for Cu followed by  $\text{Cu}_2\text{O}$  and CuO in respective order. However, considering relative-yield based statistical-reliability,  $\text{C}_{60}^+$  was concluded to be the most reliable PI beam to differentiate between the three forms of Cu in consideration.

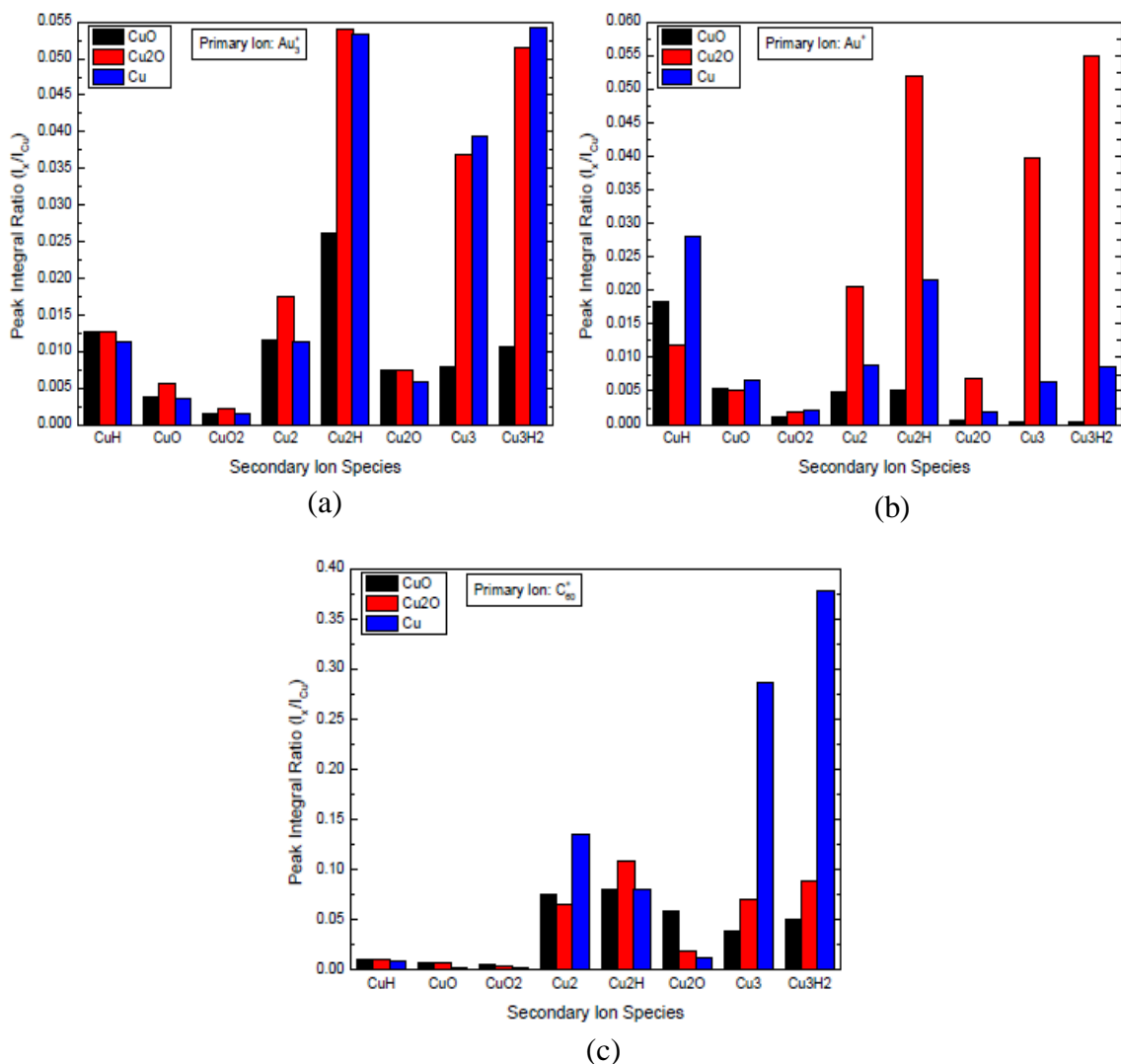
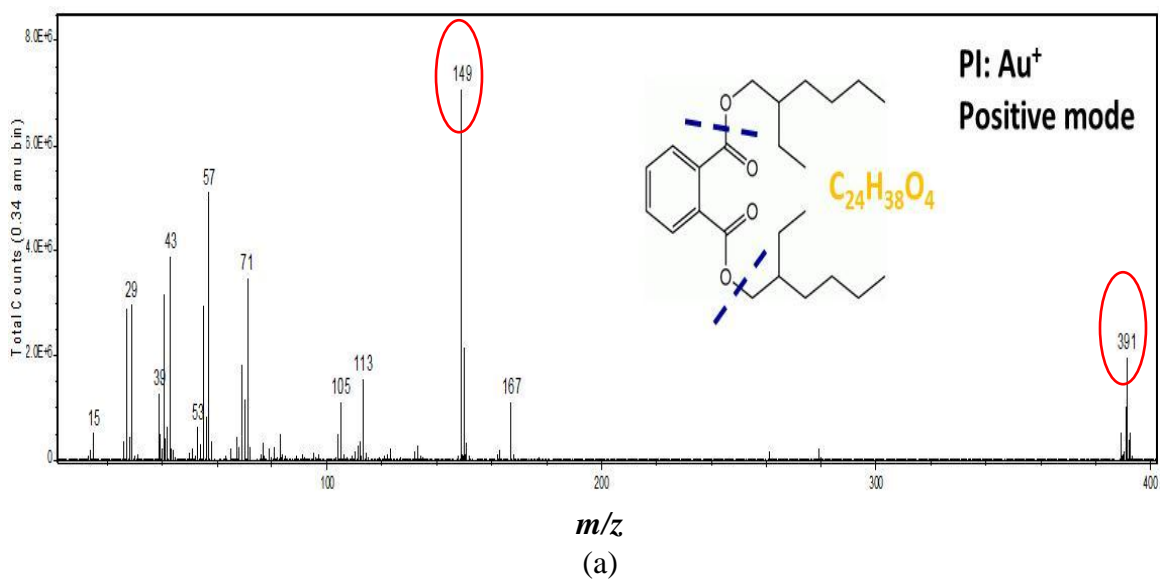


Fig. 4.7: Bar-graphs showing characteristic secondary-ion yield from Cu, Cu<sub>2</sub>O, and CuO for (a) Au<sub>3</sub><sup>+</sup> (b) Au<sup>+</sup> (c) C<sub>60</sub><sup>+</sup> primary ion beams.

The second assignment was to fingerprint bis(2-ethylhexyl) phthalate which was used to pre-dissolve the corrosion inhibitor tolyltriazole (TTAH) owing to its limited solubility in PAO-2 oil directly. This was carried out in ToF-SIMS using both Au<sup>+</sup> and C<sub>60</sub><sup>+</sup> PI beams in positive and negative SI detection mode. Irrespective of the PI beam, the positive ion detection mode was able to fingerprint the compound better. Two characteristic mass peaks were identified in this mode – ( $m/z$ ) = 149 corresponding to C<sub>8</sub>H<sub>5</sub>O<sub>3</sub><sup>+</sup>, and ( $m/z$ ) = 391

corresponding to the intact molecular ion  $C_{24}H_{39}O_4^+$ . However, the yield of the intact molecular ion was significantly higher for  $Au^+$  PI beam as compared to that of  $C_{60}^+$  PI beam. Fig 4.8 (a) displays the positive SI mass spectrum for bis(2-ethylhexyl) phthalate deposited on a Cu coupon acquired by the  $Au^+$  PI beam in the relevant  $m/z$  scale. Fig. 4.8 (b) is a bar-graph comparing the relative yields of various positive SI mass fragments normalized to the  $C_8H_5O_3^+$  yield in respective cases of the two PI beams. The  $Au^+$  PI beam was more effective in generating an even yield-distribution of mass fragments.



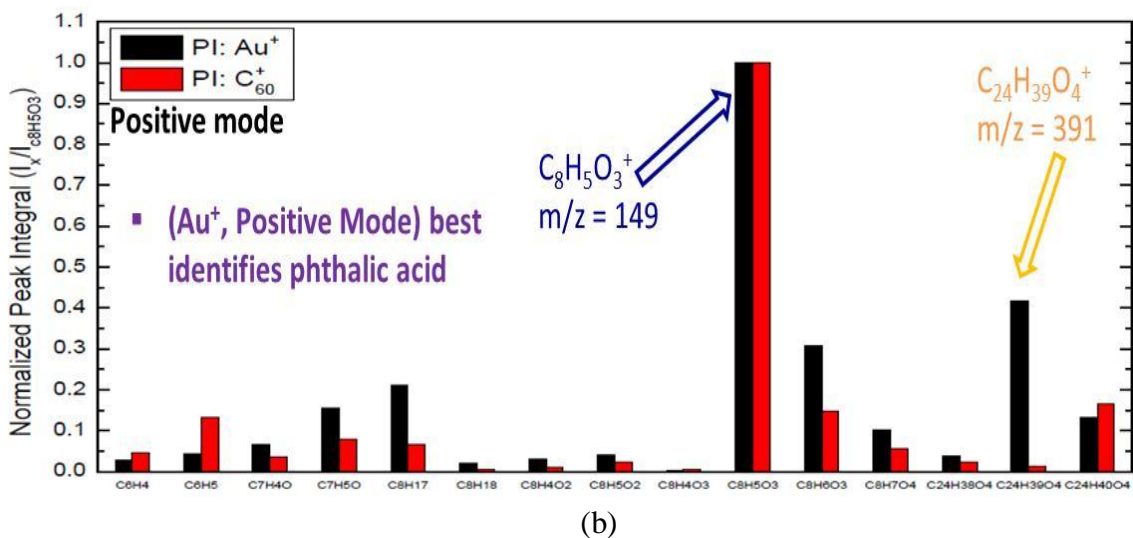


Fig. 4.8: (a) Positive ion mass spectrum for bis(2-ethylhexyl) phthalate acquired by Au<sup>+</sup> PI beam (b) Comparison of secondary ion yield distribution acquired by Au<sup>+</sup> and C<sub>60</sub><sup>+</sup> PI beams normalized to C<sub>8</sub>H<sub>5</sub>O<sub>3</sub><sup>+</sup> yield in respective cases.

PAO-2 oil was then characterized using ToF-SIMS in exactly the same fashion as that of bis(2-ethylhexyl) phthalate. The results for the same are shown in Fig. 4.9. Fig. 4.9 (a) shows the positive SI mass spectrum for PAO-2 oil deposited on a Cu coupon acquired by the Au<sup>+</sup> PI beam. The mass spectrum revealed that at lower  $m/z$ , predominant mass peaks appeared in pairs that were separated by 12 a.m.u corresponding to the mass of a C atom. Within each pair, the two mass peaks were separated from each other by 2 a.m.u corresponding to the mass of two H atoms. However, at higher  $m/z$ , this pattern broadened out due to a larger concentration of H atoms in the molecular ion fragments. This led to a higher probability of forming larger number of SI fragments differing by 1 a.m.u. Fig. 4.9 (b) shows a comparison of the relative yields of various SI fragments acquired with Au<sup>+</sup> and C<sub>60</sub><sup>+</sup> PI beams normalized to the C<sub>3</sub>H<sub>7</sub><sup>+</sup> yield in respective cases. As in the case of bis(2-ethylhexyl) phthalate, the Au<sup>+</sup> PI beam was able to generate a more uniform yield-distribution of mass fragments.

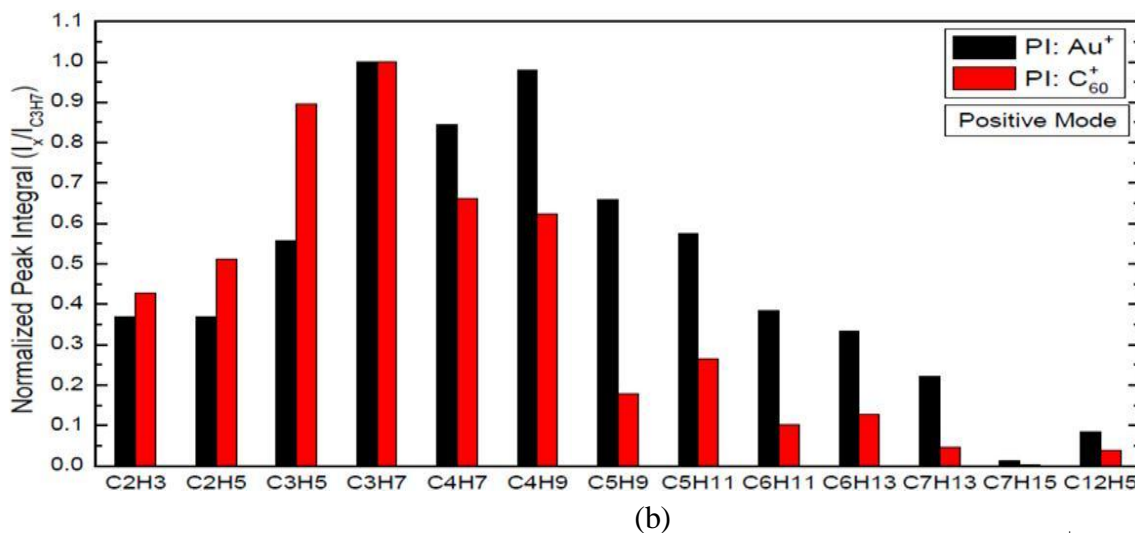
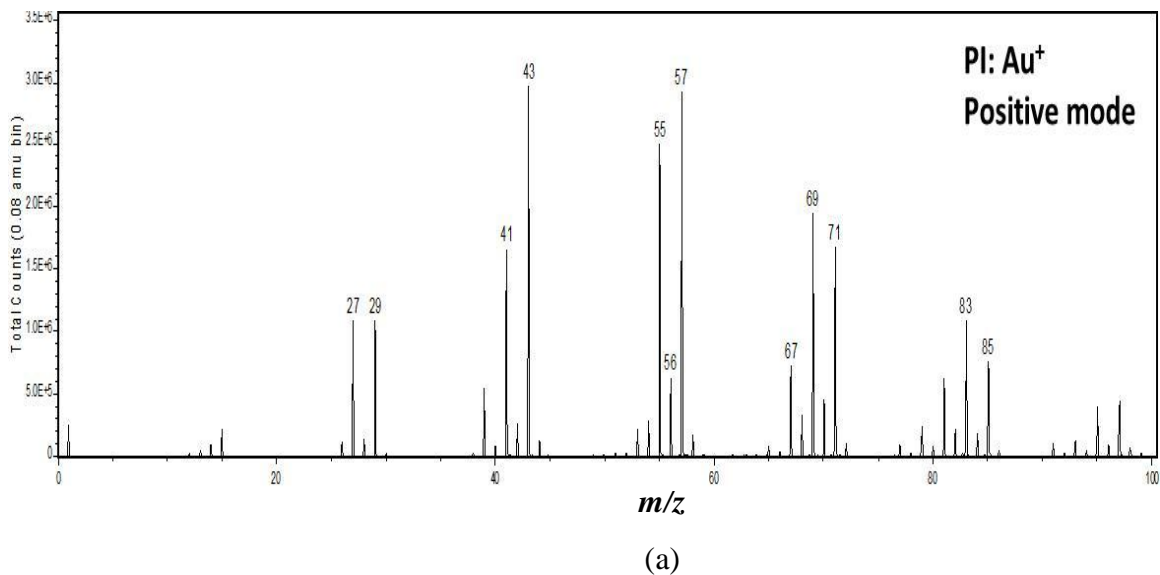


Fig. 4.9: (a) Positive secondary ion mass spectrum for PAO-2 oil acquired by Au<sup>+</sup> PI beam (b) Comparison of secondary ion yield distribution acquired by Au<sup>+</sup> and C<sub>60</sub><sup>+</sup> PI beams normalized to C<sub>3</sub>H<sub>7</sub><sup>+</sup> yield in respective cases.

Absence of SI mass peaks involving any element other than C, H, and O in ToF-SIMS characterization of the PAO-2 oil illustrated that the oil is an extremely pure form of hydrocarbon. Moreover, in the positive SI detection mode, there were no significant SI mass peaks of the type C<sub>x</sub>H<sub>y</sub>O<sub>z</sub>, which suggested that the oil was strictly of the form C<sub>x</sub>H<sub>y</sub> with no apparent tendency to oxidize under the experimental conditions. Bis(2-

ethylhexyl) phthalate and PAO-2 oil could not be directly characterized in XPS owing to its delicate UHV (ultra-high-vacuum) system. An attempt was made, but due to relatively high vapor pressures of these compounds the vacuum of the XPS was broken.

#### *4.1.3 Adhesion of PAO-2 Oil and Bis(2-ethylhexyl) phthalate on Pristine Cu Surface*

To study the adsorption behavior of TTAH on pristine Cu surface, it was important to ascertain if the other two components present in the system – bis(2-ethylhexyl) phthalate, and the oil itself, had any adhesive tendency towards the metal surface that could lead to a competitive adsorption process. For this purpose, NPA cleaned Cu coupons resulting in pristine surfaces were immersed in PAO-2 oil and bis(2-ethylhexyl) phthalate, respectively, without any additives for 3600 s (1 h). Subsequently, these samples were cleaned in the standardized process using toluene followed by XPS surface characterization. The results are shown in Fig. 4.10 and Fig. 4.11 for PAO-2 oil and bis(2-ethylhexyl) phthalate immersed samples, respectively. In either case, there was no carbon pick up, which shows that neither of the organic solvents had any adhesive affinity to the Cu surface. This conclusion is supported by the ToF-SIMS results presented in Fig. 4.8, and Fig. 4.9 of the previous section. For the corresponding ToF-SIMS experiments, even though both the organic solvents were deposited on Cu surfaces respectively, no secondary ion mass peaks of the types  $\text{Cu}_n\text{C}_x\text{H}_y$  or  $\text{Cu}_n\text{C}_x\text{H}_y\text{O}_z$  were detected. This supports the fact that both of these organic solvents in consideration do not form any kind of adsorptive bond with the Cu surface.

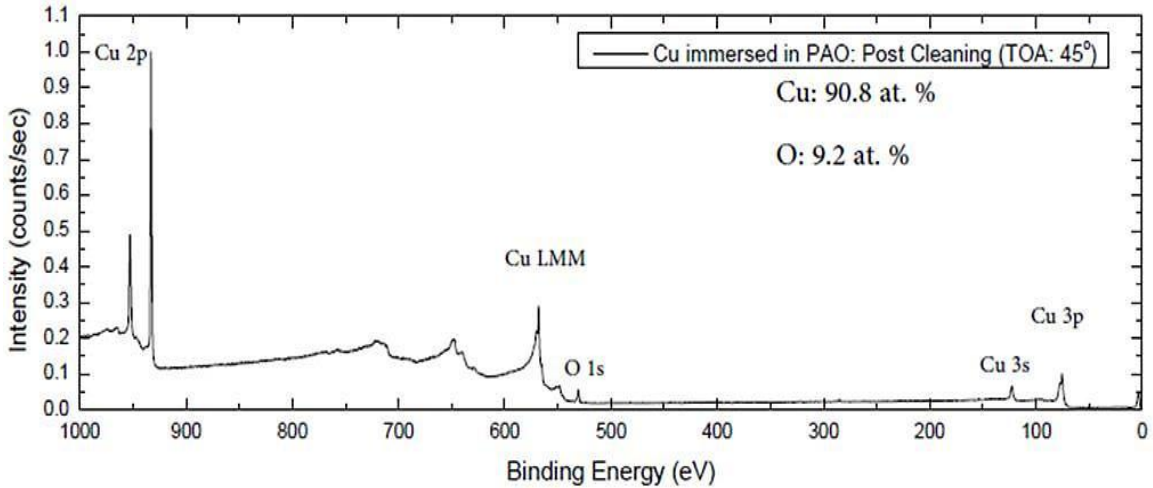


Fig. 4.10: XPS survey spectrum of Cu surface after being immersed in PAO-2 oil for 3600 s (1 h).

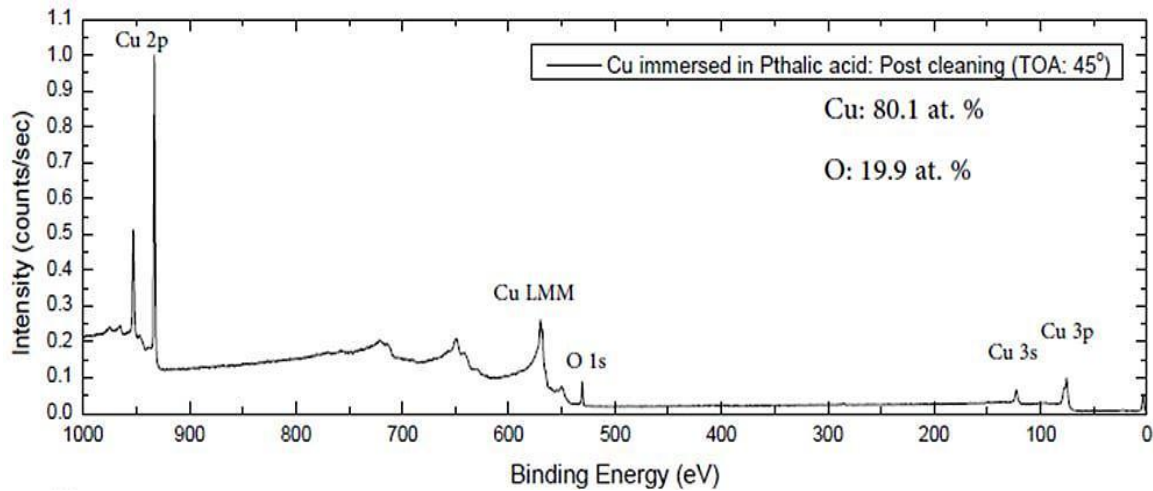


Fig. 4.11: XPS survey spectrum of Cu surface after being immersed in bis(2-ethylhexyl) phthalate for 3600 s (1 h).

As suggested by the above XPS results, both the organic solvents appeared to oxidize the Cu surface. The Cu coupons had undergone partial oxidation in the analyzed volume, the extent of oxidation being more severe in the phthalate as compared to the oil. This is attributed to the sufficiently large amounts of dissolved oxygen in these solvents. In order to ascertain that the increase in oxygen at the surface was due to the oxidation of the Cu surface and to understand the chemical nature of the oxide being formed, the Cu 2p,

Cu  $L_{3M_{4,5}M_{4,5}}$  and O 1s peaks for both the cases were closely inspected, which are shown in Fig. 4.12 (a), (b), and (c), respectively. In either case, the Cu 2p peaks did not show any satellite pre-peaks confirming the fact that there was no formation of CuO. The O 1s peaks were detected at 530.7 eV establishing the formation of  $Cu_2O$ . The Cu  $L_{3M_{4,5}M_{4,5}}$  line confirmed the same. For the phthalate immersed sample, the intensity of the LMM peak at 570 eV (corresponding to  $Cu^+$  in  $Cu_2O$ ) relative to the peak at 568 eV (corresponding to  $Cu^0$ ) was far greater than that for a freshly cleaned Cu sample. The same was intermediate for the oil immersed sample.

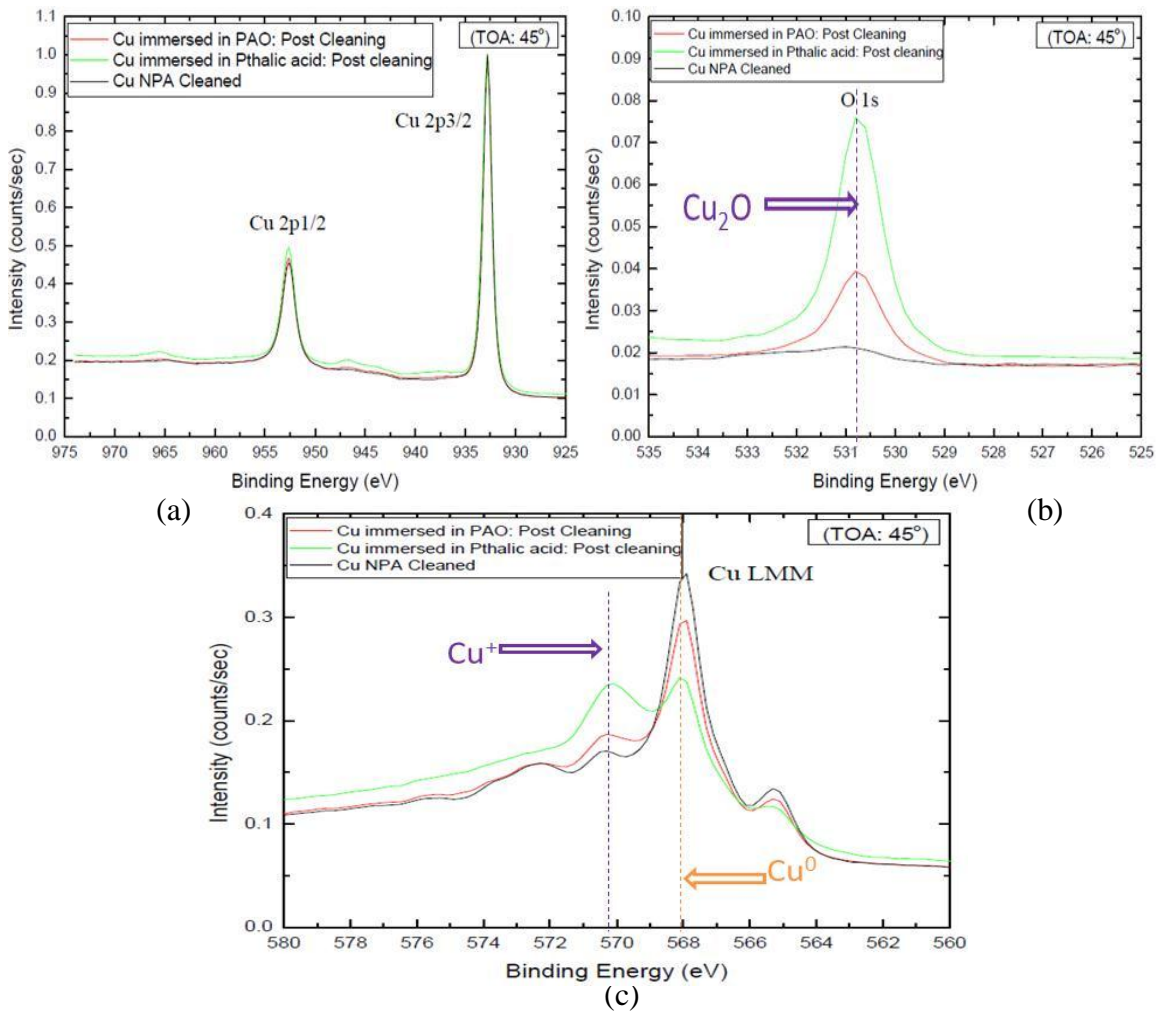


Fig. 4.12: (a) Cu 2p (b) O 1s (c) Cu  $L_{3M_{4,5}M_{4,5}}$  peaks for Cu samples immersed in PAO-2 oil and bis(2-ethylhexyl) phthalate.

## 4.2 Characterization of TTAH Adsorption Film on Cu

This section presents the ToF-SIMS and XPS results on the characterization of the TTAH adsorption film formed on Cu. The focus was to understand the chemical composition and the morphology of the surface film. For this purpose, Cu samples immersed in 0.01 wt. % (100 ppm) TTAH-containing oil solution for  $8.64 \times 10^4$  s (24 h) were primarily considered and in this entire section unless and until specified otherwise, the samples are to be assumed so. This section illustrates the presence of two distinct TTAH adsorption layers in the surface-film and also confirms the presence of a  $\text{Cu}_2\text{O}$  underlayer.

### 4.2.1 ToF-SIMS Characterization

The adsorption film was analyzed in ToF-SIMS using both  $\text{Au}^+$  and  $\text{C}_{60}^+$  PI beams. The corresponding negative SI mass spectra are shown in Fig. 4.13 (a) and (b), respectively. In both cases, nitrogen-containing fragments from TTAH were detected, which confirmed the formation and detection of the TTAH adsorption layer. However, the fragmentation pattern generated by the  $\text{Au}^+$  PI beam was found to be more suitable for the characterization of surfaces relevant to the present context. With the  $\text{Au}^+$  PI beam, high intensity peaks for intact molecular ions of TTAH, i.e.,  $\text{TTA}^-$ , and its complexes with Cu –  $[(\text{TTA})_2\text{Cu}]^-$ , and  $[(\text{TTA})_3\text{Cu}_2]^-$  were recorded, which was not the case for  $\text{C}_{60}^+$  PI beam. The detection of large fragments of TTAH-Cu complexes like these ascertained the formation of a polymeric adsorption film. For either of the PI beams, the positive SI spectrum did not reveal any information pertaining to the TTAH adsorption on Cu.

However, as shown in Fig. 4.14, with  $\text{Au}^+$  PI beam it did reveal the presence of PAO-2 oil and bis(2-ethylhexyl) phthalate in the surface film, although their intensities were insignificantly small. These peaks were observed to disappear on sputtering for 10 s with  $\text{C}_{60}^+$  ion beam over a  $500\ \mu\text{m} \times 500\ \mu\text{m}$  raster area. This can be explained on the basis that although, the oil and the phthalate do not have any adhesive tendency towards the Cu surface directly, but these organic molecules are likely to experience an attractive force from the organo-metallic adsorption film formed by TTAH on the Cu substrate and hence, adhere on top of the latter.

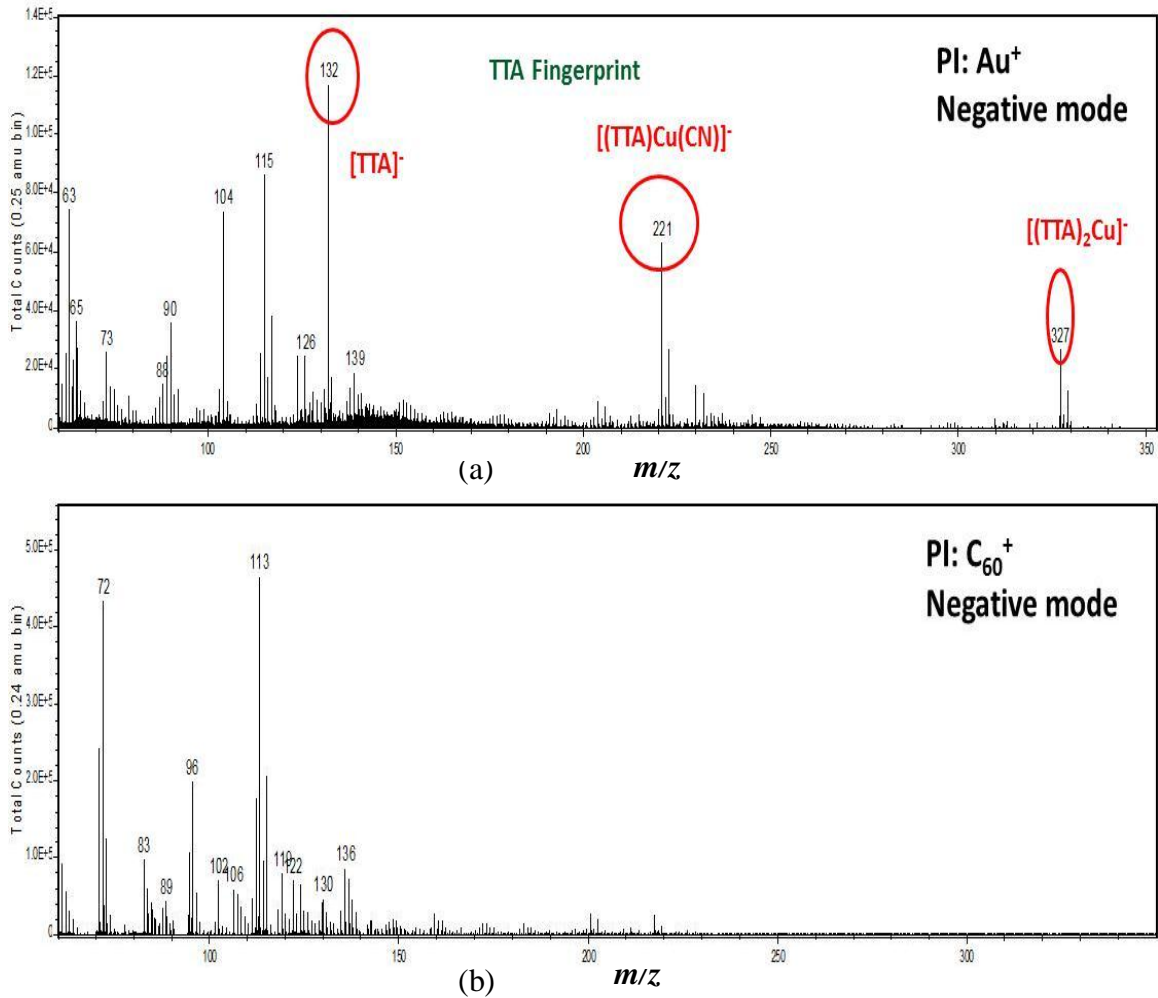


Fig. 4.13: Negative SI mass spectrum for a TTAH adsorption film on Cu formed upon immersion in oil solution for  $8.64 \times 10^4$  s (24 h) acquired by (a)  $\text{Au}^+$  (b)  $\text{C}_{60}^+$  PI beam.

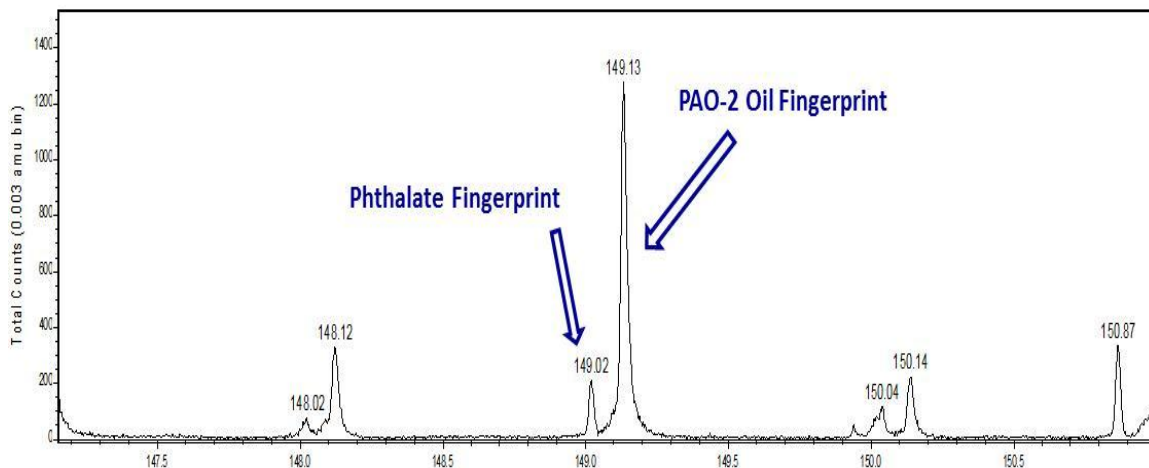


Fig. 4.14: Positive SI mass spectrum of TTAH adsorption film on Cu formed upon  $8.64 \times 10^4$  s (24 h) immersion in oil showing the presence of PAO-2 oil and bis(2-ethylhexyl) phthalate in the film.

From this point on, all the TOF-SIMS mass spectra reported in this chapter were exclusively analyzed by the  $\text{Au}^+$  PI beam, whereas sputtering was always done with the  $\text{C}_{60}^+$  beam. Table 4.1 lists some of the important negative SI fragments that were relevant to the characterization of the TTAH adsorption film formed on Cu.

Fragment Formula	Acronym	Mass: $m/z$ (a.m.u)
$\text{Cu}^-$		62.930
$\text{CuO}^-$		78.925
$\text{Cu}(\text{CHN})^-$		89.941
$\text{CuN}_2^-$		90.936
$\text{CuO}_2^-$		94.919
$\text{C}_7\text{H}_6\text{N}^-$		104.050
$\text{CuC}_2\text{N}_2^-$	$[\text{Cu}(\text{CN})_2]^-$	114.936
$\text{C}_7\text{H}_6\text{N}_3^-$	$[\text{TTA}]^-$	132.056
$\text{C}_8\text{H}_6\text{N}_4\text{Cu}^-$	$[\text{TTACu}(\text{CN})]^-$	220.989
$\text{C}_9\text{H}_6\text{N}_5\text{Cu}_2^-$	$[\text{TTACu}_2(\text{CN})_2]^-$	309.922
$\text{C}_{14}\text{H}_{12}\text{N}_6\text{Cu}^-$	$[\text{TTA}_2\text{Cu}]^-$	327.042
$\text{C}_{15}\text{H}_{12}\text{N}_7\text{Cu}_2^-$	$[\text{TTA}_2\text{Cu}_2(\text{CN})]^-$	415.975
$\text{C}_{21}\text{H}_{18}\text{N}_9\text{Cu}_2^-$	$[\text{TTA}_3\text{Cu}_2]^-$	522.028

Table 4.1: Negative SI fragments acquired by  $\text{Au}^+$  PI beam on  $8.64 \times 10^4$  s (24 h) immersed TTAH adsorption film on Cu.

Some of the SI fragments listed in Table 4.1 that are directly related to the TTAH adsorption film were imaged over a 250  $\mu\text{m}$  x 250  $\mu\text{m}$  area to examine the spatial (X-Y plane) continuity of the adsorption film. Selective images that were well representative of the general surface condition are shown in Fig. 4.15. As revealed by these images, the TTAH adsorption film was continuous and uniform over the X-Y plane. The diagonal striations observed in these images correspond to the initial Cu surface texture.

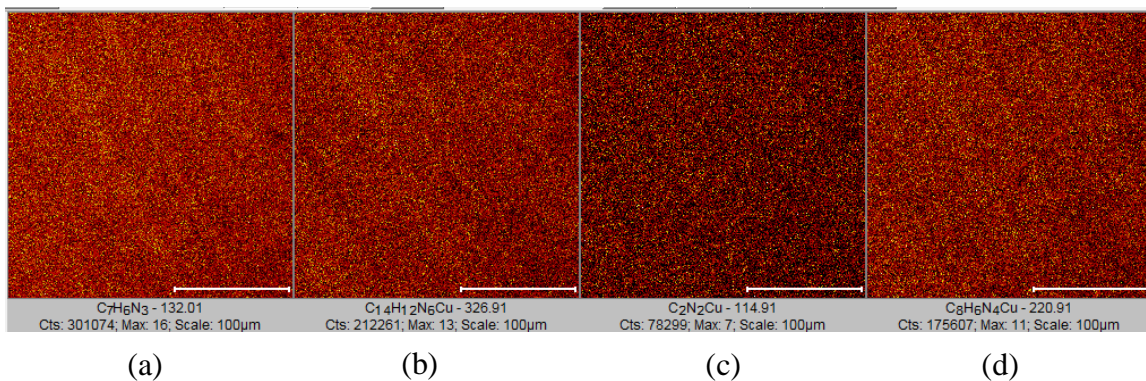


Fig. 4.15: Spatial mapping of (a)  $[\text{TTA}]^-$  (b)  $[(\text{TTA})_2\text{Cu}]^-$  (c)  $[\text{Cu}(\text{CN})_2]^-$  (d)  $[\text{TTACu}(\text{CN})]^-$

In the next undertaking, a depth-profile analysis was carried out in ToF-SIMS with the objective to understand the internal structure of the surface film. Peak integrals of the relevant SI fragments were normalized to that of the Cu peak and subsequently plotted against sputtering time. Depth-profile plots for selective SI fragments are shown in Fig. 4.16. Note, the profiles for  $[\text{TTA}]^-$ , and  $[(\text{TTA})_2\text{Cu}]^-$  differ from those of  $[\text{Cu}(\text{CHN})]^-$  and  $[\text{Cu}(\text{CN})_2]^-$ . The normalized peak integrals for the former set of ions decline monotonously with sputtering time to reach an asymptotic value of 0. The decline is rapid in the first 30 s of sputtering, beyond which, it slows down to finally reach its asymptotic value at  $\approx 200$  s, beyond which, the peaks practically disappear. However, for the latter set of ions –  $[\text{Cu}(\text{CHN})]^-$  and  $[\text{Cu}(\text{CN})_2]^-$ , the normalized peak integrals initially decrease

with sputtering time up to  $\approx 75$  s, beyond which, an increase is observed reaching a maximum at  $\approx 360$  s before decaying to lower values.

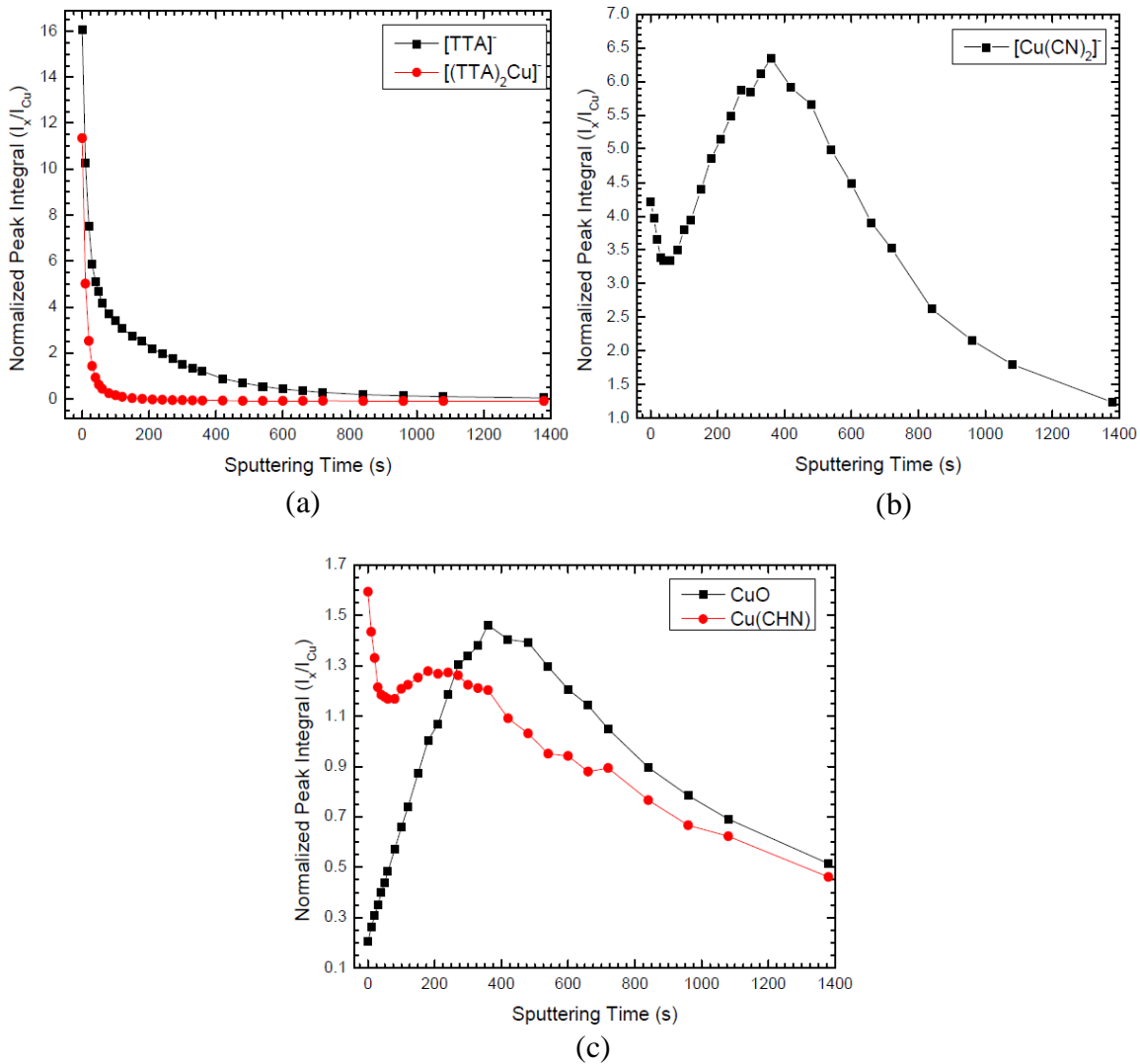
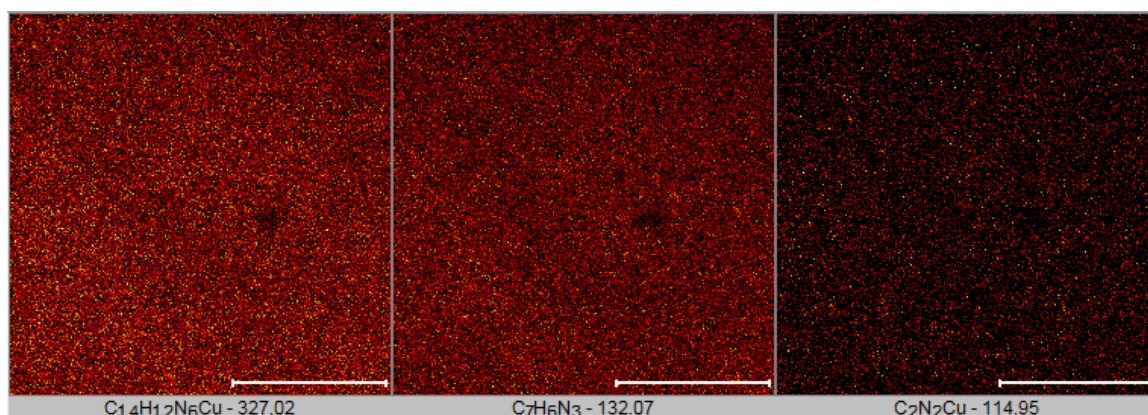


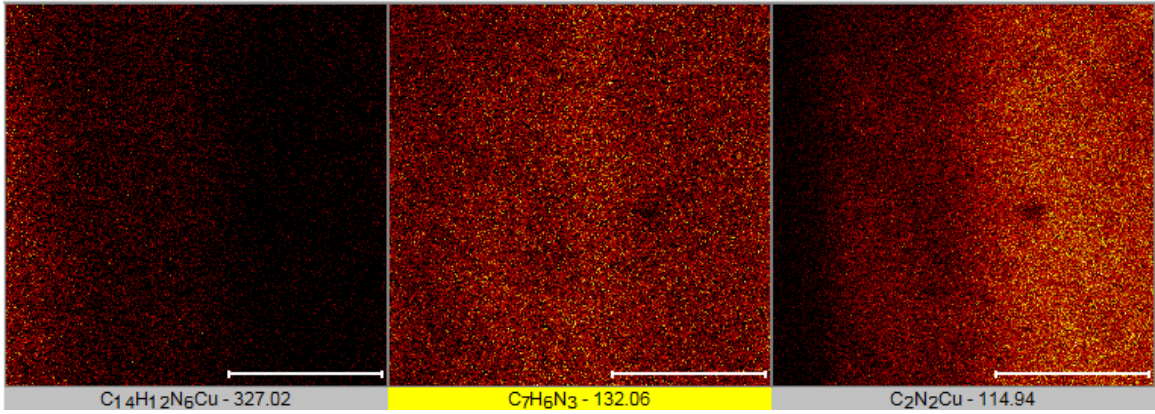
Fig. 4.16: Sputter depth-profiles for SI fragments relevant to TTAH adsorption film formed upon  $8.64 \times 10^4$  s (24 h) immersion.

Increase in the intensities of smaller fragments like  $[Cu(CHN)]^-$ , and  $[Cu(CN)_2]^-$  while those of the larger fragments like  $[(TTA)_2Cu]^-$  are decreasing, can be explained in two ways: (a) these two sets of secondary ions predominantly identify two distinct layers in

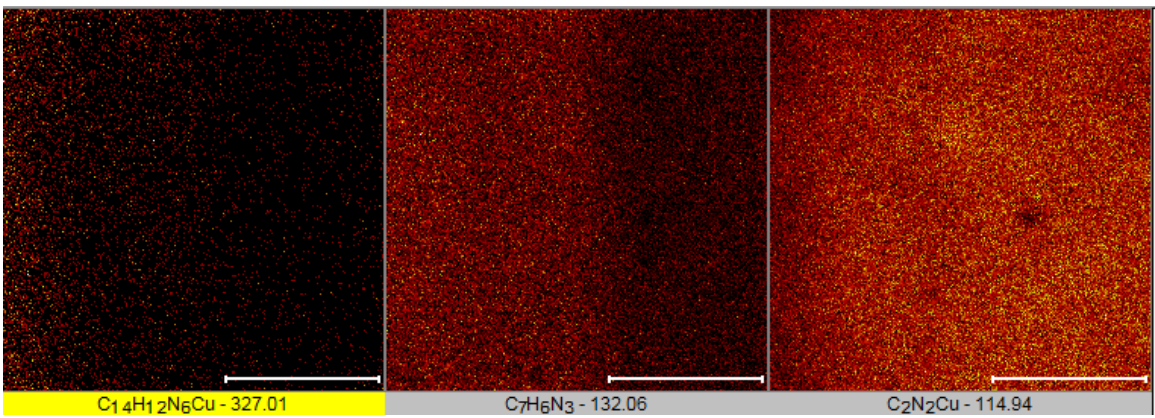
the surface film having dissimilar chemical environments, or (b) it may be a fragmentation artifact resulting from a damaged surface caused by the ion beams. However, based on the following reasons, the former explanation is reasonable. Firstly, beam-induced fragmentation should be accompanied by increasing intensity of smaller fragments. This, however, was not observed. Intensities for both sets of secondary ions were decreasing with sputtering up to  $\approx 75$  s. Moreover, the operative ion dose densities were approximately  $1/100^{\text{th}}$  of the reported static limit for such systems. Lastly, the depth profiles of these secondary ions were found to be reproducible. Based on these accounts, it was concluded that these two sets of secondary ions –  $[(\text{TTA})_2\text{Cu}]^-$ , and  $[\text{Cu}(\text{CN})_2]^-$ , predominantly identify two chemically distinct layers in the surface film. For  $[\text{CuO}]^-$ , the normalized peak integral increases with sputtering time up to  $\approx 360$  s, beyond which, it decreases progressively to lower values. Note, the time of maximum for  $[\text{CuO}]^-$  coincides with that of  $[\text{Cu}(\text{CN})_2]^-$ . Fig. 4.17 displays the surface acquired images for  $[(\text{TTA})_2\text{Cu}]^-$ ,  $[\text{TTA}]^-$ , and  $[\text{Cu}(\text{CN})_2]^-$  at progressive sputter-time intervals recorded in the course of the depth-profiling experiment. These images substantiate the information obtained from the depth-profile plots discussed above.



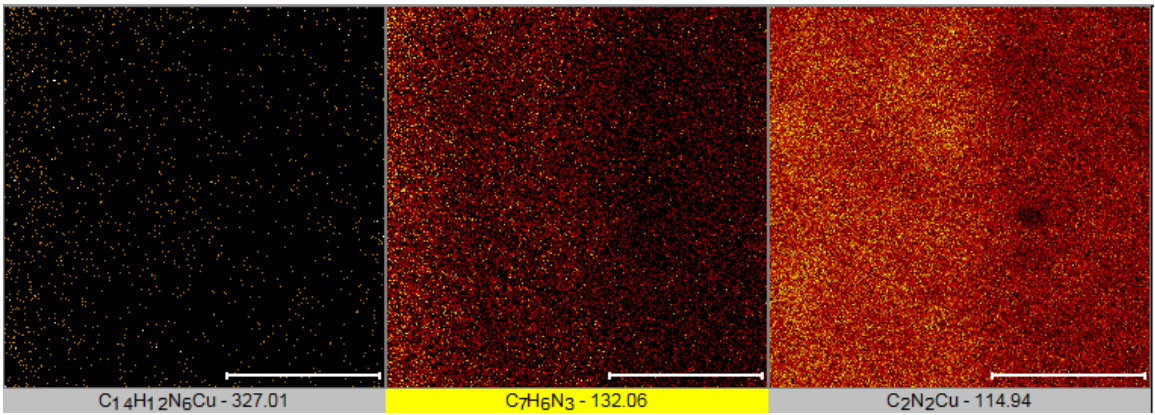
(a)



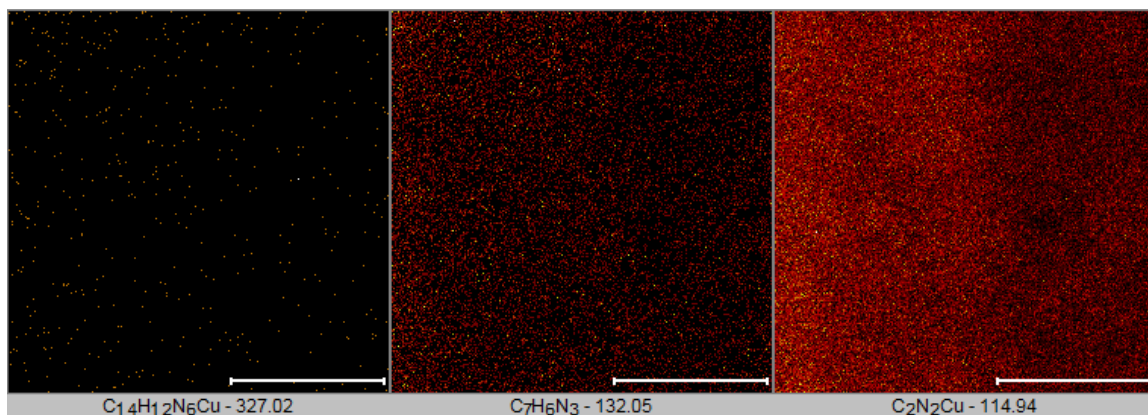
(b)



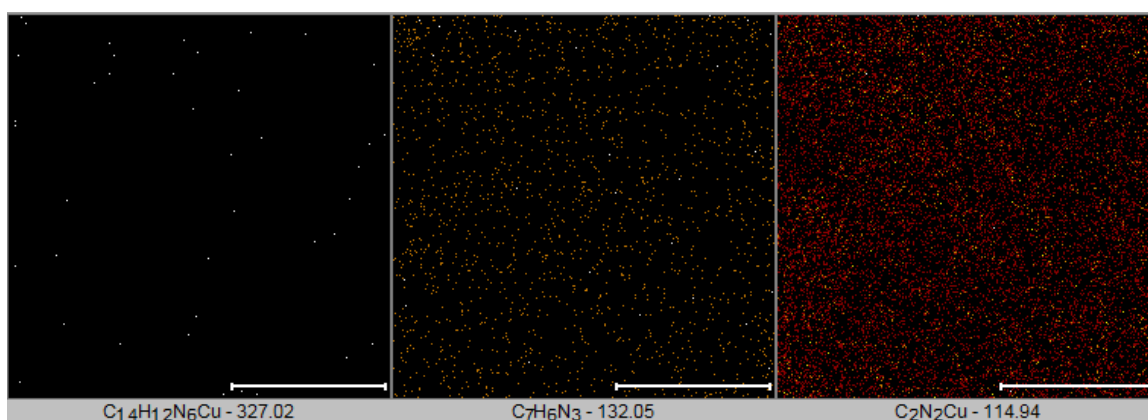
(c)



(d)



(e)



(f)

Fig. 4.17: Surface acquired images for  $[(\text{TTA})_2\text{Cu}]^-$ ,  $[\text{TTA}]^-$ , and  $[\text{Cu}(\text{CN})_2]^-$  after sputtering for (a)  $t = 0$  s (b)  $t = 120$  s (c)  $t = 360$  s (d)  $t = 600$  s (e)  $t = 810$  s (f)  $t = 1080$  s. All markers represent a length of  $100 \mu\text{m}$ .

Similar depth-profile experiments were carried out for few more selective immersion times. It was observed that for immersion times of  $2.16 \times 10^4$  s (6 h) and higher, the depth profiles were qualitatively similar. However, for immersion times below  $2.16 \times 10^4$  s (6 h), the smaller fragments in consideration –  $[\text{Cu}(\text{CHN})]^-$  and  $[\text{Cu}(\text{CN})_2]^-$ , had a marked difference in their depth profiles. These no longer show the initial decreasing segment with sputtering time and instead, start increasing right away, reaching a maximum and then decaying. The profiles for  $[(\text{TTA})_2\text{Cu}]^-$ ,  $[\text{TTA}]^-$ , and  $[\text{CuO}]^-$  were qualitatively

similar to the earlier considered case of  $8.64 \times 10^4$  s (24 h) immersion. The maxima for  $[\text{Cu}(\text{CN})_2]^-$  and  $[\text{CuO}]^-$  were still achieved at comparable sputtering times. To better illustrate this, the results on the depth-profile analysis of a  $1.08 \times 10^3$  s (3 h) immersed Cu sample are shown in Fig. 4.18. In comparison to the  $8.64 \times 10^4$  s (24 h) immersed sample, the normalized peak integral values are in general lower for  $[(\text{TTA})_2\text{Cu}]^-$ , and  $[\text{TTA}]^-$ , whereas it is higher for  $[\text{Cu}(\text{CN})_2]^-$ . However, in both cases, the rate of drop in the normalized peak integrals of  $[\text{TTA}]^-$ , and  $[(\text{TTA})_2\text{Cu}]^-$  in comparable range of magnitude are effectively similar. Also, the sputter time length at which the maxima for  $[\text{CuO}]^-$ , and  $[\text{Cu}(\text{CN})_2]^-$  are reached, is similar to that of the  $8.64 \times 10^4$  s (24 h) immersed sample.

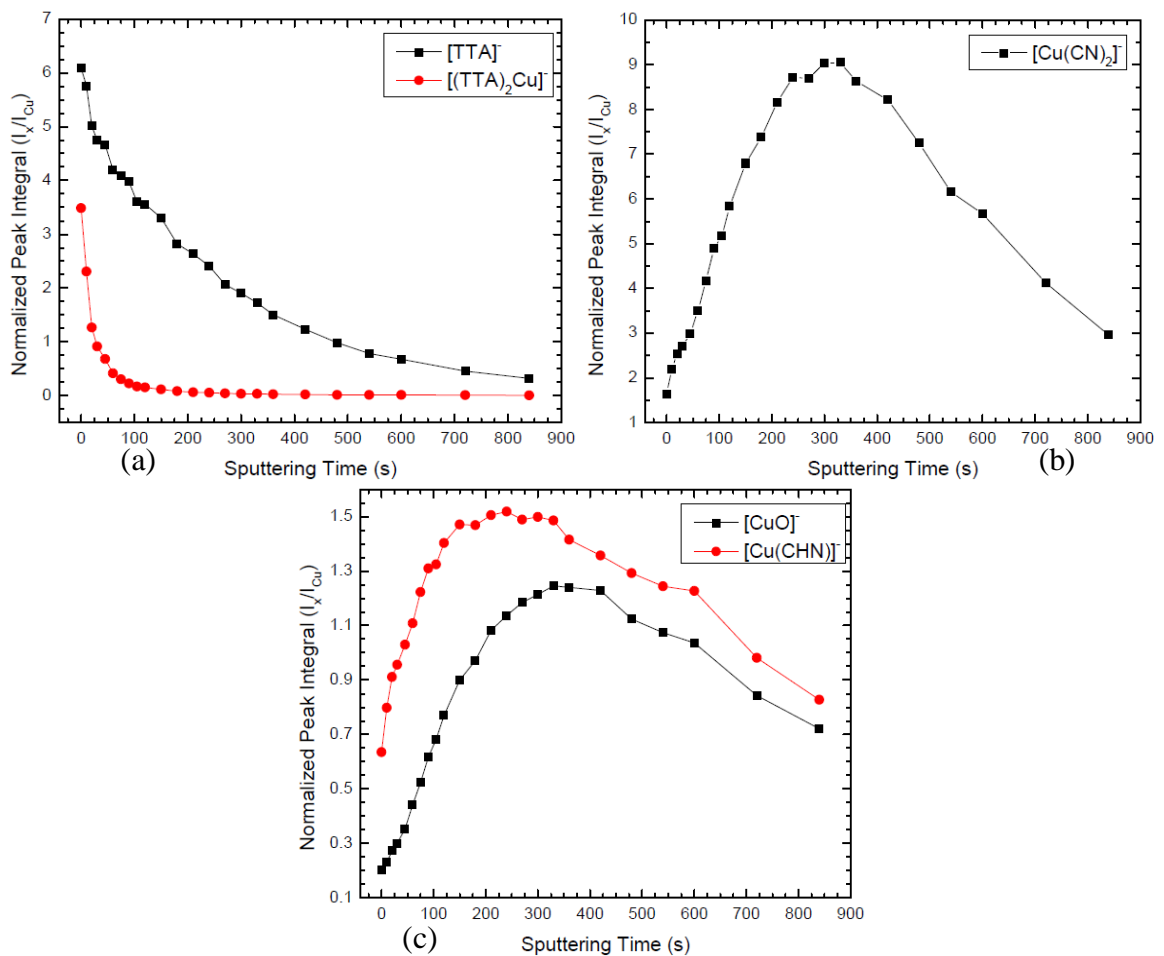


Fig. 4.18: Sputter depth-profiles for SI fragments relevant to TTAH adsorption film formed upon 10.8 Ks (3 h) immersion.

#### 4.2.2 XPS Characterization

To ensure the detection of the TTAH adsorption film in XPS, a survey spectrum was recorded at the outset. This is shown in Fig. 4.19. Cu, O, N, and C were the only elements detected. An intense N 1s peak confirmed the presence of the adsorption film as no other chemical component involved in the system other than TTAH contained nitrogen. The surface composition as calculated from the survey spectrum is shown in Table 4.2.

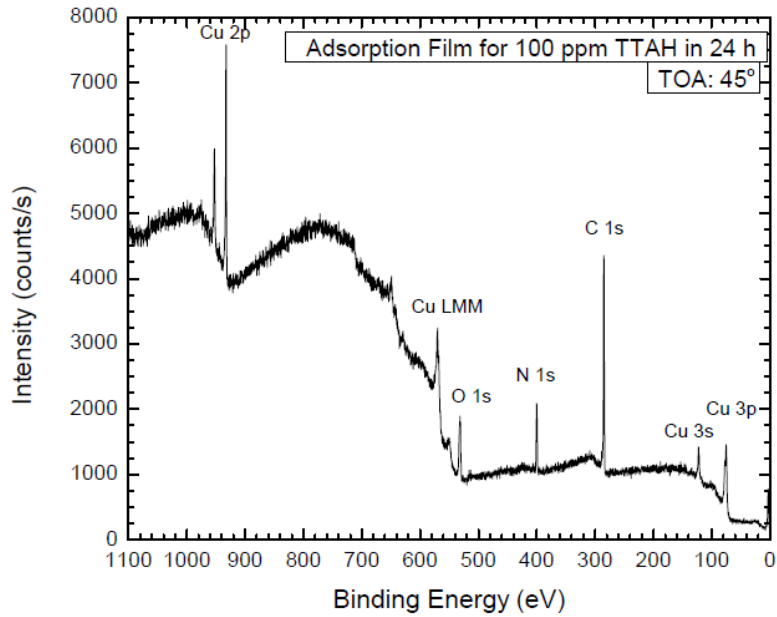
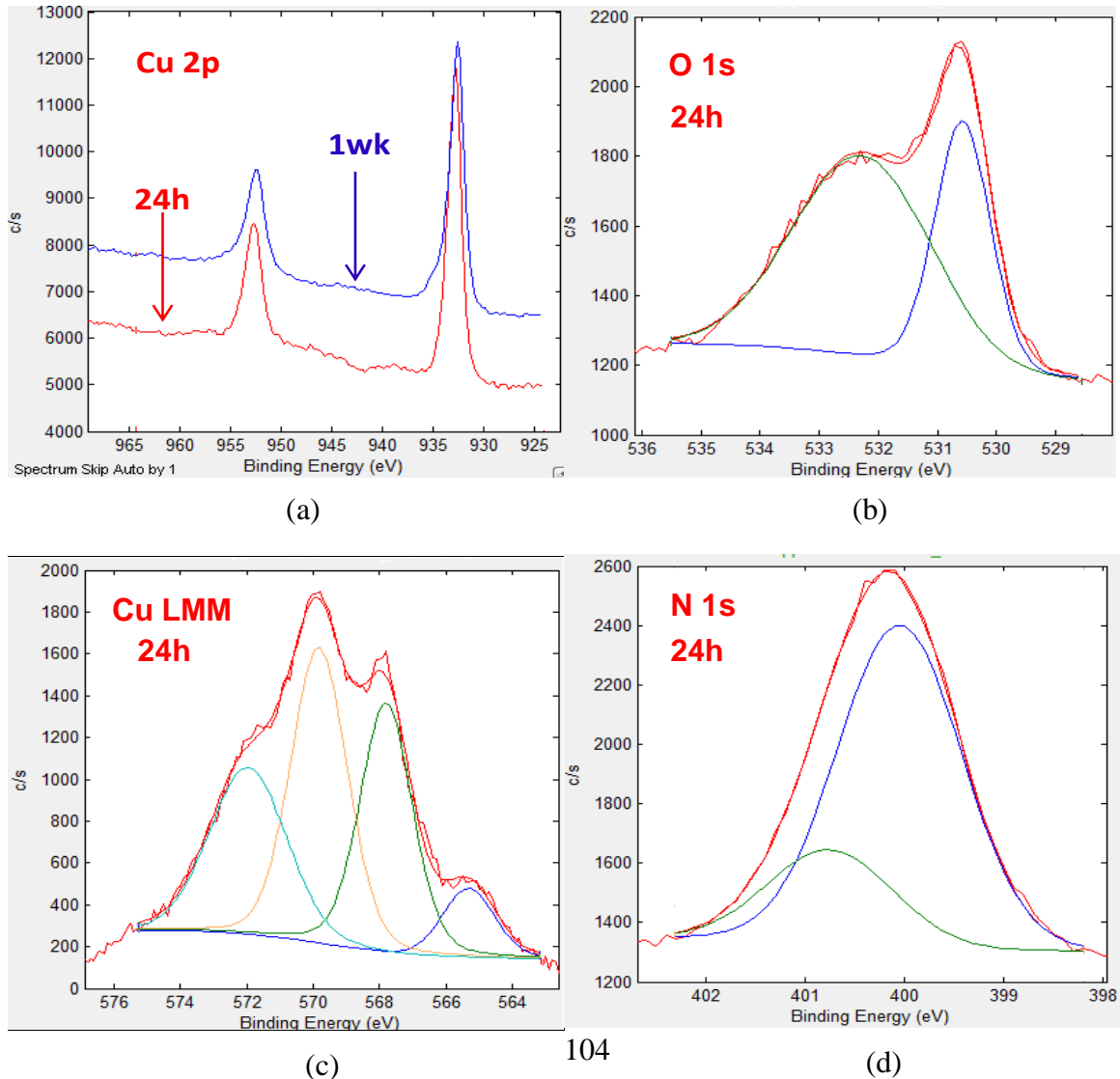


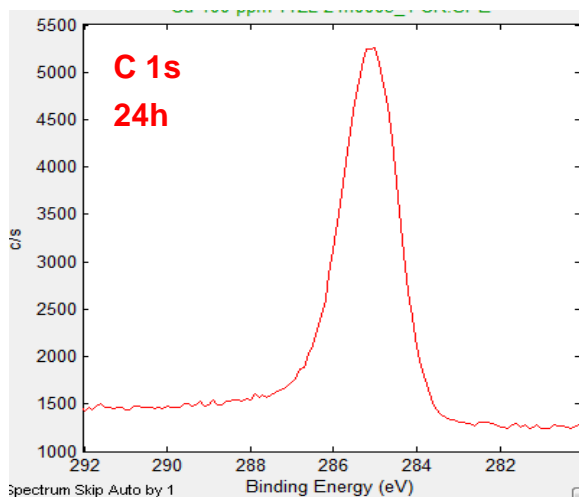
Fig. 4.19: XPS survey spectrum for TTAH adsorption film on Cu formed upon  $8.64 \times 10^4$  s (24 h) immersion in oil.

Element	Atomic %
Cu	9
N	18
O	14
C	59

Table 4.2: Surface composition for TTAH adsorption film on Cu formed upon  $8.64 \times 10^4$  s (24 h) immersion in oil.

As the above table suggests, there was an excess of C assuming that TTAH was the only source of carbon. Approximately, 40 at. % C was expected for this assumption to be true. The additional C was concluded to be associated with the adherent PAO-2 oil on top of the adsorption film as suggested by the ToF-SIMS results reported in the prior subsection. There was also an excess of O even if the entire Cu was assumed to be oxidized to CuO. Hence, to understand the chemical nature of all the elements in greater details, high resolution data was acquired for Cu 2p, Cu L<sub>3</sub>M<sub>4,5</sub>M<sub>4,5</sub>, O 1s, N 1s, and C 1s peaks, which are shown in Fig. 4.20 (a)-(e), respectively.





(e)

Fig. 4.20: XPS multiplex scans for (a) Cu 2p (b) O 1s (c) Cu  $L_{3}M_{4,5}M_{4,5}$  (d) N 1s (e) C 1s peaks for TTAH adsorption film on Cu formed upon  $8.64 \times 10^4$  s (24 h) immersion in oil.

Fig. 4.20 (a) shows the Cu 2p peaks for samples that were immersed for  $8.64 \times 10^4$  s (24 h) and  $6.05 \times 10^5$  s (1 week). There were no satellite peaks in either of the cases, hence, ruling out the formation of CuO for all immersion times up to  $6.05 \times 10^5$  s (1 week). Note, detection limits in XPS typically range from parts per thousand to parts per million. All the other peaks reported in this figure, for the rest of the elements in consideration, are exclusively for immersion time of  $8.64 \times 10^4$  s (24 h). Fig. 4.20 (b) shows the O 1s peak which indicates the presence of O in two distinct chemical states – Cu<sub>2</sub>O corresponding to the peak at 530.7 eV, and H<sub>2</sub>O corresponding to the peak at 532.8 eV. The former accounted for  $\approx 30$  % of the total oxygen detected and hence, 4 at. % in the total surface composition based on the numbers shown in Table 4.2. This illustrates that the Cu in the analyzed volume is partly present in the form of Cu<sub>2</sub>O. Although, for heterogeneous analysis volumes, like the one in consideration, quantification of the atomic fractions are not sufficiently accurate, as they are based on the assumption of

homogenous analysis volume. Hence, for the rest of this chapter, surface compositions are evaluated on the basis of intensity-peak integrals and their relative ratios for the different elements in consideration.

The Cu  $L_{3}M_{4,5}M_{4,5}$  Auger line is comprised of four distinct peaks – 565 eV, 568 eV, 570 eV, and 572 eV in the BE scale, which were de-convoluted as shown in Fig. 4.20 (c). As mentioned earlier in section 4.1.2, the peak at 568 eV corresponds to metallic Cu, whereas the one at 570 eV corresponds to  $Cu_2O$ . The peak at 572 eV corresponds to Cu-N bonding signifying TTAH adsorption. The peak at 565 eV is a part of the characteristic peak-shape of the primary metallic peak at 568 eV. Hence, for all calculation purposes beyond this section, the peak at 565 eV was ignored. The relative fraction of these four peaks were 7 %, 30 %, 36 %, and 27 % in the order of increasing BE scale position of the peaks, respectively. The N 1s peak for the same sample is shown in Fig. 4.20 (d). The peak was best fitted to be de-convoluted into two separate peaks – 400 eV, and 401 eV. The relative fractions of these two peaks were 75 % and 25 %, respectively. These individual peaks did not correspond to the different N atoms in the azole ring of the TTAH molecule. Even though for azides, the aliphatic analogue of azoles, distinct identification of the three N atoms in XPS is well established, but for azoles it is practically impossible due to substantial resonance-stabilization in the azole ring especially when they are attached to the benzene ring as in the case of  $BTA^-$  and  $TTA^-$  ions. Hence, all the three N atoms from the same molecule of  $TTA^-$  were assumed to have the same BE. On this basis, it was concluded that the two de-convoluted peaks of N

rather identified the two chemically distinct layers of the TTAH adsorption film that were revealed by the ToF-SIMS results presented in the prior sub-section.

The C 1s peak for the same sample is shown in Fig. 4.20 (e). It was not possible to deconvolute this peak in a reasonable manner so as to differentiate between carbon from the oil and the corrosion inhibitor molecules. This is because C from both the organic compounds have similar BE and the difference is below the resolution limit of XPS. Consequently, in this chapter, focus has been laid upon the quantitative analysis of Cu, O, and N, but not C. However, the C 1s peak did not show the presence of any significant amount of adventitious carbon, which usually appears at much higher binding energies corresponding to organic acids and ketones.

Tougaard background-shape analysis was carried out on the XPS survey spectrum shown in Fig. 4.19 in the vicinity of the Cu 2p peak in order to determine the TTAH adsorption film thickness formed on Cu and the morphology of the surface-film after  $8.64 \times 10^4$  s (24 h) of immersion. This analysis is based on the kinetic energy (KE) loss undergone by the characteristic photo-electrons while travelling from sub-surface regions towards the free surface that manifests as the difference in the shape of the backgrounds on the higher and lower BE sides of the photo-electron peak. Hence, the IMFP of the photo-electrons, which in turn depends on the characteristic KE of the photo-electrons, and the depth from which these photo-electrons are travelling are the two key parameters involved in this analysis. The analysis carried out on the Cu 2p photo-electrons with an appropriately chosen IMFP of 1.0 nm for the given system suggested a uniform coverage of  $\approx 2.5$  nm organic over-layer on Cu. This is in accord to the ToF-SIMS results presented in the prior

sub-section, which also revealed a continuous coverage of Cu by the adsorption film. Note, the Tougaard analysis cannot differentiate between the TTAH adsorption layer and the adhered PAO-2 oil layer atop and hence, the estimate of 2.5 nm represents the upper limit of the TTAH inhibitor layer thickness. The best background curve-fit between the modeled and experimental backgrounds obtained for the aforementioned conditions is shown in Fig. 4.21. Similar analyses were carried out for other immersion times as well, but the resulting differences in film thickness were too marginal to be analyzed by this method.

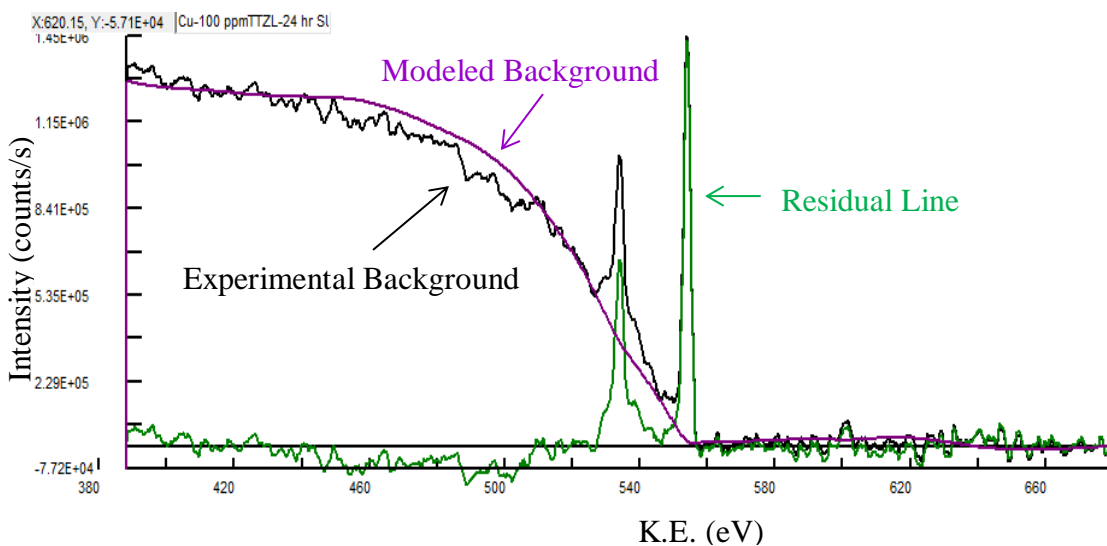


Fig. 4.21: Tougaard background curve fitting in the vicinity of Cu 2p peak for a  $8.64 \times 10^4$  s (24 h) immersed sample with 2.5 nm uniform organic over-layer.

Next, an effort was made to determine the depth-structure of the surface film by means of ARXPS. This study was exclusively carried out on a Cu sample immersed in 100 ppm TTAH oil solution for  $5.4 \times 10^3$  s (1.5 h). High-resolution data was acquired in XPS at multiple take-off-angles (TOA) of  $5^\circ$ ,  $20^\circ$ ,  $45^\circ$ , and  $90^\circ$  for Cu  $L_3M_{4,5}M_{4,5}$ , O 1s, and N 1s peaks, which are shown in Fig. 4.22 through Fig. 4.24, respectively.

As stated earlier, the Cu  $L_3M_{4,5}M_{4,5}$  peak was de-convoluted into three peaks – 568 eV, 570 eV, and 572 eV signifying metallic Cu,  $Cu_2O$ , and Cu bonded to N, respectively. The integral (over BE) for each of these individual peaks were recorded and compared. The relative fraction of the peak at 572 eV decreased with increasing TOA, whereas the same for 568 eV peak increased with increasing TOA. This illustrated that the Cu bonded to TTAH was closer to the free surface.

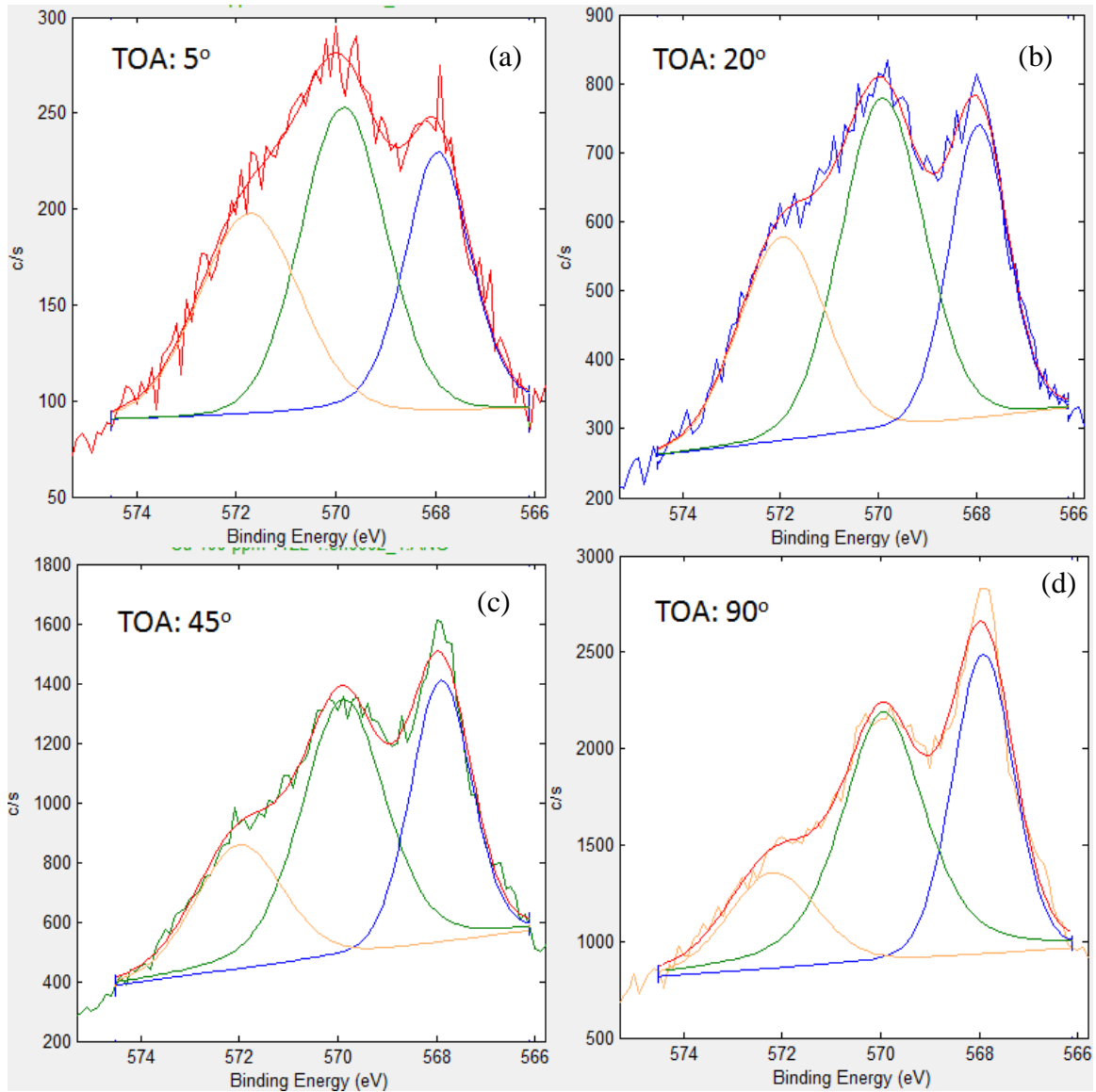


Fig. 4.22: Cu  $L_3M_{4,5}M_{4,5}$  peak acquired at TOA (a) 5° (b) 20° (c) 45° (d) 90°.

Similarly, the O 1s peak was de-convoluted into two peaks – 530.7 eV, and 532.8 eV corresponding to  $\text{Cu}_2\text{O}$ , and  $\text{H}_2\text{O}$ , respectively. Evidently, the relative fraction of the O 1s peak at 530.7 eV increased with increasing TOA suggesting that the  $\text{H}_2\text{O}$  layer was present closer to the free surface relative to the  $\text{Cu}_2\text{O}$  layer.

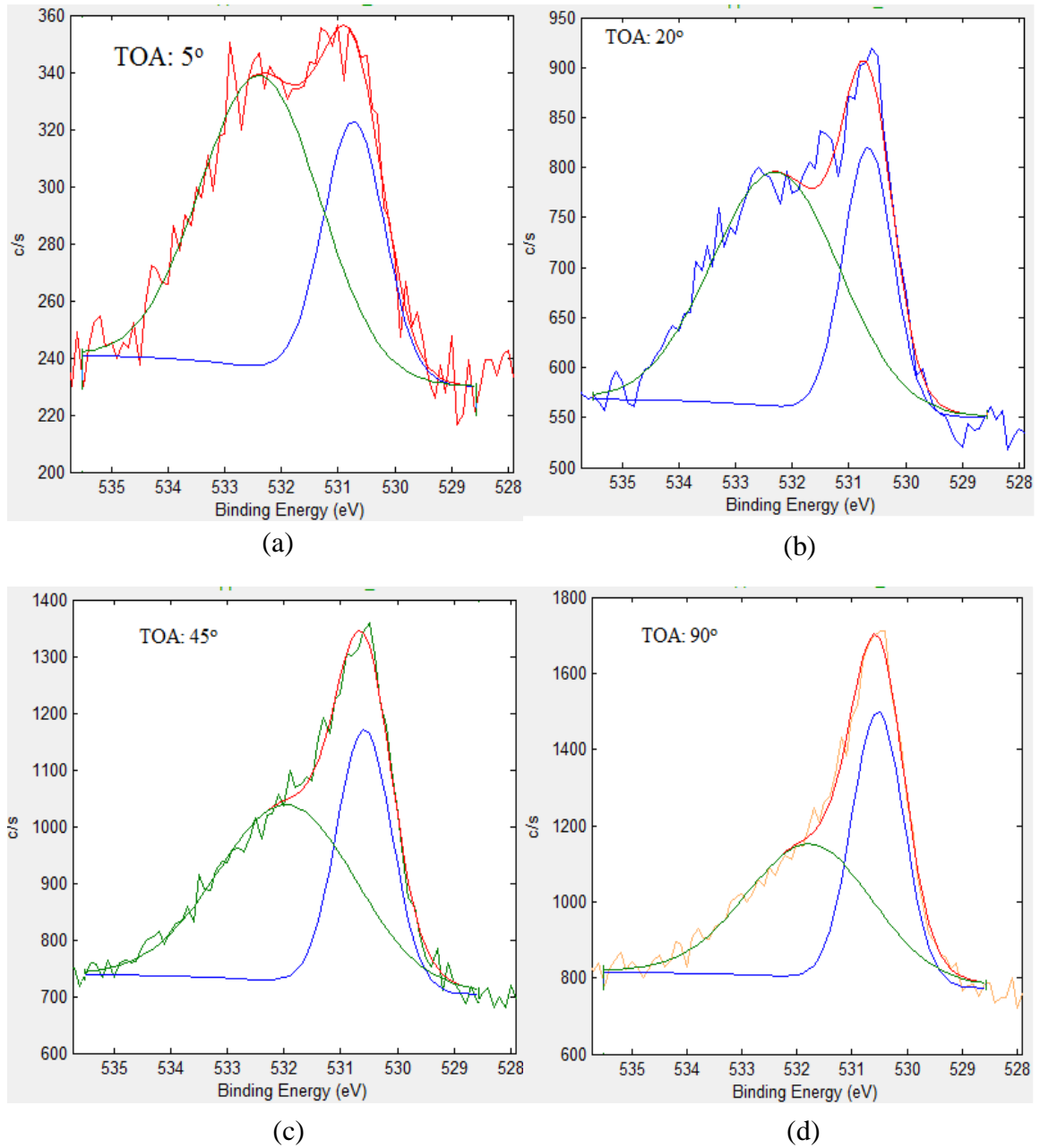


Fig. 4.23: O 1s peak acquired at TOA (a) 5° (b) 20° (c) 45° (d) 90°.

Finally, for the N 1s peak that was de-convoluted into 2 peaks – 400 eV, and 401 eV, the relative fraction of the former increased with increasing TOA suggesting a bi-layered structure in the TTAH adsorption film formed over Cu.

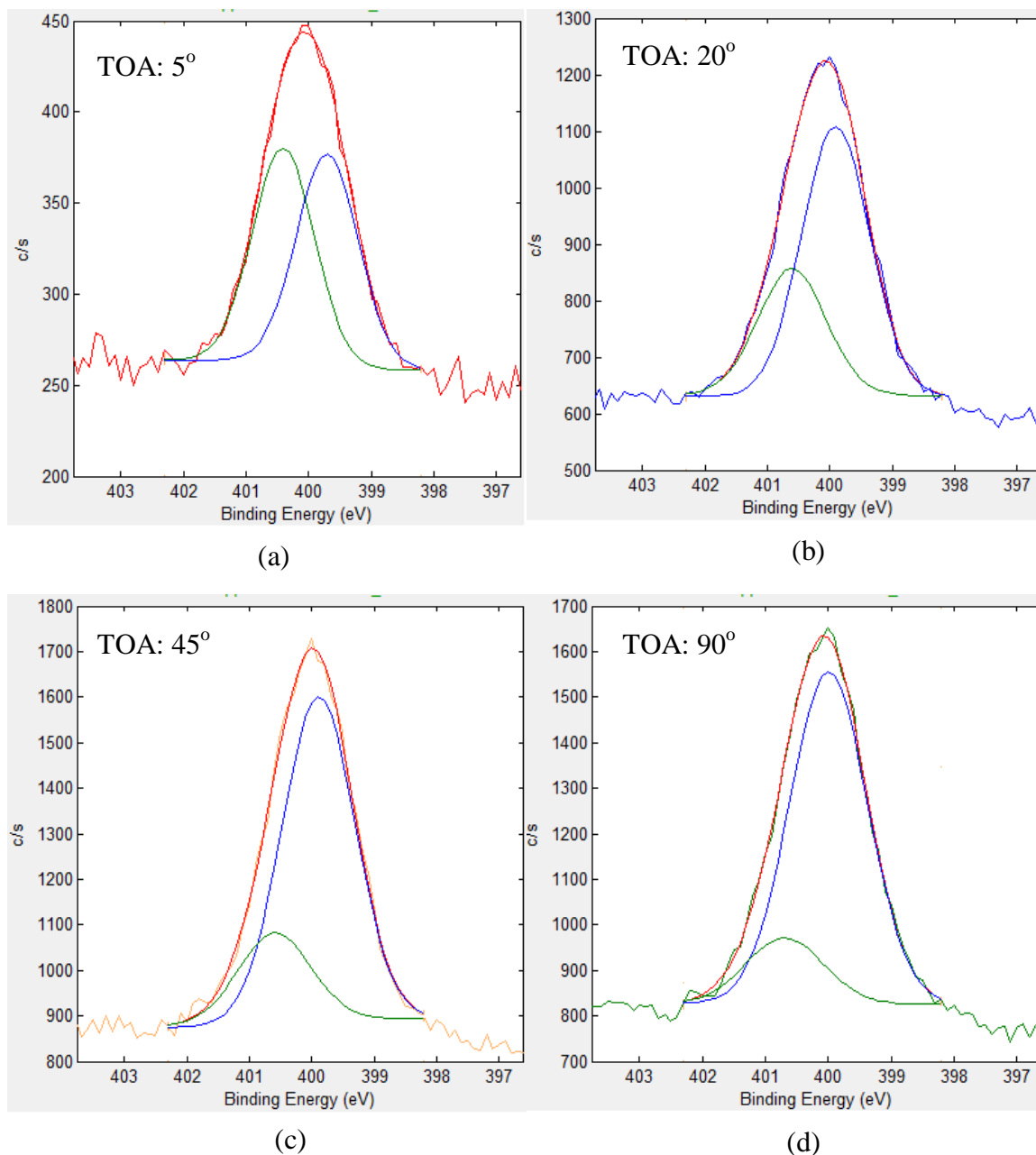


Fig. 4.24: N 1s peak acquired at TOA (a) 5° (b) 20° (c) 45° (d) 90°.

To determine the overall structure of the film, the following peak-integral ratios were calculated and plotted against TOA, which are shown in Fig. 4.25.

- Cu  $L_{3M_{4,5}M_{4,5}}$  peak at 568 eV ( $Cu_M$ ) to Cu  $L_{3M_{4,5}M_{4,5}}$  peak at 570 eV ( $Cu_2O$ ): As shown in Fig. 4.25 (a), it increases monotonously with increasing TOA. This confirms the obvious, that the  $Cu_2O$  layer was formed above the metallic substrate.
- O 1s peak at 530.7 eV ( $Cu_2O$ ) to convoluted N 1s peak: Shown in Fig. 4.25 (a), it also increases monotonously with increasing TOA, illustrating the presence of  $Cu_2O$  layer under the N-containing layer, i.e., the TTAH adsorption film.
- O 1s peak at 532.8 eV ( $H_2O$ ) to convoluted N 1s peak: This is again shown in the same figure, revealing a monotonously decreasing pattern with increasing TOA that suggests the presence of  $H_2O$  above the N-containing layer.
- Cu  $L_{3M_{4,5}M_{4,5}}$  peak at 570 eV ( $Cu_2O$ ) to Cu  $L_{3M_{4,5}M_{4,5}}$  peak at 572 eV (Cu-N): This plot, shown in Fig. 4.25 (b), confirms the presence of  $Cu_2O$  layer below the Cu layer that bonds to N from the TTAH molecules based on its monotonously increasing pattern with increasing TOA.
- N 1s peak at 400 eV to N 1s peak at 401 eV: This graph is shown in Fig. 4.25 (c), which shows a monotonously increasing pattern with increasing TOA suggesting that the TTAH adsorption layer with predominant N 1s peak at 401 eV was spatially above the other, chemically distinct, TTAH adsorption layer with predominant N 1s peak at 400 eV.

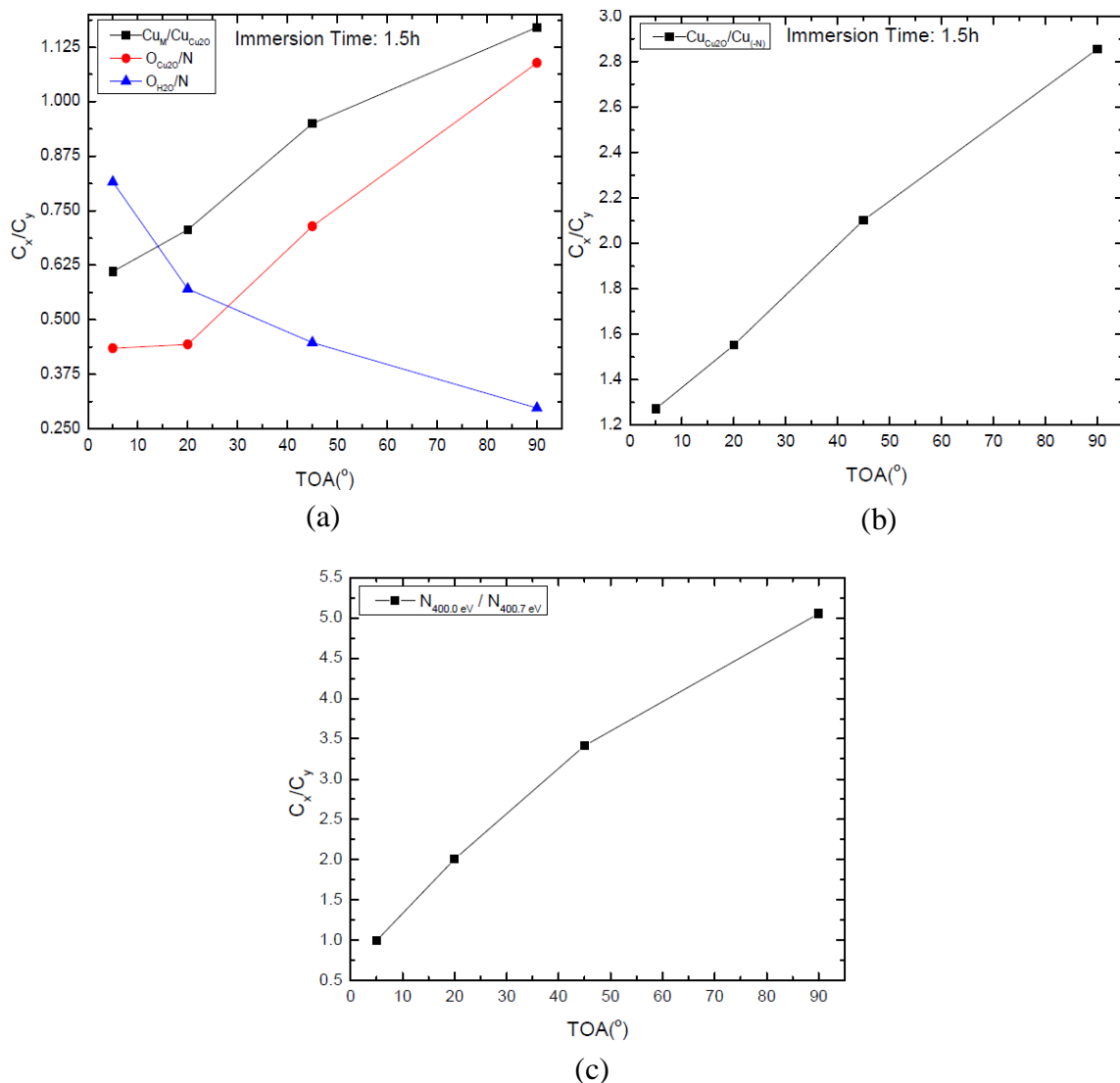


Fig. 4.25: Plots of peak-integral ratio vs. TOA for various elemental peaks.

Finally, the structure of the surface film was inferred by integrating the results obtained from ToF-SIMS depth-profile analysis, and ARXPS. The resulting structure is shown in Fig. 4.26. The O 1s peak at 532.8 eV may have a component of metallic hydroxides as well, but the film structure that has been determined is not compatible with the formation of copper hydroxides at the top most layer.

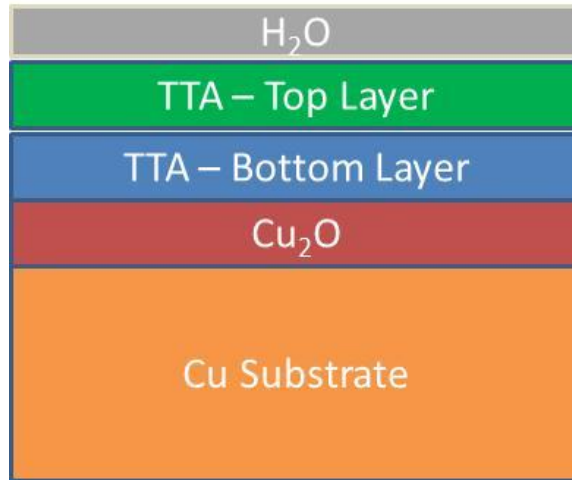


Fig. 4.26: Proposed structure for the surface film

### 4.3 Temporal Evolution of the TTAH Adsorption Film Structure on Cu

This section deals with the XPS and ToF-SIMS results on the characterization of the immersion-time interrupted TTAH adsorption film on Cu aiming to understand the time-dependent interactions between the different compositional layers revealed in section 4.2, and hence, the growth mechanism of the adsorption film. This section illustrates the dynamic nature of the individual layers of the surface film and suggests significant time-dependent interactions amongst them.

Fig. 4.27 through Fig. 4.29 show the XPS results for ten different immersion times – 1 s, 60 s (1 min), 600 s (10 min), 1.2 Ks (20 min), 2.7 Ks (45 min), 5.4 Ks (1.5 h), 10.8 Ks (3 h), 21.6 Ks (6 h), 86.4 Ks (24 h), and 604.8 Ks (1 week). Photo-electron peak-integral ratios for the involved elements were plotted against immersion time. In all the figures showing XPS results, there are two parts (a), and (b) that show results for immersion times up to 2700 s (45 min), and beyond, respectively. To confirm the reproducibility of

the surface film on Cu, three samples were prepared and subsequently characterized in XPS for selective immersion times – 1 s, 600 s (10 min), 2.7 Ks (45 min). In Fig. 4.27 through Fig. 4.29, the data points pertaining to these three immersion times are the respective average values from the three characterized samples at each condition. For all other immersion times, the data points are representative of only one characterized sample. Appropriate standard deviation error bars are shown in these figures for the three immersion times. The surface composition of the samples prepared under identical conditions varied within acceptable limits and hence, it was concluded that the surface film was largely reproducible.

Fig. 4.27 shows the temporal variations in the ratios for N/Cu, and N/O<sub>Cu<sub>2</sub>O</sub>, where N represents the total photo-electron intensity under the N 1s peak and Cu represents that of under Cu 2p<sub>3/2</sub> peak. O<sub>Cu<sub>2</sub>O</sub> represents the O associated to Cu<sub>2</sub>O only, based on deconvolution of the O 1s peak. Evidently, N increased with time in comparison to both O associated to Cu<sub>2</sub>O, and total Cu. After a week of immersion, the relative gain in N was by 150 %, and 400 %, respectively. However, this relative increase in N was not monotonous with time in either case. There were three distinct time intervals – 1 s to 60 s (1 min), 1200 s (20 min) to 2700 s (45 min), and 10800 s (3 h) to 86400 s (24 h) for which the relative fraction of N decreased consistently with time in an overall increasing behavior over the entire range of tested immersion times. The lowest values for both N/Cu, and N/O<sub>Cu<sub>2</sub>O</sub> were recorded upon 60 s (1 min) immersion at 1.1 and 0.55, respectively, whereas the respective highest values of 7.7 and 1.8 were observed after immersing for 6.05 x 10<sup>5</sup> s (1 week). Note that the variation of N with total Cu was

directly correlated to its variation with O associated to  $\text{Cu}_2\text{O}$ . This indicated to a possible correlation between the growth of the TTAH adsorption film, and the growth of the  $\text{Cu}_2\text{O}$  under-layer.

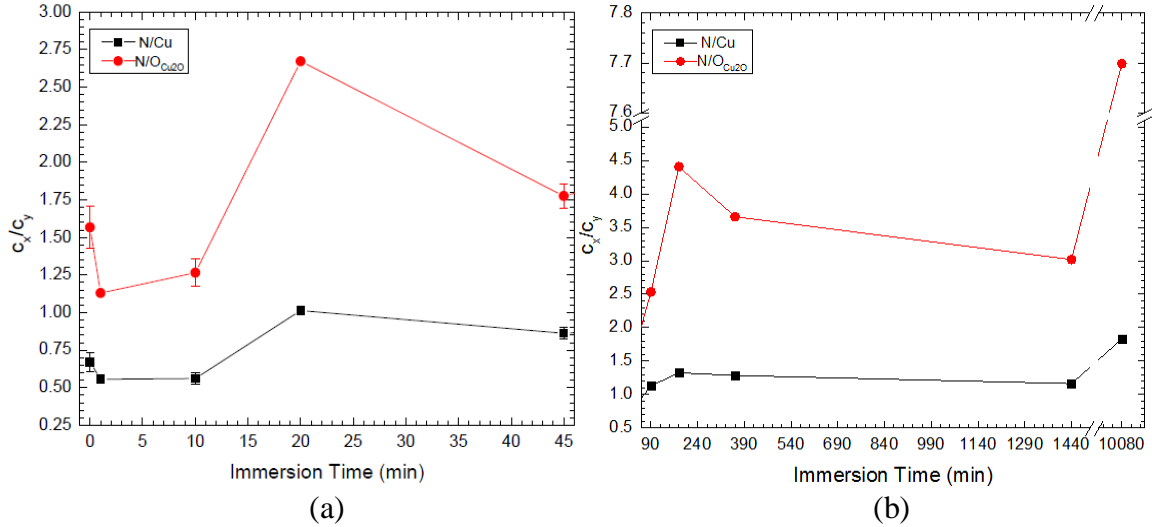


Fig. 4.27: Immersion-time-dependent variations for N/Cu, and N/Cu<sub>2</sub>O in (a) 1 s to 2700 s (45 min) (b) 5400 s (90 min) to 6.05 x 10<sup>5</sup> s (1 week).

To investigate this further, the  $\text{Cu}_{(-\text{N})}/\text{Cu}_{\text{Cu}_2\text{O}}$ , and  $\text{Cu}_{\text{Cu}_2\text{O}}/\text{Cu}_\text{M}$  ratios were plotted against immersion time as shown in Fig. 4.28, where  $\text{Cu}_{(-\text{N})}$  represents the Cu bonded to TTAH,  $\text{Cu}_{\text{Cu}_2\text{O}}$  represents Cu associated with  $\text{Cu}_2\text{O}$ , and  $\text{Cu}_\text{M}$  represents the metallic Cu in the substrate. These calculations were based on the Cu L<sub>3</sub>M<sub>4,5</sub>M<sub>4,5</sub> peak de-convolution. In general, with increasing immersion time, the relative fraction of Cu bonded to TTAH increased with respect to that associated with  $\text{Cu}_2\text{O}$ , whereas the latter decreased in comparison to metallic Cu. But again, rather than a monotonous behavior, there were intermittent inflection points in the time dependence of both  $\text{Cu}_{(-\text{N})}/\text{Cu}_{\text{Cu}_2\text{O}}$ , and  $\text{Cu}_{\text{Cu}_2\text{O}}/\text{Cu}_\text{M}$  at exactly the same immersion times as that of N/Cu, and N/Cu<sub>2</sub>O. Also, the variations in the time dependence of both these ratios were inversely correlated to each

other. These observations led to the conclusion that the Cu-TTAH bonding occurred at the expense of the  $\text{Cu}_2\text{O}$  under-layer, while the latter appeared to grow intermittently. These observations suggest that the engaged chemical transformations must occur coherently over a large area of the surface that is being probed.

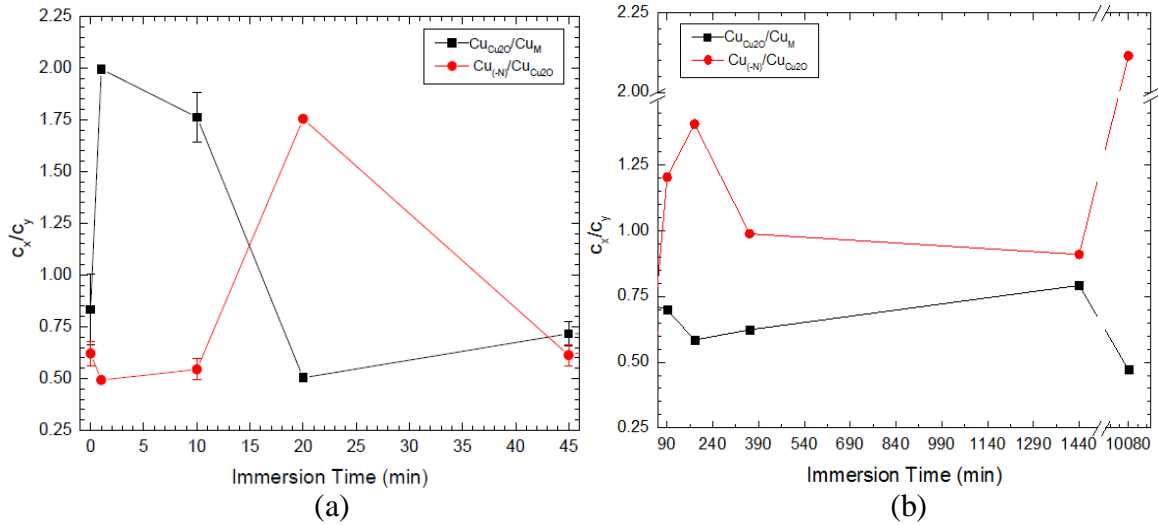


Fig. 4.28: Immersion-time-dependent variations for  $\text{Cu}_{(-N)}/\text{Cu}_{\text{Cu}_2\text{O}}$ , and  $\text{Cu}_{\text{Cu}_2\text{O}}/\text{Cu}_M$  in (a) 1 s to 2700 s (45 min) (b) 5400 s (90 min) to  $6.05 \times 10^5$  s (1 week)

Finally, for the sake of confirmation, the  $\text{O}_{\text{Cu}_2\text{O}}/\text{Cu}$  ratio was also plotted against immersion time, shown in Fig. 4.29, where both  $\text{O}_{\text{Cu}_2\text{O}}$  and Cu stand as per their prior definitions. In the whole range of tested immersion times, there was an overall decrease in O, associated with  $\text{Cu}_2\text{O}$ , as compared to total Cu. This plot shows the intermittent inflection points as well at the same immersion times as the other plots. The time-dependent behavior for  $\text{O}_{\text{Cu}_2\text{O}}/\text{Cu}$  was in accord to the results obtained on the basis of the Cu  $\text{L}_3\text{M}_{4,5}\text{M}_{4,5}$  peak analysis, shown in Fig. 4.28 and the time-dependent variations of all the five ratios, considered in Fig. 4.27 through Fig. 4.29, were in agreement to each other.

Moreover, all these ratios showed fluctuations with immersion time, the significance of which is discussed in the following chapter.

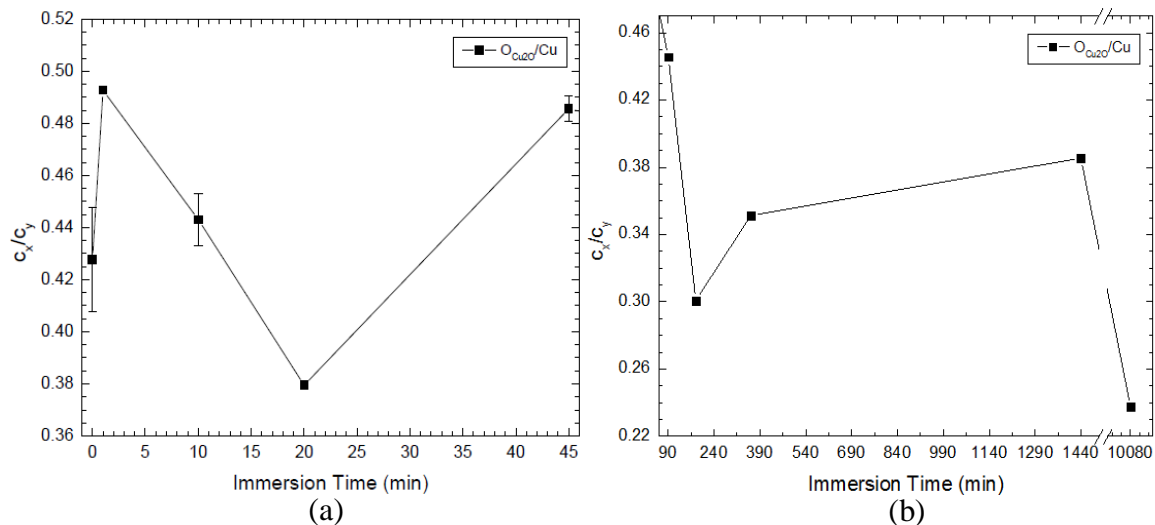


Fig. 4.29: Immersion-time-dependent variation for  $O_{Cu_2O}/Cu$  in (a) 1 s to 2700 s (45 min) (b) 5400 s (90 min) to  $6.05 \times 10^5$  s (1 week)

An analogous ToF-SIMS study was carried out for the same immersion times except for  $6.05 \times 10^5$  s (1 week). ToF-SIMS results revealed certain complimentary aspects of the TTAH adsorption film growth. The  $[TTA_2Cu]^-/[Cu(CN)_2]^-$ , and  $[TTA]^-/[TTA_2Cu]^-$  ratios were plotted against immersion time, as shown in Fig. 4.30 (a), and (b), respectively. These plots helped to get an insight into the time-dependence of the polymerization behavior of the adsorption film. There was a strong inverse correlation between these two plots. Evidently, the degree of polymerization in the TTAH adsorption film, i.e., the relative fraction of the polymerized layer present atop increased, with respect to the other TTAH adsorption configuration present underneath, for the first 1.2 Ks (20 min) of immersion, beyond which, it dropped substantially to lower values. The drop continued until 10.8 Ks (3 h) of immersion and subsequently, it fractionally increased again to an

apparent equilibrium value. The continuous growth of the polymerized layer in the early phase was indicative of two plausible scenarios – a) the formation of the polymer is the first step of corrosion inhibitive film formation on Cu surface and with time the other layer builds up underneath, or b) the lower layer is indeed the nucleating step of film formation, but under the prevailing conditions, the formation of the polymerized top-layer is kinetically favored, although after sometime as the conditions change, the polymerized layer gets saturated and the bottom layer starts growing more rapidly. These two hypothetical scenarios are discussed in further details in the following chapter.

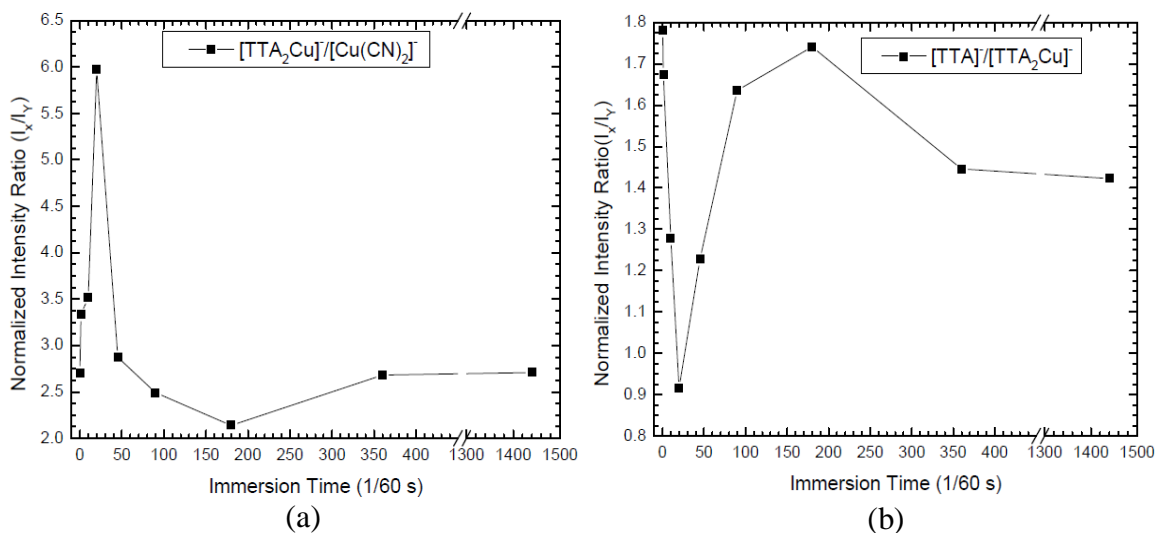


Fig. 4.30: Immersion-time-dependent variation for the ratios (a)  $[TTA_2Cu]/[Cu(CN)_2]$  (b)  $[TTA]/[TTA_2Cu]$

#### 4.4 Corrosion of Cu in Sulfide Solution

This section presents all the results on the Cu corrosion study in sulfide-containing oil solution, which was exclusively carried out in XPS. Sec-butyl disulfide, shown in Fig. 3.3, was used as the source for active sulfur. An active component refers to the fact

that it is available to bond with the metallic substrate, which in turn corrodes the substrate. All the immersion tests were conducted at 80°C. At such an elevated temperature, the disulfide bonds cleave to produce butyl sulfide free radicals. This section reveals the chemical nature of the Cu corrosion products in the initial stages of sulfide attack, and their depth-distribution. This section also reveals the significant effect of temperature on the TTAH adsorption film formation on Cu.

#### *4.4.1 Cu Corrosion by Sulfide in Absence of TTAH*

The objective of studying Cu corrosion by sulfide in the absence of TTAH was to realize the initial surface reactions leading to corrosion. In this case, there were oxygen and butyl sulfide free radicals present in the system, both of which have the tendency to react with the Cu surface. The focus was to ascertain the chemical species that interacts with the Cu surface first and identify the consequent corrosion products being formed on the surface. For this purpose, the immersion time and S concentration in the oil were varied. In this sub-section, immersion test results are presented for four different conditions:

- 0.36 wt. % S in PAO-2 oil for  $1.8 \times 10^3$  s (30 min) at 80°C
- 0.36 wt. % S in PAO-2 oil for  $8.64 \times 10^4$  s (24 h) at 80°C
- 0.72 wt. % S in PAO-2 oil for  $8.64 \times 10^4$  s (24 h) at 80°C
- 0.72 wt. % S in PAO-2 oil for  $6.05 \times 10^5$  s (1 week) at 80°C

The S contents were chosen to be representative of actual lubricant oils. The XPS survey spectrum for the case of  $8.64 \times 10^4$  s (24 h) immersion time in 0.36 wt. % S containing oil

is shown in Fig. 4.31. The surface composition as calculated from this survey spectrum is shown in Table 4.3. The survey spectra for the other considered cases were qualitatively similar except for the case of  $1.8 \times 10^3$  s (30 min) immersion time in 0.36 wt. % S-containing oil for which there were no detectable S peaks.

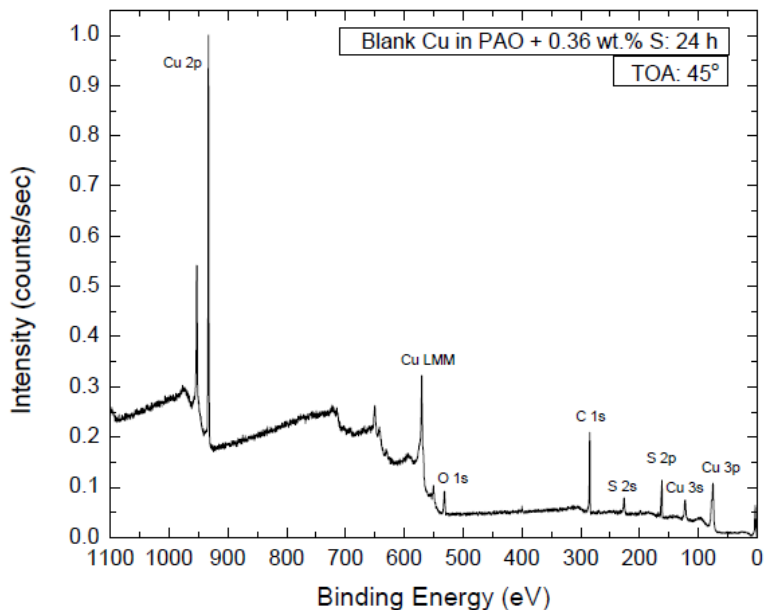


Fig. 4.31: XPS survey spectrum for Cu surface upon  $8.64 \times 10^4$  s (24 h) immersion in oil containing 0.36 wt. % S.

Element	Atomic %
Cu	33
S	8
O	25
C	34

Table 4.3: Surface composition of Cu surface upon  $8.64 \times 10^4$  s (24 h) immersion in oil containing 0.36 wt. % S.

As mentioned in earlier sections, due to the heterogeneity of the surface film, comparative calculations were based on the ratios of pure intensities of the relevant XPS

peaks of involved elements rather than their atomic percentages. To understand the chemical nature of the O, and S, high resolution data were acquired for O 1s and S 2p peaks and subsequently de-convoluted as shown in Fig. 4.32 (a) and (b), respectively.

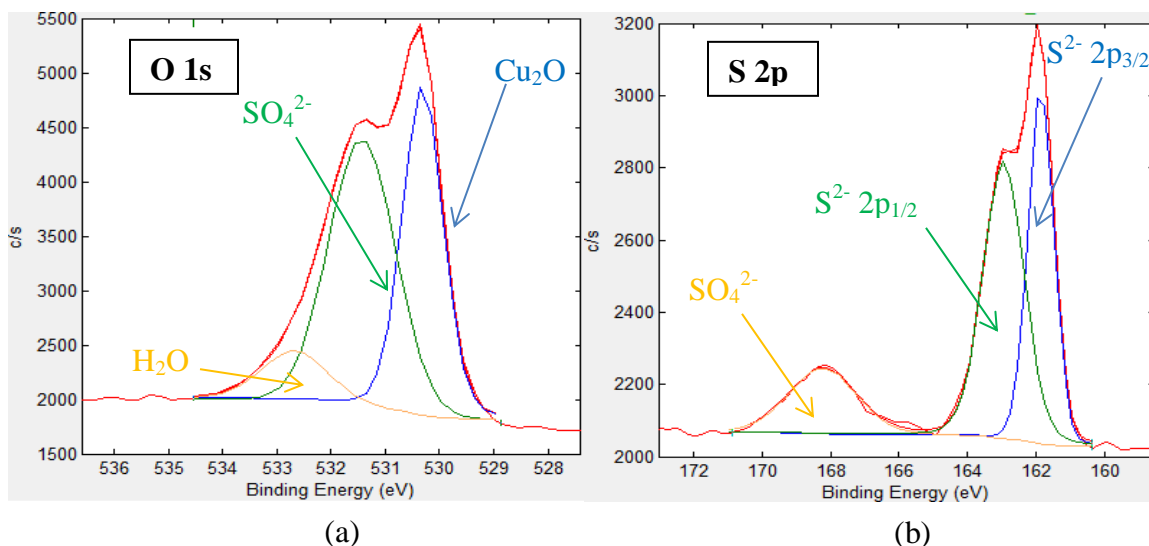


Fig. 4.32: XPS multiplex scans for (a) O 1s (b) S 2p peaks acquired on Cu surface film formed upon  $8.64 \times 10^4$  s (24 h) immersion in oil containing 0.36 wt. % S.

There were three distinct peaks identified within the O 1s peak – 530.5 eV, 531.6 eV, and 532.8 eV peaks corresponding to Cu<sub>2</sub>O, SO<sub>4</sub><sup>2-</sup>, and H<sub>2</sub>O, respectively. Similarly for S, two distinct chemical states were identified – SO<sub>4</sub><sup>2-</sup> that corresponded to the 168.4 eV peak and S<sup>2-</sup> corresponding to the peak in the vicinity of 162.6 eV. The sulfide peak had two further distinct components, which were related to the 2p<sub>1/2</sub>, and 2p<sub>3/2</sub> photo-electron peaks at 163.2 eV, and 162.1 eV, respectively. Note that even the sulfate peak is comprised of two analogous components corresponding to the 2p<sub>1/2</sub>, and 2p<sub>3/2</sub> photo-electrons, but this feature was not well observed in the present experiments owing to the low intensity of photoelectrons from the SO<sub>4</sub><sup>2-</sup> ions. For all calculation purposes related to S, no distinction between the 2p<sub>1/2</sub>, and 2p<sub>3/2</sub> photo-electrons were made and all

comparisons were made on the basis of the peak integrals for the overall 2p peaks for  $S^{2-}$  and  $SO_4^{2-}$ , respectively.

Next, a comparative study was carried out on the variations in the Cu 2p, Cu  $L_3M_{4,5}M_{4,5}$ , O 1s, and S 2p peaks under the different testing conditions that revealed evidence for Cu corrosion by sulfide. The respective plots are shown in Fig. 4.33. No satellite peaks for Cu 2p photo-electrons were detected in either of the conditions, as shown in Fig. 4.33 (a). Hence, the formation of CuO and  $CuSO_4$  were ruled out. Note that neither CuS nor  $Cu_2S$  leads to the appearance of satellite peaks. Also, the Cu 2p peak positions, reported in the literature, are practically unaltered for these two forms of copper sulfides. Thus, no conclusion regarding the oxidation state of Cu in the sulfide could be drawn from its 2p peaks. The analysis of Cu  $L_3M_{4,5}M_{4,5}$  peak shapes and positions, shown in Fig. 4.33 (b), proved to be insensitive to differentiate between the compositions of the resultant surface films formed under the different testing conditions except for the fact that the respective peak for  $8.65 \times 10^4$  s (24 h) immersion in 0.36 wt. % S-containing oil showed a higher metallic component as compared to the other two cases. Broadly, the Cu  $L_3M_{4,5}M_{4,5}$  peaks in all cases were similar to that of  $Cu_2O$ . In the literature, the predominant  $L_3M_{4,5}M_{4,5}$  peak for  $Cu_2O$ , and  $Cu_2S$  have been reported at the same KE (BE position), whereas a small shift of  $\approx 0.5$  eV to higher KE (lower BE) has been reported for CuS. In the experimental results obtained in the course of this project, no such shift was observed and hence, the Cu associated to sulfide was concluded to be present as  $Cu_2S$ . Comparing the O 1s peaks under the different testing conditions, shown in Fig. 4.33 (c), the relative fraction of O associated with  $Cu_2SO_4$ , as compared to that of  $Cu_2O$ , increased with

increasing immersion time, and S concentration in the oil. Moreover, as observed from the S 2p peaks, shown in Fig. 4.33 (d), the relative fraction of sulfate as compared to sulfide, was the highest for  $8.65 \times 10^4$  s (24 h) immersion time and 0.36 wt. % S, while the sulfide fraction increased substantially with increasing S concentration in the oil.

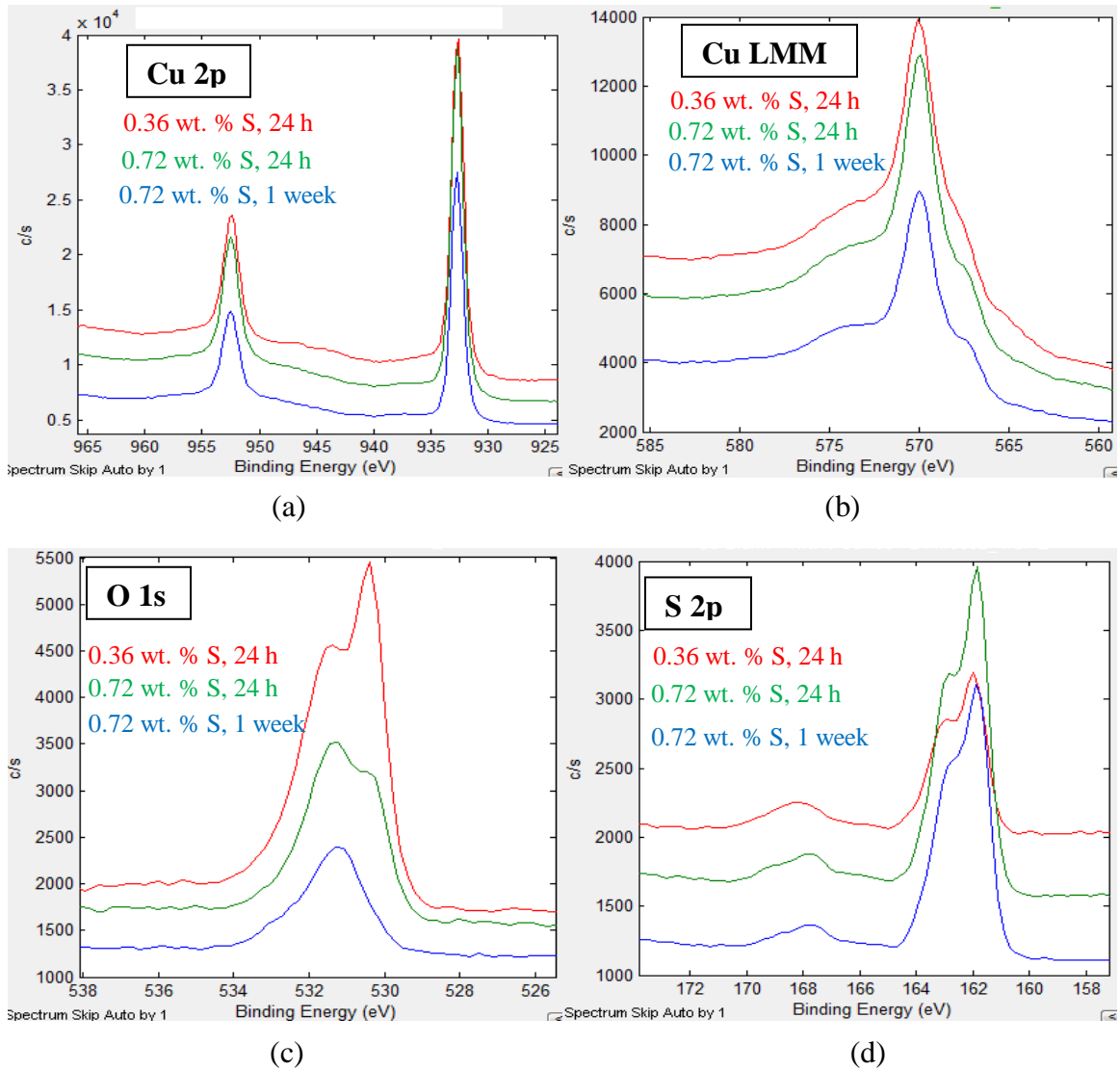


Fig. 4.33: Comparative plots of (a) Cu 2p (b) Cu  $L_{3}M_{4,5}M_{4,5}$  (c) O 1s (d) S 2p peaks acquired on Cu surface films formed under different conditions.

Calculations were carried out for better understanding the compositional differences amongst the above discussed cases, the results of which are summarized in Fig. 4.34. For this purpose, peak integrals for the individual components were normalized to that of the Cu 2p peak for the respective cases.

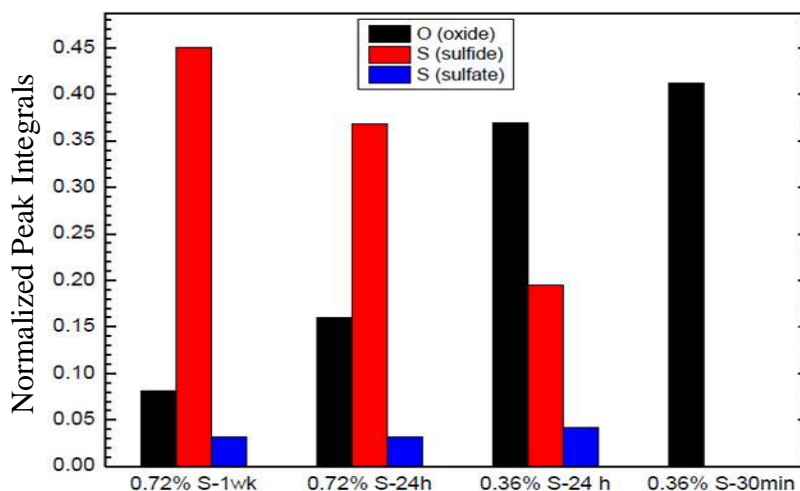


Fig. 4.34: Quantitative comparison of O (in  $\text{Cu}_2\text{O}$ ), S (in  $\text{Cu}_2\text{S}$ ), and S (in  $\text{Cu}_2\text{SO}_4$ ) content in the surface film formed under different conditions.

The  $\text{Cu}_2\text{O}$  content in the surface film was the highest for the sample immersed for  $1.8 \times 10^3$  s (30 min) in 0.36 wt. % S-containing oil. The  $\text{Cu}_2\text{O}$  fraction decreased, while the  $\text{Cu}_2\text{S}$  fraction increased in the surface film with increasing immersion time and S concentration in the oil. Similar experiments were done for 0.1 and 0.2 wt. % S content in the oil as well, but neither of these cases showed any detectable evidence for Cu corrosion by sulfide, even after  $6.05 \times 10^5$  s (1 week). These results suggested that interaction of oxygen with the Cu surface leading to the formation of  $\text{Cu}_2\text{O}$  is the first surface reaction step even in the presence of sulfide radicals. It was also implied that there is an incubation time for the sulfide attack to initiate, which decreases with

increasing S concentration in the medium. In all the considered cases revealing Cu corrosion by sulfide attack, the sulfate content of the surface film practically remained the same. This was indicative of two plausible scenarios: (a)  $\text{Cu}_2\text{S}$  is directly formed on the substrate surface ( $\text{Cu}_2\text{O}$ ) as result of corrosion. On exposure to the atmosphere, the top layer of the  $\text{Cu}_2\text{S}$  oxidizes to  $\text{Cu}_2\text{SO}_4$ . (b)  $\text{Cu}_2\text{SO}_4$  is first formed on  $\text{Cu}_2\text{O}$ , and upon reaching a critical thickness of this layer,  $\text{Cu}_2\text{S}$  starts to grow on top of it.

Thus, the formation of the  $\text{Cu}_2\text{SO}_4$  layer is either the first stage of Cu corrosion by sulfide attack or the last. This question was answered by determining the corrosion film structure by means of ARXPS, which is included in the following sub-section.

#### *4.4.2 Cu Corrosion by Sulfide in Presence of TTAH*

Corrosion of Cu by sulfide attack in presence of TTAH was studied under the following conditions:

- Cu immersed in Oil + 0.01 wt. % TTAH + 0.72 wt. % S for 60 s (1 min) at 80°C
- Cu immersed in Oil + 0.01 wt. % TTAH + 0.72 wt. % S for  $6.05 \times 10^5$  s (1 week) at 80°C
- Cu immersed in Oil + 0.01 wt. % TTAH for 3600 s (1 h) at room temperature and then immediately immersed in Oil + 0.01 wt. % TTAH + 0.72 wt. % S for  $6.05 \times 10^5$  s (1 week) at 80°C

- Cu immersed in Oil + 0.01 wt. % TTAH for 3600 s (1 h) at room temperature and then immediately immersed in Oil + 0.72 wt. % S for  $6.05 \times 10^5$  s (1 week) at 80°C

The purpose of studying Cu corrosion by sulfide under these different testing conditions was to realize the efficacy of TTAH in inhibiting this particular form of corrosion and better understand the related micro-mechanism of protection. The last two experimental conditions were deliberately aimed at determining the nature of the protective film being formed by TTAH on Cu, i.e., whether the TTAH adsorption film was essentially static or dynamic.

The normalized N content of the surface films, formed under different conditions, is shown in Fig. 4.35, whereas the same for O in  $\text{Cu}_2\text{O}$  and S in  $\text{Cu}_2\text{S}$ , and  $\text{Cu}_2\text{SO}_4$ , respectively are shown in Fig. 4.36. The N content was significantly higher, approx. 2 times as much, at 80°C as compared to that of room temperature for corresponding immersion times. The room temperature data is shown in Fig. 4.27. The N/Cu ratios at room temperature, and 80°C were calculated to be 0.6, and 1, respectively, upon 60 s (1min) of immersion, whereas the same reached a value of 1.8, and 3.6, respectively after  $6.05 \times 10^5$  s (1 week). This suggested a greater extent of reactivity between Cu and TTAH and faster adsorption kinetics at elevated temperatures. The sample that was subjected to a room temperature pre-coat of TTAH before immersing in the S- and TTAH-containing oil solution, showed an even higher N content (N/Cu = 4.7) in the film composition as compared to that of the sample without the TTAH pre-coat. However, the N/Cu ratio dropped to 0.1 for the TTAH pre-coated sample that was immersed in S-

containing oil solution devoid of TTAH, which suggested that the TTAH layer was practically destroyed in this case. This leads to the conclusion that the structure, molecular- and chemical-composition of the TTAH adsorption film forming on Cu vary with progressing reaction time.

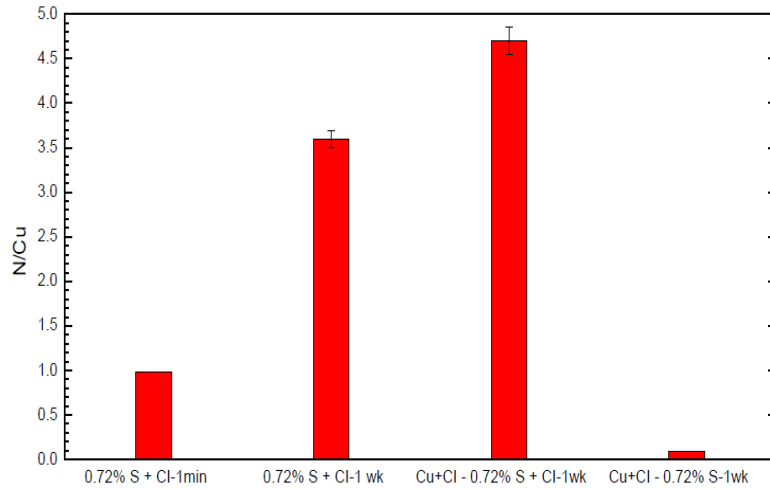


Fig. 4.35: Normalized N content in the Cu surface film formed under different conditions.

For the same set of samples, the  $\text{Cu}_2\text{O}$  in the surface film, measured in terms of normalized O associated with  $\text{Cu}_2\text{O}$ , was inversely correlated to the extent of Cu corrosion by sulfide that these samples had undergone after  $6.05 \times 10^5$  s (1 week) of immersion. There is a strong correlation between O associated with  $\text{Cu}_2\text{O}$ , and N detected on the surface. However, an exception was observed for the samples immersed for  $6.05 \times 10^5$  s (1 week) with, and without the room temperature pre-coat of TTAH. For these two samples, the N/Cu ratio increased from 3.6 to 4.7, whereas the  $\text{O}_{\text{Cu}_2\text{O}}/\text{Cu}$  ratio dropped from 1.2 to 0.8, respectively. Understandably, the decreasing Cu corrosion by sulfide attack with increasing N was also offset for these two samples. The normalized S, associated with sulfide, was  $< 0.05$  for the sample without the room temperature pre-coat

of TTAH as compared to that of 0.15 for the other sample with the pre-coat. In fact, the TTAH pre-coat was able to provide only a nominal protection to the Cu surface from sulfide attack. This was evident from the results for the sample with the initial pre-coat immersed in TTAH free S-containing oil solution for  $6.05 \times 10^5$  s (1 week) that revealed an  $S_{\text{sulfide}}/\text{Cu}$  ratio of 0.4 as compared to that of 0.45 for the sample tested under exactly the same conditions but without any TTAH, at either stage. The above results suggested TTAH to be generally effective in inhibiting sulfide-corrosion of Cu provided an optimized concentration of the inhibitor was maintained in the oil medium, although it allowed preferential oxidation of the Cu surface underneath. It was also clear that the room temperature pre-coat of TTAH made the Cu surface more prone to sulfide attack at  $80^\circ\text{C}$ , which was counter-intuitive.

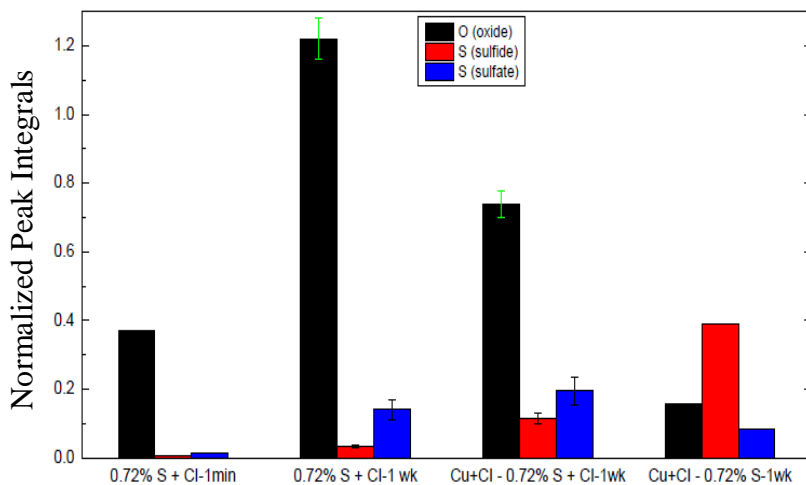
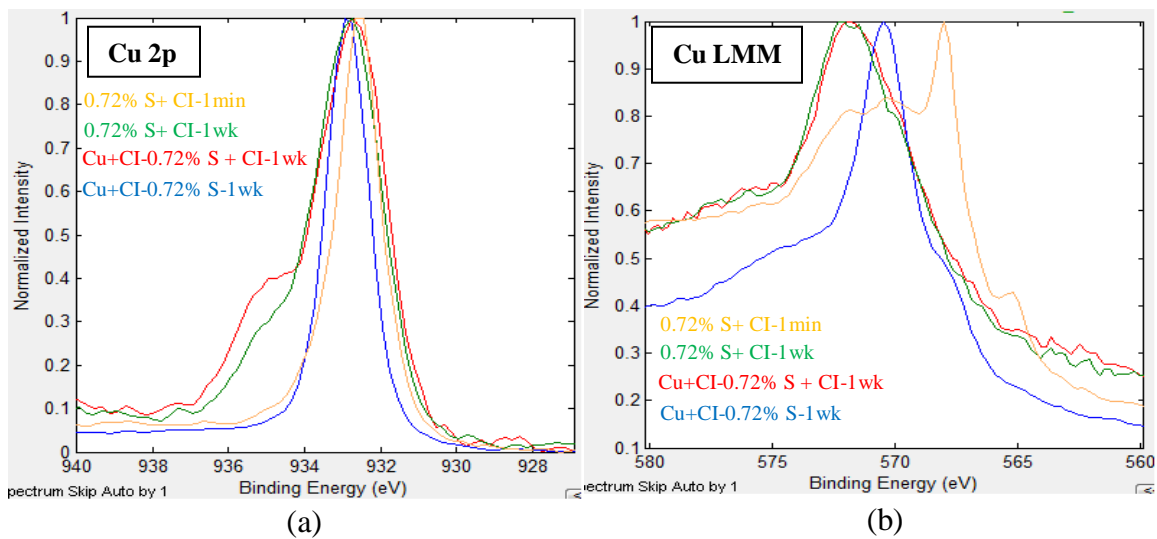


Fig. 4.36: Normalized  $\text{O}_{\text{Cu}_2\text{O}}$ ,  $\text{S}_{\text{Cu}_2\text{S}}$ , and  $\text{S}_{\text{Cu}_2\text{SO}_4}$  content in the Cu surface film formed under different conditions.

To further understand the chemical interactions involving sulfide radicals, TTAH, and dissolved oxygen in the medium with the Cu surface, qualitative peak shape analysis was

carried out for Cu 2p, Cu L<sub>3</sub>M<sub>4,5</sub>M<sub>4,5</sub>, O 1s, N 1s, and S 2p peaks. For this purpose, all these peaks were individually normalized to a scale of 0 to 1 and subsequently, peak respective comparisons were done for each of the four samples considered in this subsection. The comparative photo-electron peak-plots are laid out in Fig. 4.37 except for that of N 1s peak which did not show any noticeable difference from one sample to the other. As shown in Fig. 37 (a), the Cu 2p peak for the two samples – with, and without the room temperature pre-coat of TTAH, immersed in 80°C oil solution containing TTAH for  $6.05 \times 10^5$  s (1 week) revealed a considerable shoulder-peak at a higher BE of 935.1 eV as compared to the corresponding metallic peak at 932.8 eV. This higher BE peak was related to the Cu-N complex formation. For the sample with the TTAH pre-coat, the relative fraction of this peak at 935.1 eV (24 %) was higher than that of the sample without the pre-coat (18 %). The other two samples – immersed in oil solution containing TTAH for 60 s (1 min) without any pre-coat, and pre-coated one immersed in TTAH free oil solution for  $6.05 \times 10^5$  s (1 week), essentially showed the metallic peak only. Considering the Cu L<sub>3</sub>M<sub>4,5</sub>M<sub>4,5</sub> peaks shown in Fig. 4.37 (b), the 60 s (1 min) immersed sample had a predominant peak at 568 eV corresponding to the metallic component of Cu, and two minor peaks at 570 eV, and 572 eV corresponding to Cu<sub>2</sub>O, and Cu-N complex formation, respectively. However, the TTAH pre-coated sample immersed for  $6.05 \times 10^5$  s (1 week) in TTAH free oil solution had the predominant peak at 570 eV corresponding to Cu<sub>2</sub>O, and Cu<sub>2</sub>S, whereas the other two samples – with, and without the pre-coat, immersed for the same length of time in TTAH-containing oil solution, showed largely predominant peaks at 572 eV. Note, for such an extended length of immersion time, both the Cu 2p, and the Cu L<sub>3</sub>M<sub>4,5</sub>M<sub>4,5</sub> peaks underwent considerable

changes in their peak-shapes from room temperature to 80°C immersion, that were representative of a substantially greater extent of Cu-N complex formation at the elevated temperature. The O 1s peak, shown in Fig. 4.37 (c), demonstrated shift in BE from 530.5 eV to 531.6 eV, illustrating chemical predominance shift from Cu<sub>2</sub>O to Cu<sub>2</sub>SO<sub>4</sub> in the following order of samples: 60 s (1 min) immersion in TTAH-containing oil solution, 6.05 x 10<sup>5</sup> s (1 week) immersion in TTAH free oil solution in pre-coated condition, and in TTAH-containing oil solution in absence and presence of pre-coat. As evident from Fig. 4.37 (d), the 60 s (1 min) immersed sample did not show any detectable S peak, whereas sulfate was the predominant form of sulfur present on the samples immersed in TTAH-containing oil solution for 6.05 x 10<sup>5</sup> s (1 week), to a larger extent in case of the uncoated sample. However, for the sample immersed in oil solution devoid of any TTAH, and for the same length of time, sulfide was the primary form of sulfur present on the surface. Thus, it was conclusive that the results from the qualitative peak shape analysis were consistent with the quantitative analysis discussed earlier.



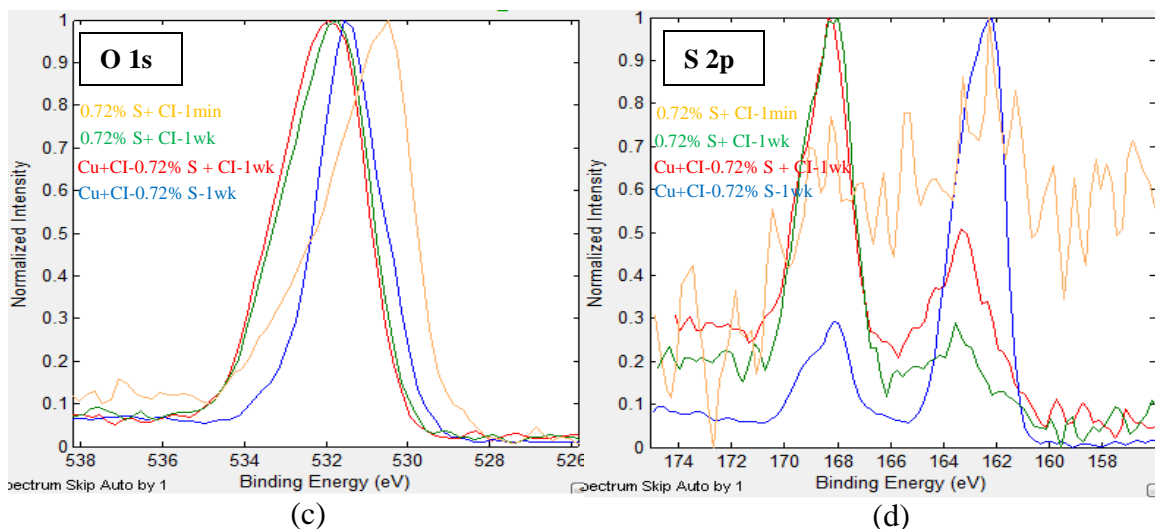


Fig. 4.37: Comparative plots of (a) Cu 2p (b) Cu  $L_{3}M_{4,5}M_{4,5}$  (c) O 1s (d) S 2p peaks acquired on Cu surface films formed under different conditions.

ARXPS was carried out to determine the structure of the corrosion film formed on Cu surface in the presence of TTAH. The objective was to determine the depth-distribution of  $Cu_2O$ ,  $Cu_2S$ ,  $Cu_2SO_4$ , and corrosion inhibitive TTAH layer in the surface film. For this purpose, the variation of the two components of the O 1s peak –  $O_{sulfate}$ , and  $O_{oxide}$ , and the two components of the S 2p peak –  $S_{sulfate}$ , and  $S_{sulfide}$ , were studied with TOA. Fig. 4.38 shows the variation of the de-convoluted O 1s peak with TOA. The relative fraction of the oxide component of this peak increased with increasing TOA, which implied that  $Cu_2O$  was present underneath the  $Cu_2SO_4$  layer.

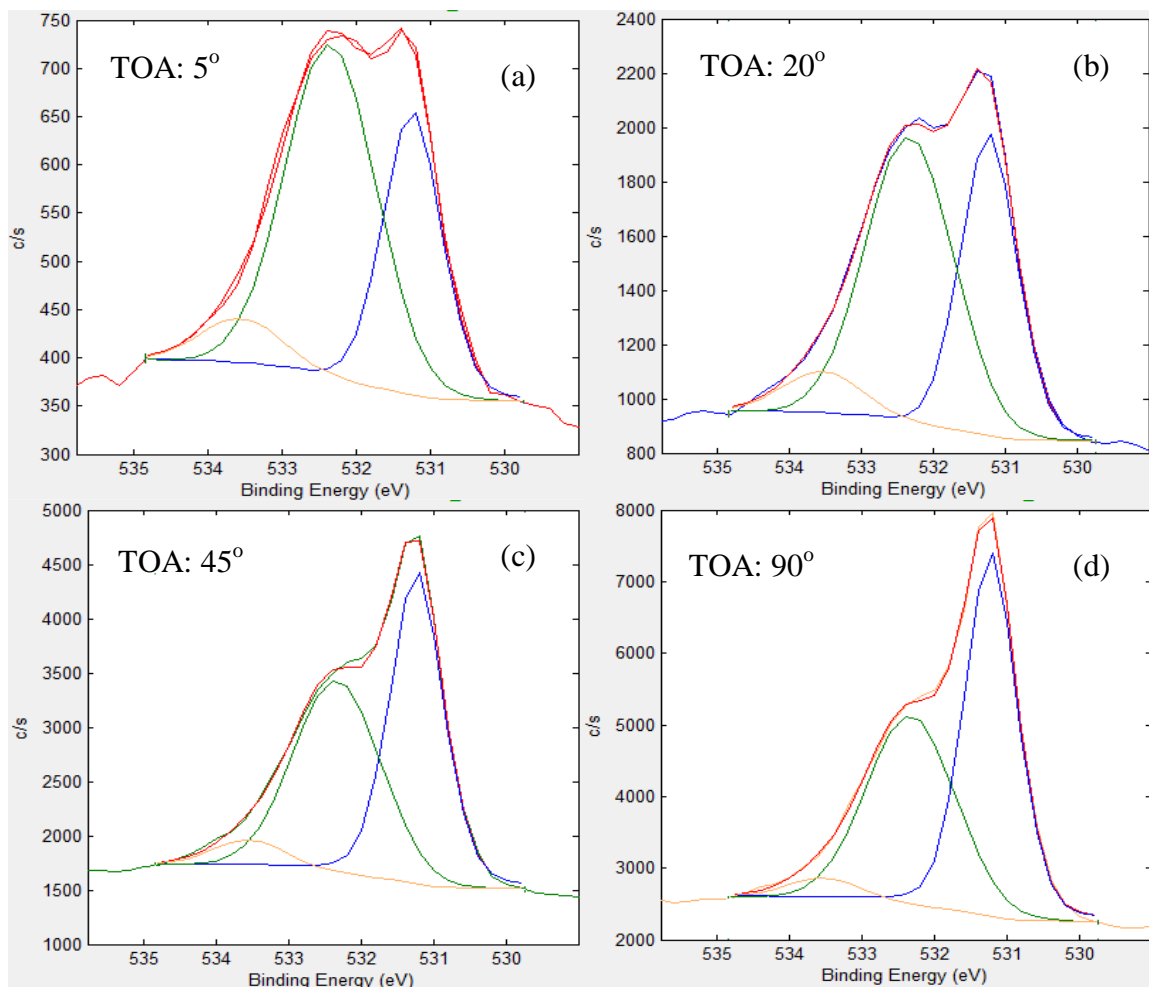


Fig. 4.38: O 1s peak acquired at TOA (a) 5° (b) 20° (c) 45° (d) 90° on a Cu sample surface corroded upon sulfide attack.

For a visual comparison of the S 2p peaks, the sulfide component of the peaks were normalized to a scale of 0 to 1 in respective cases and subsequently, the corresponding sulfate components were compared, as shown in Fig. 4.39. With increasing TOA, the relative fraction of the sulfate peak increased, implying that the  $\text{Cu}_2\text{S}$  layer was formed above the  $\text{Cu}_2\text{SO}_4$  layer.

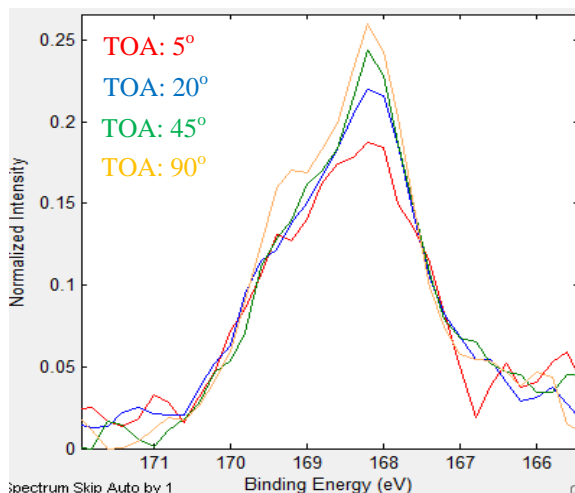


Fig. 4.39: Sulfate component of the S 2p peaks upon normalizing the respective sulfide components acquired at TOA 5°, 20°, 45°, and 90° on a Cu sample surface corroded upon sulfide attack.

Quantitative plots confirming the variations in the relative fractions of the two component peaks of O, and S, respectively with TOA are shown in Fig. 4.40. These plots affirmed the conclusions on the morphology of the corrosion film that were stated earlier. In the same figure, a plot for the  $N/S_{\text{sulfate}}$  ratio is also shown, which decreases with increasing TOA and hence, suggesting that the Cu sulfide-corrosion product layer was formed beneath the TTAH protective layer.

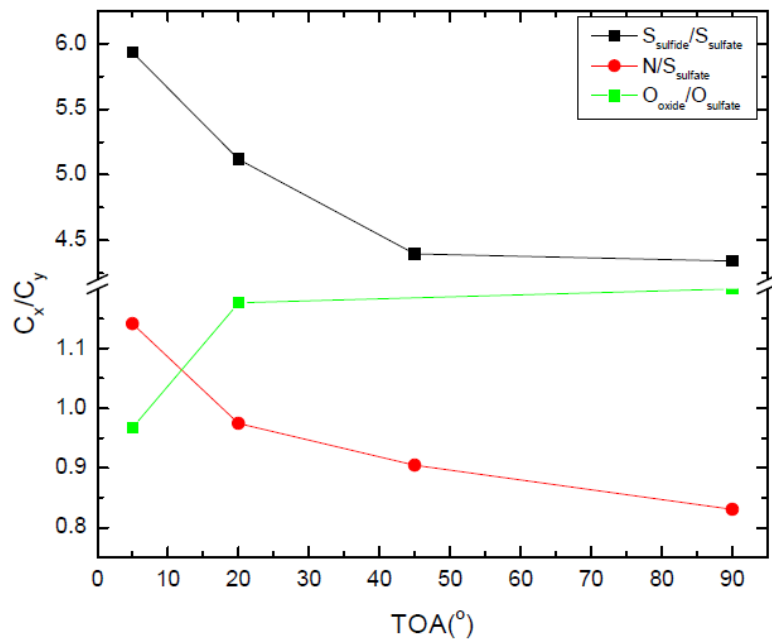


Fig. 4.40: Plots of peak-integral ratio vs. TOA for various elemental peaks acquired on Cu sample surface corroded upon sulfide attack.

Ultimately, based on the above ARXPS results, Fig. 4.41 depicts a schematic for the layered-structure of the surface film formed on the Cu surface undergoing corrosion by sulfide attack in the presence of TTAH corrosion inhibitor.

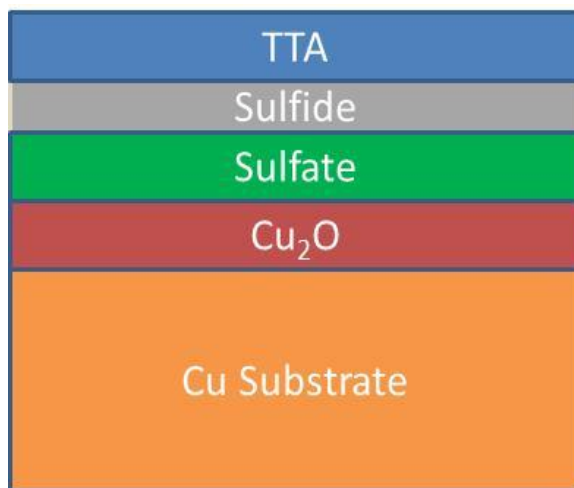


Fig. 4.41: Proposed structure for the corrosion surface film formed on Cu in presence of TTAH.

#### 4.5 O<sup>18</sup> Isotope Tracer Study in ToF-SIMS

This section presents the results on the corrosion study of Cu in S-containing oil solution, carried out by means of ToF-SIMS characterization. This experiment was primarily aimed at understanding the role of the surface oxide. The surface oxide was confirmed to be dynamic in nature and was proven to interact with the S radicals resulting in the formation of Cu<sub>2</sub>SO<sub>4</sub>. The present section also reveals the significant difference in the thickness of the surface films formed at room temperature and 80°C.

In the studied system, there were two sources of oxygen involved – O dissolved in the PAO-2 oil and O from the atmosphere. As suggested by the results presented in the earlier sections of this chapter, the Cu appeared to be oxidized by the O dissolved in the oil. In order to confirm this phenomenon, in the final experiment undertaken in this PhD project, a Cu sample with pristine surface was immediately oxidized in O<sup>18</sup> atmosphere at 80°C for 3600 s (1 h). This operation was carried out in a specially designed furnace capable of producing a vacuum chamber that could be flooded with a desired gas at a controlled flow rate. The resultant sample was characterized in XPS to reveal a predominantly Cu<sub>2</sub>O surface. A similarly oxidized sample was then immediately immersed in 0.01 wt. % TTAH and 0.72 wt. % S-containing oil for 6.05 x 10<sup>5</sup> s (1 week). Subsequently, a depth-profile characterization in ToF-SIMS was carried out on this sample, the results for which are shown in Fig. 4.42 through Fig. 4.44. Fig. 4.42 shows the depth-profiles for the ionic species that identify the TTAH adsorption film formed on Cu, whereas Fig. 4.43 shows the same for the ionic species identifying the Cu corrosion

products –  $\text{Cu}_2\text{S}$ , and  $\text{Cu}_2\text{SO}_4$ . Finally, Fig. 4.44 shows the depth-profile characteristic to the  $\text{Cu}_2\text{O}$  layer.

The  $[\text{TTA}]^-$  depth-profile shown in Fig. 4.42 (a) showed an identical pattern to that described in section 4.2 dealing with a  $8.64 \times 10^4$  s (24 h) immersion sample at room temperature. The only major difference was that in the present case, the depth-profile for the  $[\text{TTA}]^-$ , based on its normalized peak-integral, reached an asymptotic value after sputtering for  $\approx 2000$  s, whereas for the room temperature sample, it took only  $\approx 125$  s of sputtering for the same to happen. For  $[\text{Cu}(\text{CN})_2]^-$ , shown in Fig. 4.42 (b), the normalized peak-integral depth-profile showed a monotonous gain up to 10080 s (2.8 h) of sputtering. In comparison, the same for the room temperature treated sample decreased consistently for the first 60 s of sputtering, followed by an inflection and hence, increasing monotonously up to 360 s, beyond which, it decayed to negligible values by  $\approx 900$  s of sputtering. This led to the conclusion that the TTAH adsorption layer, based on the  $[\text{TTA}]^-$  depth-profile, was at the least 16 times thicker upon immersion at  $80^\circ\text{C}$  for  $6.05 \times 10^5$  s (1 week) as compared to  $8.64 \times 10^4$  s (24 h) immersion at room temperature. This in turn meant a conservative estimate of 40 nm TTAH adsorption film under the presently considered conditions. However, based on the  $[\text{Cu}(\text{CN})_2]^-$  depth-profile, the adsorption film was estimated to be at least 70 nm. Moreover, in the present case, extremely low yields for the higher-order ion-clusters, like  $[\text{TTA}_2\text{Cu}]^-$ , were observed. The  $[\text{TTA}_2\text{Cu}]^-/[\text{TTA}]^-$  depth-profile was plotted as shown in Fig. 4.42 (c), revealing an increasing pattern with sputtering time. Note that in the present case, this ratio was in the range of 0.02 to 0.08, which was an order of magnitude smaller than that of the typically

observed values at the surface of the room temperature treated samples. For the latter samples, this ratio was in the range of 0.5 to 1.1 at the very surface. This led to the conclusion that at 80°C the TTAH adsorption film showed lower polymerization tendency as compared to that of room temperature. However, due to extremely low counts of  $[\text{TTA}_2\text{Cu}]$ , no other conclusions were drawn from the  $[\text{TTA}_2\text{Cu}]/[\text{TTA}]$  depth-profile.

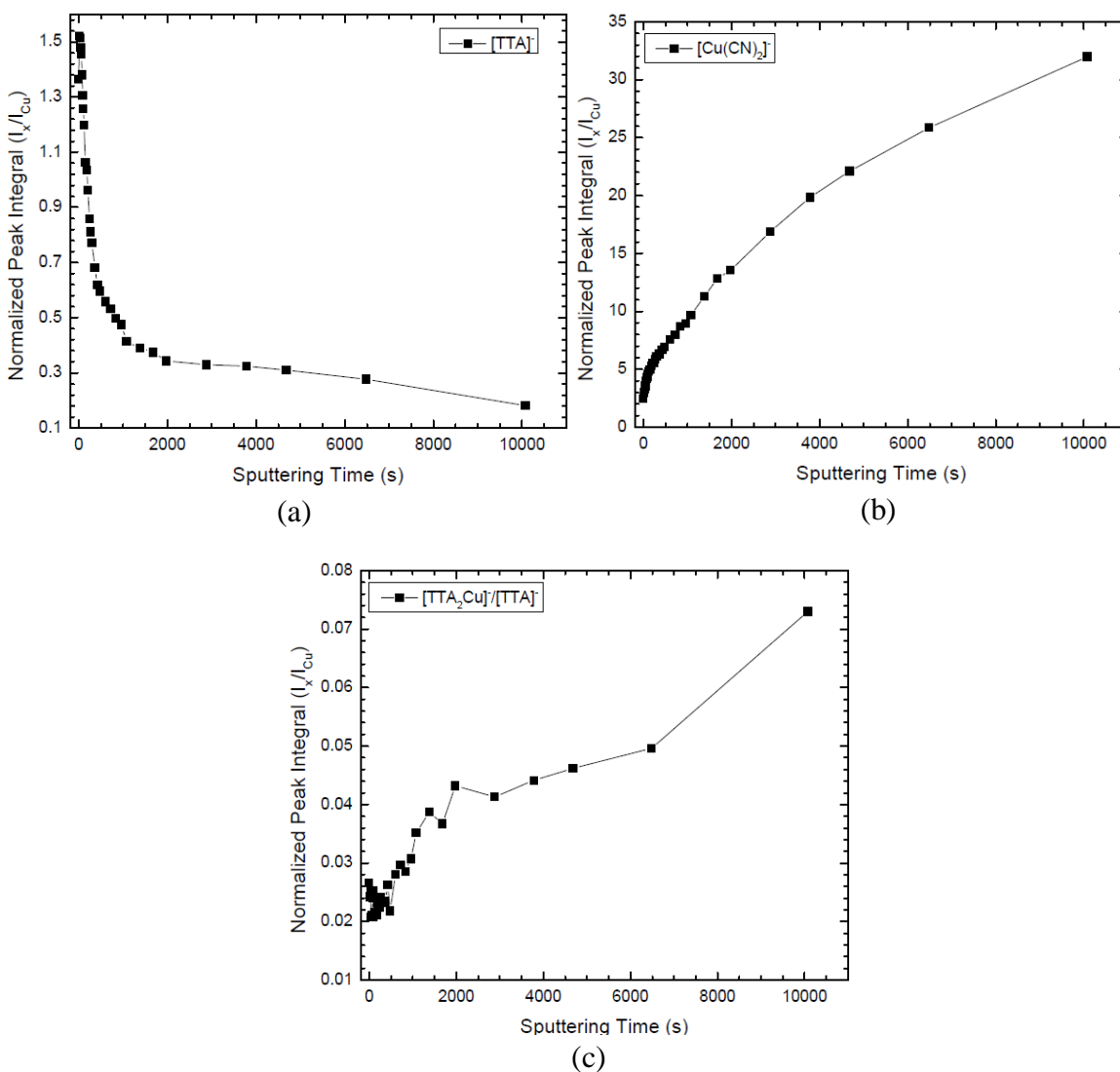


Fig. 4.42: Sputter depth-profiles for SI fragments relevant to TTAH adsorption film formed upon  $6.05 \times 10^5$  s (1 week) immersion in TTAH- and S-containing oil at 80°C.

Fig. 4.43 (a), and (b) show the depth-profiles for  $[\text{CuS}]^-$ , and  $[\text{SO}_4]^-$ , respectively. The normalized peak-integral for  $[\text{CuS}]^-$  monotonously increased from 0.07 to 0.7 in the entire range of sputtering time – 0 s to 10080 s. This was consistent with the fact that the  $\text{Cu}_2\text{S}$  layer was underneath the TTAH adsorption layer, as revealed by XPS results presented in section 4.4. The sulfate depth-profile is shown for two distinct ionic species –  $[\text{SO}^{16}_4]^-$ , and  $[\text{SO}^{18}_4]^-$ . Evident from Fig. 4.43 (b), the deeper zones of the  $\text{Cu}_2\text{SO}_4$  layer, closer to the Cu substrate, were richer in the  $\text{O}^{18}$ , whereas the upper regions, closer to the free surface, were richer in the  $\text{O}^{16}$ . This revealed two important facts regarding the chemical interactions involved in the formation of the surface film. Firstly, the initial  $\text{Cu}_2\text{SO}_4$  in the deepest zone was formed by the interaction of S with the  $\text{Cu}_2\text{O}$  layer and the O in the  $\text{Cu}_2\text{SO}_4$  was supplied by  $\text{Cu}_2\text{O}$ . Hence, the  $\text{Cu}_2\text{SO}_4$  layer must have formed at the expense of the  $\text{Cu}_2\text{O}$  layer on the very same interface. This, in turn, implied that the former should be below the  $\text{Cu}_2\text{S}$  layer, as already established by ARXPS results in section 4.4. Secondly, a comparable yield of the  $[\text{SO}^{16}_4]^-$  suggested that the sulfate ions were also formed due to interaction with O dissolved in the oil. This proved the dissolved O in the oil to be an active chemical reagent participating in the dynamic chemical reactions undergoing in the surface film.

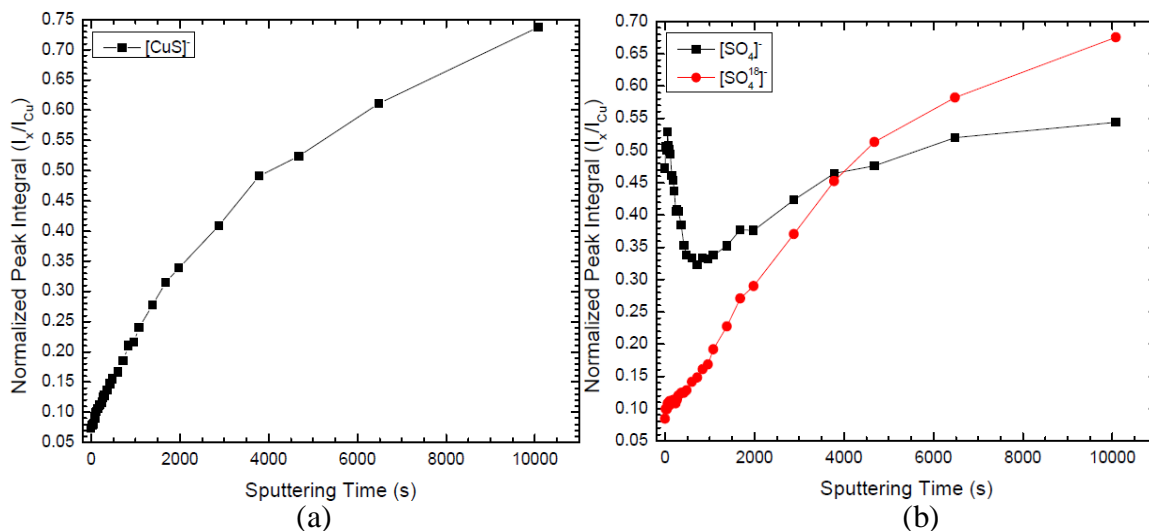


Fig. 4.43: Sputter depth-profiles for SI fragments relevant to Cu sulfide corrosion products formed upon  $6.05 \times 10^5$  s (1 week) immersion in TTAH- and S-containing oil at  $80^\circ\text{C}$ .

Ultimately, Fig. 4.44 shows the depth-profiles for  $[\text{CuO}^{16}]^-$ , and  $[\text{CuO}^{18}]^-$ . Again, both these profiles showed monotonously increasing behavior with sputtering time, which was consistent with the fact that the  $\text{Cu}_2\text{O}$  was the deepest surface layer, present immediately above the metallic Cu substrate. Note, the  $[\text{CuO}^{16}]^-$  to  $[\text{CuO}^{18}]^-$  ratio was approximately 1:1 in the entire span of depth-profiling – up to 10080 s of sputtering. The comparative value for the same ratio was recorded to be 1:3 on a freshly oxidized sample in controlled  $\text{O}^{18}$  atmosphere. This again illustrated the dynamic nature of the oxide layer by confirming the formation of fresh  $\text{Cu}_2\text{O}$  while the Cu sample was immersed in the oil. Thus, it was established that the dissolved O in the oil played an active role to support the undergoing chemical reactions in the surface film formed over the Cu foil.

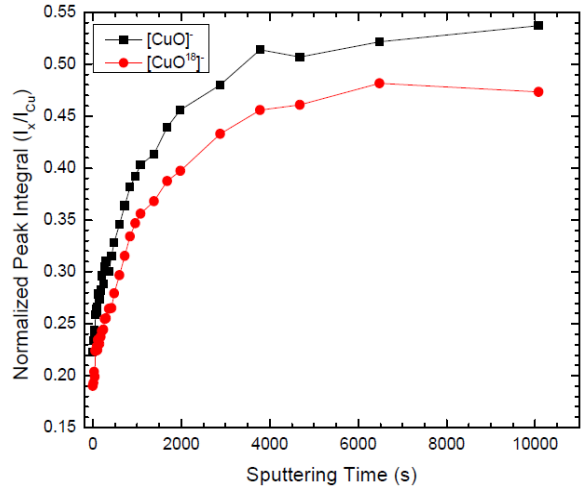


Fig. 4.44: Sputter depth-profiles for SI fragments characteristic to Cu<sub>2</sub>O layer formed upon  $6.05 \times 10^5$  s (1 week) immersion in TTAH- and S-containing oil at 80°C.

In light of all the results presented in this chapter, the following chapter attempts to rationalize the microscopic mechanisms for TTAH adsorption film formation on Cu, and the protection that it provides against sulfide attack, in perspective to known facts from the published literature.

## Chapter 5

### Discussion

This chapter focuses on unifying all the experimental results presented in the previous chapter, to put forward a microscopic mechanism for the growth of the TTAH adsorption-film formed on the Cu surface, and explain how it protects the Cu surface from corroding in sulfide solution. The hence proposed mechanisms are then validated with respect to the observations reported in the literature.

#### 5.1 TTAH Adsorption-Film Formation Mechanism

The results presented in section 4.1.3 established that neither of the two solvents – PAO-2 oil, and bis(2-ethylhexyl) phthalate, adhere to the pristine Cu surface. Hence, in the absence of butyl-sulfide radicals, only two chemical entities in the presently studied system – O dissolved in the oil and TTAH – have the affinity to bond with the pristine Cu surface upon immersion. Results from sections 4.1.3, and 4.2.2 prove that the O dissolved in the oil oxidizes the pristine Cu surface to  $\text{Cu}_2\text{O}$ , both in the absence and presence of TTAH. Additionally, results from section 4.3 establish that the pristine Cu surface instantaneously reacts with both O and TTAH to form  $\text{Cu}_2\text{O}$  and TTAH-Cu complex, respectively. This leads to the conclusion that the kinetics of these two reactions proceed at comparable rates. However, as illustrated in Fig. 4.27 through Fig. 4.29, there is a net growth in the TTAH adsorption-film over an immersion time of 0.6 Ms (1 week), whereas the  $\text{Cu}_2\text{O}$  layer, formed in the initial stages of immersion, tends to decompose

over longer immersion times. This has two implications, proven that, the thickness of the surface film formed on Cu is always less than the depth of analysis in XPS, in the range of tested immersion times at room temperature:

- The TTAH-Cu-complex-forming reaction is favored with progressing immersion time. This, in turn, impedes the oxidation of Cu to Cu<sub>2</sub>O.
- The Cu associated with the initially formed Cu<sub>2</sub>O transforms to the TTAH-Cu complex.

The former can be explained on the following basis. As the TTAH-Cu complex formation proceeds with time, it provides a physical barrier to the availability of O at the Cu surface. However, the complex structure of this film is open enough to allow diffusion of O through it. This results in continued oxidation of the Cu, although at a progressively reduced rate with increasing thickness of the TTAH-Cu surface film. The second implication is indicative of the fact that the stability of Cu<sub>2</sub>O and TTAH-Cu complex, i.e., the Gibbs free energy of formation ( $\Delta G_f^\circ$ ) for these two products must be in a similar range, and room temperature is sufficient to provide the activation energy required for such a transformation reaction. It is known that  $\Delta G_f^\circ$  of Cu<sub>2</sub>O is  $\approx -70$  kJ/mol of Cu. Note, typical  $\Delta G^\circ$  of chemisorption reactions are  $< -40$  kJ/mol [Umo08].

In context to the present discussion in this section, Fig. 5.1 shows a schematic outlining the surface film formation mechanism.

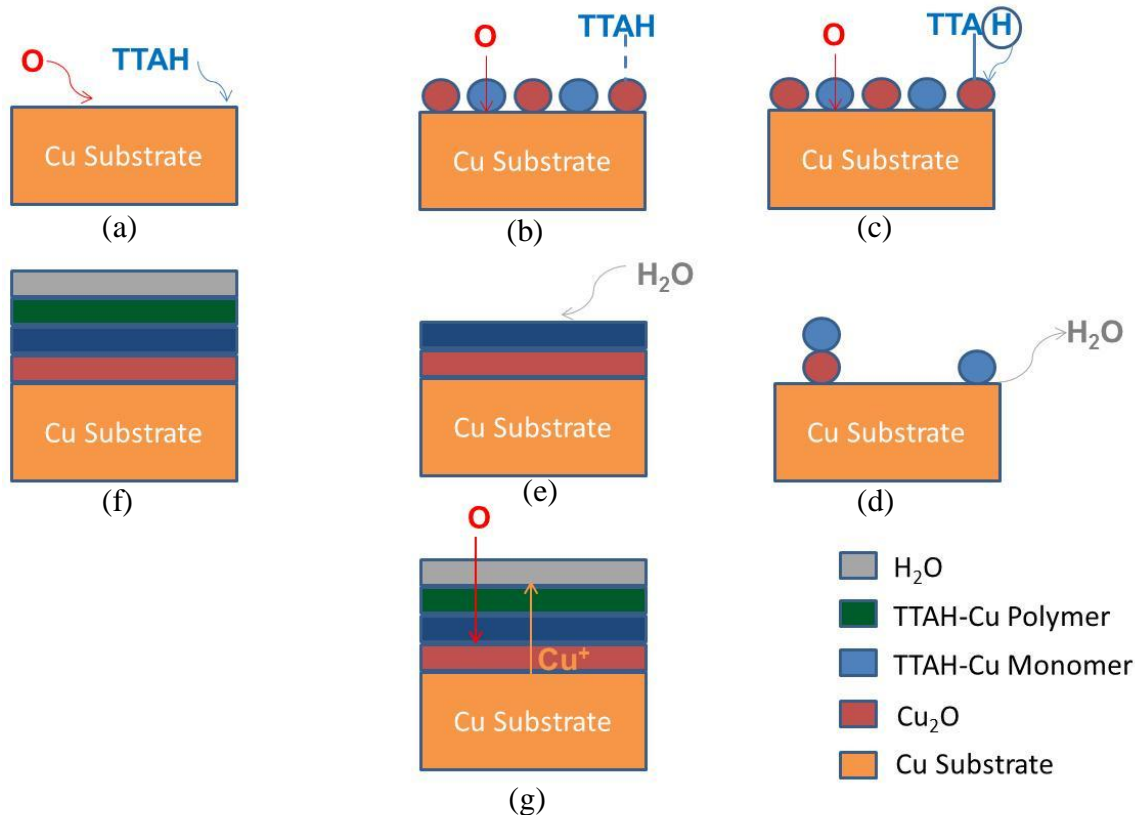


Fig. 5.1: Schema of the surface film formation mechanism. (a) Pristine Cu surface immersed in oil. (b) Initial formation  $\text{Cu}_2\text{O}$  and TTAH-Cu complex on the surface. (c) Interaction of TTAH with  $\text{Cu}_2\text{O}$ . (d) Continued formation of  $\text{Cu}_2\text{O}$  under-layer and simultaneous growth of TTAH-Cu at the expense of  $\text{Cu}_2\text{O}$ . (e) Development of uniform TTAH adsorption layer and  $\text{Cu}_2\text{O}$  under-layer. (e) Polymerization of top layer of the TTAH-Cu complex. (f) Diffusion current of O and  $\text{Cu}^+$  through various layers of surface film sustaining the formation of  $\text{Cu}_2\text{O}$  and TTAH-Cu complex

The time-dependent surface film composition profiles, shown in Fig. 4.27 through Fig. 4.29, reveal compositional fluctuations, especially significant in the early stages of film growth. This is characteristic of mechanism involving competing reactions – oxidation of Cu to  $\text{Cu}_2\text{O}$ , and formation of TTAH-Cu complex, in the present case. This is in agreement to the observation made by Levin *et al.*, that ellipsometry data on TTAH film growth on Cu surface required at least two time-constants to mathematically fit the experimental data <sup>[Lev07]</sup>. Such compositional fluctuations (near perfect oscillations in

extreme cases) can arise for systems that are sufficiently far from the state of thermodynamic equilibrium, and involve competing reactions with different rates. Such reactions are broadly classified as *chemical clock reactions*, of which *Belousov-Zhabotinsky*, and *Briggs-Rauscher* reactions are the most widely studied [Bel59], [Zha64], [Bri73]. These systems lead to the establishment of non-linear oscillators far from thermodynamic equilibrium for which a number of theoretical models have been developed including Lotka-Volterra model [Lot25], [Vol31], the Brusselator [Pri10], and the Oregonator [Fie07]. In fact, in the literature, Cu complexes have been reported to show such behavior in the presence of oxidants [Hux03]. In the present case, the recorded compositions are in reality average compositions over 300  $\mu\text{m}$ -diameter spot. This indicates that the compositional fluctuations are not a localized effect and imply significant lateral interactions of atoms and molecules with their neighbors.

In the course of the present project, it was established that the surface film is multi-layered – Cu substrate /  $\text{Cu}_2\text{O}$  / TTAH-Cu complex / polymerized TTAH-Cu complex. The schematic of the same is shown in Fig. 4.26. However, it is unlikely for the TTAH molecules in the oil medium to be transported to the  $\text{Cu}_2\text{O}/\text{Cu}$  surface, across the self-barrier of the initially formed layer of the TTAH-Cu complex. Hence, it is comprehended that the  $\text{Cu}^+$  from the Cu/ $\text{Cu}_2\text{O}$  interface diffuses outward through the  $\text{Cu}_2\text{O}$  and the TTAH-Cu layer to the TTAH-Cu/oil-medium interface, where it reacts with the TTAH molecules present in the oil to sustain the growth of the TTAH-Cu surface film. Simultaneously, O dissolved in the oil diffuses inwards through the TTAH-Cu layer to the TTAH-Cu/ $\text{Cu}_2\text{O}$  interface. A fraction of the outward diffusing  $\text{Cu}^+$  interacts with the

inward diffusing O to form  $\text{Cu}_2\text{O}$  at the intermediate TTAH-Cu/ $\text{Cu}_2\text{O}$  interface, depending upon the relative availability of the two species, and the corresponding reaction kinetics. The rest of the  $\text{Cu}^+$  makes its way through the existing TTAH-Cu layer to form new layers of the same. This diffusion model is based on the prior-established fact regarding the growth-mechanism of  $\text{Cu}_2\text{O}$ , that the outward-diffusion of Cu atoms through  $\text{Cu}_2\text{O}$  is the rate determining step <sup>[Zhu06]</sup>. The above discussed model explains the results on the structural analysis of the surface film, presented in section 4.2, showing that the  $\text{Cu}_2\text{O}$  layer was formed underneath TTAH-Cu layer.

In ToF-SIMS, all the intact molecular peaks related to TTAH were detected in the de-hydrogenated form –  $[\text{TTA}]^-$ ,  $[\text{TTA Cu (CN)}]^-$ ,  $[\text{TTA}_2\text{Cu}]^-$ , etc. However, in ToF-SIMS, non-equilibrium conditions prevail in the time-frame of the ion-flights. This does not allow the conclusive determination of the exact form of existence of the TTAH molecules in the adsorption-film – with or without the loss of  $\text{H}^+$ . Nevertheless, the total absence of all possible TTAH related peaks with the H intact –  $[\text{TTAH Cu (CN)}_2]^-$ ,  $[\text{TTAH TTA}_2\text{Cu}]^-$ , etc., suggests that TTAH forms complex with Cu in a de-hydrogenated form. This is in agreement with the results from the DFT study that showed higher bonding energy for chemisorption of  $\text{TTA}^-$  on Cu (111) as compared to that of TTAH <sup>[Kok10]</sup>. However, since PAO-2 oil is a non-polar solvent, the  $\text{H}^+$  released upon formation of TTAH-Cu complex bonds with the available O to form  $\text{H}_2\text{O}$ . This  $\text{H}_2\text{O}$  adsorbs on top of the TTAH-Cu layer, as detected in the XPS characterization of the surface film presented in section 4.2. The approximate surface concentration of the O associated with  $\text{H}_2\text{O}$  was  $\approx 10$  at. %, suggesting the presence of 1-2 molecular layers of  $\text{H}_2\text{O}$  atop.

Both XPS and ToF-SIMS results, presented in section 4.2, suggest the existence of two distinct layers in the TTAH adsorption-film. The two layers are inferred to have distinct configurations that give rise to the difference in their N 1s photo-electron binding energy (BE) in XPS, and their respective fragmentation behavior in ToF-SIMS. The top layer showed fractionally higher BE (401 eV) for N 1s photo-electrons as compared to that of the lower layer (400 eV). This is consistent with the former being a polymeric layer, and the latter a monomeric layer as the N electrons are expected to be bound tighter upon polymerization. In ToF-SIMS, the underlying monomeric layer predominantly fragmented into relatively smaller secondary-ion species. This indicates that the physical orientation of this layer is such, that it has an effectively higher projected surface area exposed to the primary-ion beam than the other layer. Thus, it is inferred that the polymeric layer, atop, has a vertical orientation, whereas the monomeric layer, underneath, has a flatter orientation with respect to the Cu surface. Fig. 2.1 refers to a vertical orientation, whereas Fig. 2.2 refers to a flat/parallel orientation. This inference on the molecular orientation of the two layers is speculative and needs more careful consideration. The orientation sensitivity of the fragmentation behavior in ToF-SIMS, for adsorbed organic molecules, can be validated by studying the fragmentation behavior of 2,5-diphenyl-1,3,4-oxadiazole (PPD) molecules adsorbed on Cu(111) that show a sharp transition in their orientation – flat to vertical with increase in surface coverage. Xue *et al.* suggested a plausible structure for the BTAH-Cu polymeric complex, which is shown in Fig. 5.2 <sup>[Xue91]</sup>.

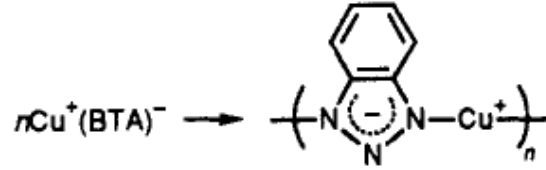


Fig. 5.2: BTAH-Cu polymeric film structure suggested by Xue *et al.* [Xue91]

Conceptually, the structure for TTAH-Cu polymeric complex is expected to be alike that of BTAH-Cu. In this structural arrangement, each  $\text{TTA}^-$  ion is attached to two  $\text{Cu}^+$  ions, and vice versa. Fig. 4.30 illustrated that the initial phase of TTAH adsorption-film formation is dominated by polymeric film growth, whereas beyond 1.2 Ks (20 min) of immersion, it is dominated by the monomeric film growth. As proven earlier, the polymeric film is morphologically on top, and assuming that the TTAH molecules in the oil-medium cannot diffuse through the self-formed barrier of pre-existing TTAH-Cu polymeric film to continue reacting with Cu, there must be reversibility between the polymerized and non-polymerized film layers. The observations made in sections 4.2 and 4.3 are best explained if the TTAH-Cu monomer layer forms first and subsequently the near oil-interface region of this film gets transformed to a polymerized layer. Hence, in the initial phase of film growth, a larger fraction of the TTAH adsorption-film is in the polymerized state, thus explaining the observed rapid growth in the polymerized layer in this time-phase. However, beyond a certain stage of growth, the monomeric configuration of TTAH-Cu complex is stabilized and it appears that the TTAH-Cu polymeric film undergoes a reversal to the monomeric state.

The depth of analysis ( $d$ ) in XPS is given by  $d = 3\lambda \sin\theta$  (5.1), where  $\lambda$  is the IMFP (inelastic mean free path), and  $\theta$  is the TOA of the photo-electrons. With  $\theta$  being  $45^\circ$  and

$\lambda$  for Cu 2p photo-electrons  $\approx 2\text{nm}$ ,  $d$  is  $\approx 4\text{nm}$ . Moreover, it was established in section 4.2 that the TTAH adsorption-film thickness was  $\approx 2.5\text{ nm}$  after 86.4 Ks (24 h) of immersion at room temperature. This implies that the XPS data was representative of the entire thickness of the surface film. This is confirmed by the distinctly visible component of metallic Cu in the Cu  $L_3M_{4,5}M_{4,5}$  peak at 568 eV, for all immersion times up to 0.6 Ms (1 week) at room temperature. In ToF-SIMS, the  $C_{60}^+$  ion-beam sputter rate through this surface film was calibrated to be  $\approx 7\text{ pm/s}$  for  $500\text{ }\mu\text{m} \times 500\text{ }\mu\text{m}$  raster area. This calibration of sputtering rate implies that the thickness of the polymerized layer, on top, is  $\approx 0.9\text{ nm}$  as compared to that of  $\approx 1.7\text{ nm}$  for the non-polymerized lower layer, after 86.4 Ks (24 h) of immersion at room temperature. Assuming a vertical orientation of the TTAH molecule axis, the polymerized layer consists of 1-2 molecular layers of TTAH under the same conditions.

### *5.1.1 Effect of Temperature*

Sections 4.4 and 4.5 established that the rate of TTAH adsorption-film formation is much higher at an immersion temperature of  $80^\circ\text{C}$  than at room temperature. The N/Cu ratio after 60 s (1 min) in the former case was recorded to be 1 (Fig. 4.35), as compared to 0.5 at room temperature (Fig. 4.27). The value for the same parameter after 0.6 Ms (1 week) of immersion was recorded to be 3.6 and 1.8, respectively. Note, the film thickness after 60 s (1min) immersion at  $80^\circ\text{C}$  is less than the depth of analysis ( $d$ ) in XPS, whereas after 0.6 Ms (1 week), it is  $\gg d$ . This is substantiated by the results shown in Fig. 4.37 (b), as the metallic component of the Cu  $L_3M_{4,5}M_{4,5}$  peak that was predominant after 60 s

(1 min) immersion completely disappeared after 0.6 Ms (1 week). The increased kinetics of surface film growth is explained in terms of faster formation, and diffusivity of  $\text{Cu}^+$  at  $80^\circ\text{C}$ . As the rate of availability of  $\text{Cu}^+$  at the TTAH-Cu/oil-medium interface increases, the rate of film formation escalates. This explains the typical observation of thicker adsorption films in polar solvents, based on the higher rate of extraction of  $\text{Cu}^+$  from the metallic substrate. The ToF-SIMS data presented in Fig.4.42 leads to a conservative estimate of  $\approx 70$  nm for the TTAH adsorption-film thickness after 0.6 Ms (1 week) immersion at  $80^\circ\text{C}$ . This is in agreement with the XPS data, which reveals a film thickness  $\gg d$ . Moreover, the TTAH adsorption film shows lower tendency to polymerize at  $80^\circ\text{C}$ , implying that the monomer configuration of the TTAH-Cu complex is more stable at elevated temperatures.

## **5.2 Mechanism for Protection against Corrosion of Cu in Sulfide Solution**

In section 4.4, it was shown that the presence of a thick TTAH adsorption-film leads to the formation a substantial oxide layer while protecting the surface from sulfide attack. This indicates that  $\text{O}$  can infiltrate through the adsorption-film, whereas the butyl-sulfide radical cannot. This is attributed to the size difference between the two species. The butyl-sulfide radical, being much bigger in size, is screened off by the steric hindrance of TTAH-Cu complex film. Therefore, the mechanism of protection against corrosion in sulfide solution is the formation of an effective physical barrier by TTAH and not surface passivation by means of blocking active sites on the Cu surface.

In section 4.4, the composition of the TTAH adsorption-film was established to be changing with time. The sample with a room-temperature pre-coat of TTAH (Fig. 4.36), immersed in S-containing oil without TTAH underwent corrosion comparable to that observed for the sample without TTAH coating (Fig. 4.34), although the extent of corrosion was fractionally lower in the former case. Moreover, in the absence of any TTAH reinforcement, the TTAH pre-coat was nearly completely decomposed in the S-containing oil. The N/Cu ratio at the sample surface was  $\approx 1$  after the formation of the room-temperature pre-coat of TTAH. However, upon subsequent immersion into S-containing oil without any TTAH for 0.6 Ms (1 week), it dropped down to 0.1. Such drastic reduction in the N fraction indicates to substantial desorption of TTAH in the latter case, and the Cu bonded to TTAH transforms to sulfide/oxide. The overall surface film thickness in this case is  $\gg d$ , but the TTAH-Cu film is the top most layer with thickness  $< d$ .

There are two differences between the samples with and without TTAH pre-coat, immersed in S-, and TTAH- containing oil for 0.6 Ms (1 week). As illustrated by Fig. 4.35, and Fig. 4.36, in the prior case, a higher value for the N/Cu ratio was observed at the surface, but this sample also underwent more considerable corrosion by sulfide attack. For these samples, a higher N/Cu ratio does not imply a thicker TTAH adsorption-film because the film thickness is  $\gg d$ . Instead, it means that the TTAH adsorption-film for the sample without the TTAH pre-coat, having lower N/Cu ratio, was richer in  $\text{Cu}^+$  ions. This, in turn, means that the TTAH adsorption-film on this sample is expected to have higher density, or in other words, a more closely packed structure as compared to

the other sample. This leads to a better physical barrier to the infiltration of the butyl-sulfide radicals on the sample without the TTAH pre-coat, which in turn, explains the second difference between these two samples, namely that the one showing lower N/Cu ratio experienced lower corrosion by sulfide attack. These observations indicate that the presence of the room-temperature pre-coat of TTAH must be modifying the surface potential of the Cu substrate such that the  $\text{Cu}^+$  formation is suppressed.

From the ARXPS results shown in Fig. 4.40, it was established that  $\text{Cu}_2\text{SO}_4$  forms below the  $\text{Cu}_2\text{S}$  layer. This suggests that the formation of  $\text{Cu}_2\text{SO}_4$  is the initiating step of Cu corrosion by sulfide radicals. This can be explained on the basis that the initial sulfide radicals that penetrate through the TTAH adsorption-film come in contact with the  $\text{Cu}_2\text{O}$  surface. At this interface, the sulfide radicals react with the  $\text{Cu}_2\text{O}$  to form  $\text{Cu}_2\text{SO}_4$ . Note,  $\Delta G_f^\circ(\text{Cu}_2\text{SO}_4) \ll \Delta G_f^\circ(\text{Cu}_2\text{S})$ , i.e.,  $\text{Cu}_2\text{SO}_4$  is thermodynamically a more stable product than  $\text{Cu}_2\text{S}$ . But beyond a certain stage of growth in  $\text{Cu}_2\text{SO}_4$ , for the sulfide corrosion to proceed,  $\text{Cu}^+$  ions have to diffuse through the  $\text{Cu}_2\text{SO}_4$  layer where they encounter the sulfide radicals, consequently forming  $\text{Cu}_2\text{S}$ . The optimized value of the  $\text{Cu}_2\text{SO}_4$  layer thickness is determined by the comparative diffusion rates of the  $\text{Cu}^+$  through the  $\text{Cu}_2\text{O}$ , and  $\text{Cu}_2\text{SO}_4$  layers from the  $\text{Cu}/\text{Cu}_2\text{O}$ , and  $\text{Cu}_2\text{O}/\text{Cu}_2\text{SO}_4$  interfaces, respectively to reach the  $\text{Cu}_2\text{SO}_4/\text{Cu}_2\text{S}$  interface. Ideally, the diffusion rate of the sulfide radical through the  $\text{Cu}_2\text{SO}_4$  layer in the opposite direction to that of  $\text{Cu}^+$  should also play a role, but it can be fairly assumed that owing to its size, the sulfide radical has a much lower diffusivity as compared to  $\text{Cu}^+$  and hence, the overall reaction is governed by the diffusivity of the  $\text{Cu}^+$ . This explains the relative predominance of  $\text{Cu}_2\text{S}$  over  $\text{Cu}_2\text{SO}_4$  in the corrosion product

even though the latter is thermodynamically more stable. The results from the ToF-SIMS study involving the  $O^{18}$  isotope, presented in section 4.5, substantiated this model by confirming that the O associated with the  $Cu_2O$  surface oxide is significantly transferred to  $Cu_2SO_4$ . In Fig. 4.43 (b), the initial drop in the  $[SO_4^{16}]^-$  is likely to be related to the  $Cu_2SO_4$  formed by the oxidation of the prior-formed  $Cu_2S$  nearer to the free surface, as a result of exposure to the atmosphere or as an action of the O dissolved in the oil.

### **5.3 Validation of the Proposed Mechanism against Observations Reported in the Literature**

This section attempts to rationalize the presently proposed mechanisms in perspective to the observations related to both BTAH-, and TTAH- Cu systems, cited in the literature. The present project revealed that the surface film reactions are far from thermodynamic equilibrium. They are transport-controlled. The controlling factors are the diffusivity of O, and sulfide radicals through the TTAH-Cu complex,  $Cu_2S$ , and  $Cu_2SO_4$  layers and diffusivity of  $Cu^+$  in the opposite direction through the same layers along with that in  $Cu_2O$ . This explains the commonly reported effects of the surface oxides on the BTAH, and TTAH adsorption-film formation on Cu <sup>[Lev07], [Xue91]</sup>. The limiting factor is the rate of availability of  $Cu^+$  for reacting with BTAH, or TTAH, which is lower in the presence of  $Cu_2O$ , leading to the formation of a less effective BTAH-, TTAH- Cu adsorption-film. This is in agreement with the fact that in aqueous medium, the BTAH adsorption-film has a higher corrosion resistance when tested on pristine Cu surface than that of  $Cu_2O$  <sup>[Xue91]</sup>. The presently proposed mechanism also explains the observation that in oily medium, a thinner TTAH adsorption-film on furnace-oxidized CuO surface as compared to that on a

mechanically polished Cu surface <sup>[Lev07]</sup>. This effect of O and surface-oxides may be better illustrated by considering further experiments in the future, involving O, and Ar purged immersion, at various flow rates. The mechanism put forward in the present work is also in agreement with the observation that Cu-Ag alloys upon reacting with BTAH in aqueous medium undergo a substantial Ag enrichment at the surface <sup>[Man06]</sup>. The present work also confirms chemisorption to be the active mode of TTAH adsorption on Cu under the conditions considered here.

The involvement of multiple kinetic parameters in the formation process of the surface film explains the observed sensitivity of the system against temperature. In the course of the present project, the significant effect of temperature on the TTAH adsorption behavior was established. However, adsorption-isotherm studies on the BTAH-Cu system in aqueous media were not able to detect any appreciable difference in the corresponding adsorption behavior in the temperature range of 35°C to 55°C <sup>[Kha10]</sup>. The present work also ascertained multi-layered adsorption of TTAH on Cu. Adsorption-isotherm studies, on the other hand, mostly revealed mono-layered adsorption <sup>[Kah10], [Rav05]</sup>. Moreover, most of the adsorption-isotherm studies fail to account for the interactions amongst adsorbed corrosion inhibitor molecules, which is expected to be significant in structures similar to that revealed in the present study <sup>[Bas06], [Bas97]</sup>. These key differences emphasize the inefficiency of adsorption-isotherm studies for investigating into similar systems, especially at elevated temperatures. Further work is required to optimize the temperature for most effective surface protection, specific to chemical environments. Based on the present study, it may be interesting to study the behavior and performance of a TTAH

adsorption-film formed at elevated temperature under lower temperature service conditions.

The present study also contradicts with the observation made by Levin *et al.*, that TTAH adsorbed on Cu, in oily-medium, did not show any appreciable tendency to polymerize at room temperature, which was based on the absence of an appreciable peak for  $[\text{TTA}_2\text{Cu}]^-$  species <sup>[Lev07]</sup>. Lastly, the present work contradicts Trouiller *et al.* in respect that,  $[\text{CuO}]^-$  secondary ions in ToF-SIMS were found to be related to the  $\text{Cu}_2\text{O}$  layer, rather than surface contamination as suggested by the latter <sup>[Tro08]</sup>.

To sum up, for a given concentration of the TTAH corrosion inhibitor, a chemical state of the Cu surface, and the solvent that enable easier availability of  $\text{Cu}^+$  in the initial phases, leads to the formation of a more protective TTAH adsorption film. However, further research is required on the molecular orientation of TTAH in the adsorption-film.

## Chapter 6

### Conclusion

The present PhD project was able to identify the microscopic-mechanism for TTAH adsorption on Cu. The efficacy of TTAH in protecting the Cu surface against corrosion in oily sulfide solution was attributed to the formation of a physical barrier rather than surface passivation. The surface film formation was shown to be a kinetics-controlled process with profound temperature sensitivity. The outward diffusion of  $\text{Cu}^+$  was identified to be the most critical step in the formation of the TTAH adsorption film. Based on the mechanism proposed in this project, more realistic kinetic modeling can be carried out to predict the behavior of practical systems. The presently proposed model is able to explain a number of observations for TTAH- and BTAH-Cu systems reported in the literature. Based on the present study, the key mechanistic features of TTAH adsorption on Cu, in both oily and aqueous media are expected to be similar except for the fact that aqueous media extract  $\text{Cu}^+$  from the metallic substrate more effectively. On the basis of the present model, this difference implies that the adsorption film formed in aqueous media should have better anti-corrosion properties than that formed in oily media (under identical conditions). Based on the present work, there can be multiple approaches to achieve better corrosion protection for Cu in the future:

- Identify newer corrosion inhibitors that are capable of forming better packed organo-metallic structures than TTAH-Cu system, hence providing a more effective physical barrier.

- Optimization of operating temperature: It may be beneficial to expose the initial Cu surface to form a corrosion inhibitive adsorption film at a higher temperature before subjecting it to lower temperature service conditions. This is based on the fact that according to the present model, CI adsorption film formed at higher temperature is expected to be more corrosion resistant than the one formed at room temperature.
- Research into the synergistic effects of additives in modifying the surface potential such that the extraction of  $\text{Cu}^+$  from the substrate is facilitated in the initial phases.

The present project established the potency of XPS and ToF-SIMS, used in conjunction, to investigate organo-metallic systems, in spite of the lacking lateral-resolution offered by these instruments. The strength of these experimental techniques lies with their ability to reveal extremely depth sensitive information without significantly damaging the surface, which is imperative for probing into thin and soft organo-metallic layers. The complimentary nature of information imparted by these two techniques regarding the state of chemical-bonding in the adsorption film ensures nearly complete characterization of such systems. High-resolution TEM study on both cross-sectional and planar samples may be attempted to overcome the limitation on the lateral-resolution posed by XPS and ToF-SIMS. TEM study would reveal direct evidence for the structure of the surface film and its lateral homogeneity at molecular scale. This would help to understand the lateral molecular interactions. However, it may be challenging to prepare a TEM sample keeping the thin and soft organo-metallic adsorption film intact.

Finally, having shown that the physical principles governing the TTAH adsorption film-formation on Cu in oily media are generic, it will be useful to study the reaction mechanisms for other organic corrosion inhibitor and metal systems. The larger objective of such research work will be to develop a broader understanding on the microscopic interactions of organic corrosion inhibitors with metallic systems, which would ultimately lead to more effective corrosion protection of metallic alloys in the future.

## Appendix I

### XPS Neutralizer Beam Induced Surface Modification

Modern XPS instruments, including the one installed in SCSAM that was exclusively used in the course of this PhD project, are equipped with dual beam neutralizers – an electron-beam, and an ion-beam. The idea is to simultaneously flood the surface with low-energy electrons, and positive ions to neutralize the surface which in turn minimizes the shift in the binding energy (BE) of photo-electrons from their true values caused as an artifact of surface charging. This feature is extremely helpful for characterizing insulating samples in XPS that are prone to surface charge accumulation. The PHI Versa Probe 5000 XPS installed in SCSAM uses  $\text{Ar}^+$  for ion-beam neutralization. Typically, 1 eV electron-beam, and 10 eV  $\text{Ar}^+$  beam are used for this purpose. Presently, it is quite customary to use these neutralizer beams irrespective of the conductivity of the sample.

It is well-known that continuous bombardment of the sample surface with high-energy ion-beam tends to modify the chemical state of the surface. One of the most commonly observed effects is the reduction of the metallic species in the sample to lower oxidation numbers. A number of transition metal oxides – Fe oxides, W oxides, etc. have been studied for this purpose <sup>[Xie12], [Alo08], [Sil06]</sup>. But in the literature, this surface-reduction artifact has been studied only with high-energy sputtering ion-beams with energies in the range of few KeVs – typically 1-6 KeV. However, in the course of the present PhD project, it was observed that Cu oxide systems are prone to similar surface-reduction effects even with low-energy neutralizer beams. This chapter articulates the chemical

modifications at the surface of Cu oxide specimens under dual-beam neutralizer with 1 eV electron-beam, and 10 eV Ar<sup>+</sup> beam. For this purpose, three different states of Cu oxides were studied – Cu<sub>2</sub>O formed by HNO<sub>3</sub> etching, CuO formed by furnace oxidation, and native oxide formed on pristine Cu surface upon exposure to the atmosphere for 5 days.

In order to study the effect of the neutralizer beams, the sample surface was intermittently exposed to the neutralizer beams, while data was repeatedly collected over the same area with the neutralizer beams off. The Cu 2p, Cu L<sub>3</sub>M<sub>4,5</sub>M<sub>4,5</sub>, and O 1s peaks were compared, respectively, for all cycles of data acquisition on each sample. For each sample, the Cu 2p, and the Cu L<sub>3</sub>M<sub>4,5</sub>M<sub>4,5</sub> peaks were normalized to a scale of 0 to 1 in order to clearly reveal the shift in the chemical nature of the Cu with increasing neutralization time. However, the O 1s peaks were not normalized to illustrate the reduced intensity of the same with increasing neutralization time. Fig. AI.1 (a) shows the modifications observed in the Cu L<sub>3</sub>M<sub>4,5</sub>M<sub>4,5</sub> peak with increasing neutralization time, as acquired on the specimen with Cu<sub>2</sub>O at the surface. The Cu metallic peak at 568.0 eV was normalized to 1 for each data set. Evidently, the relative intensity of the peak corresponding to Cu<sup>+</sup> in Cu<sub>2</sub>O, at 570.0 eV, decreased with increasing neutralization time. Correspondingly, as shown in Fig. AI.1 (b), the intensity of the O 1s peak also dropped substantially with increasing neutralization time. The variations in the atomic (at.) % of Cu, and O with neutralization time, recorded in the near-surface analyzed volume, are shown in Fig. AI.2 (a). The at. % of Cu increased from 67 % in the initial surface condition to 95 % after 22680 s (6.3 h) of neutralization. Similarly, the variations

in the relative fraction of the Cu  $L_3M_{4,5}M_{4,5}$  peak at 568.0 eV, and 570.0 eV were plotted against neutralization time, as shown in Fig. AI.2 (b). These plots were in good agreement with the fact that the Cu surface became more metallic in nature with increasing neutralization.

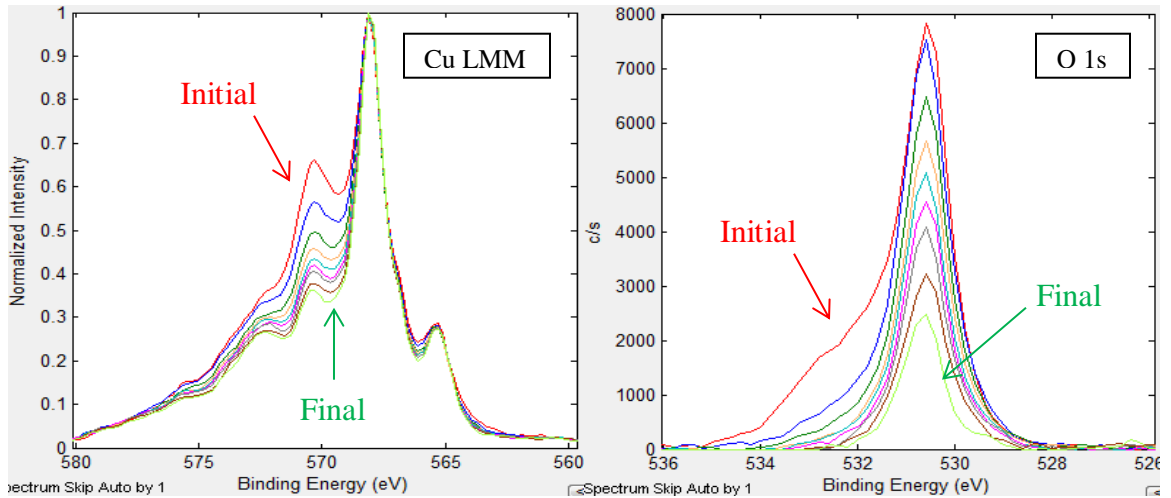


Fig. AI.1: Comparison of (a) Cu  $L_3M_{4,5}M_{4,5}$  (b) O 1s peaks acquired on  $Cu_2O$  specimen with increasing neutralization time.

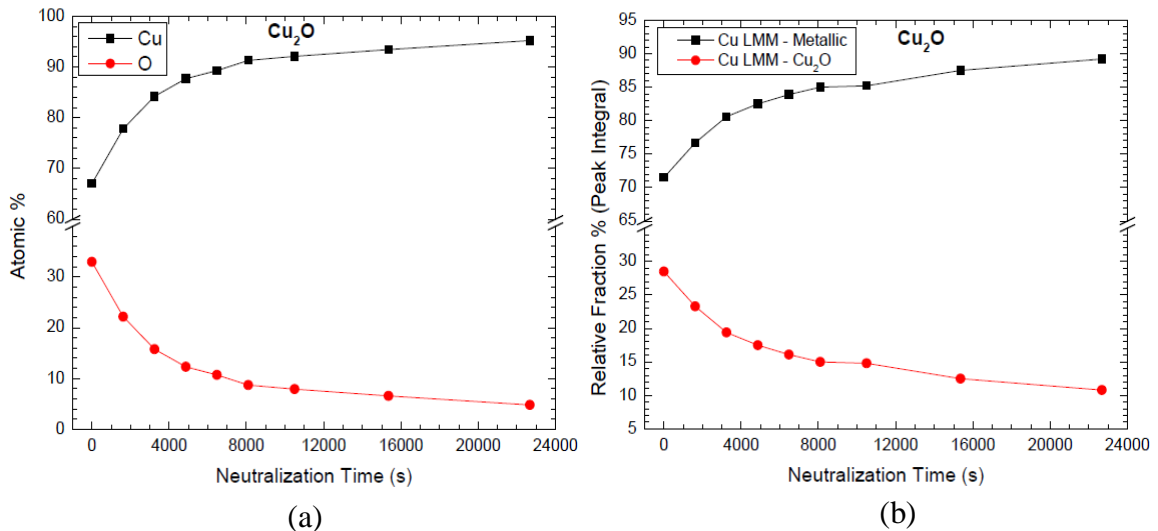


Fig. AI.2: Comparison of relative fractions of (a) Cu and O at. % (b) Cu metallic to  $Cu_2O$  component in Cu  $L_3M_{4,5}M_{4,5}$  peak acquired on  $Cu_2O$  specimen with increasing neutralization time.

In order to verify if this was a mechanical sputtering effect leading to a largely dislodged oxide layer or an actual chemical reduction of the Cu at the surface, a similar experiment was carried on a furnace oxidized Cu sample that was completely transformed into a black CuO foil. The results for this sample are shown in Fig. AI.3, and Fig. AI.4. Even in this case, a significant Cu enrichment of the surface was observed. This proved that it was not a uniform sputtering effect of the top layer, as in that case, no shift in the peaks were expected with the CuO foil being  $\approx 25 \mu\text{m}$  thick ( $\gg$  analyzed or sputter depth). As shown in Fig. AI.3 (a), the intensity of the satellite peaks for Cu  $2p_{3/2}$ , and Cu  $2p_{1/2}$  peaks relative to their corresponding main peaks reduced significantly with increasing neutralization time confirming the reduction of Cu in CuO. The shift in the Cu  $L_3M_{4,5}M_{4,5}$  peak, shown in Fig AI.3 (b), from 569.0 eV in the initial state to predominantly 570.0 eV in the final state confirmed that  $\text{Cu}^{2+}$  in CuO was being reduced to  $\text{Cu}^+$  in  $\text{Cu}_2\text{O}$ . The intensity of the O 1s peak, shown in Fig. AI.3 (c), dropped again with increasing neutralization time. Moreover, the O 1s peak also showed a chemical-shift in BE. In the initial surface condition, the O 1s peak was predominantly at 529.7 eV corresponding to CuO, whereas upon neutralization, the relative fraction of the O 1s peak at 530.7 eV corresponding to  $\text{Cu}_2\text{O}$  increased monotonously. On the final state of the surface, data was acquired for a prolonged time in the vicinity of the Ar 2p peak so as to ascertain if the  $\text{Ar}^+$  ion-beam had sufficient energy to incorporate  $\text{Ar}^+$  ions into the sample surface. However, as shown in Fig. AI.3 (d), no signs were detected for the presence of Ar on the surface. The variations in the atomic % of Cu, and O with neutralization time, recorded at the surface of the CuO sample, are shown in Fig. AI.4.

Cu content of the surface increased from 50 %, in the beginning, to 60 % after 71460 s (19.8 h) of neutralization.

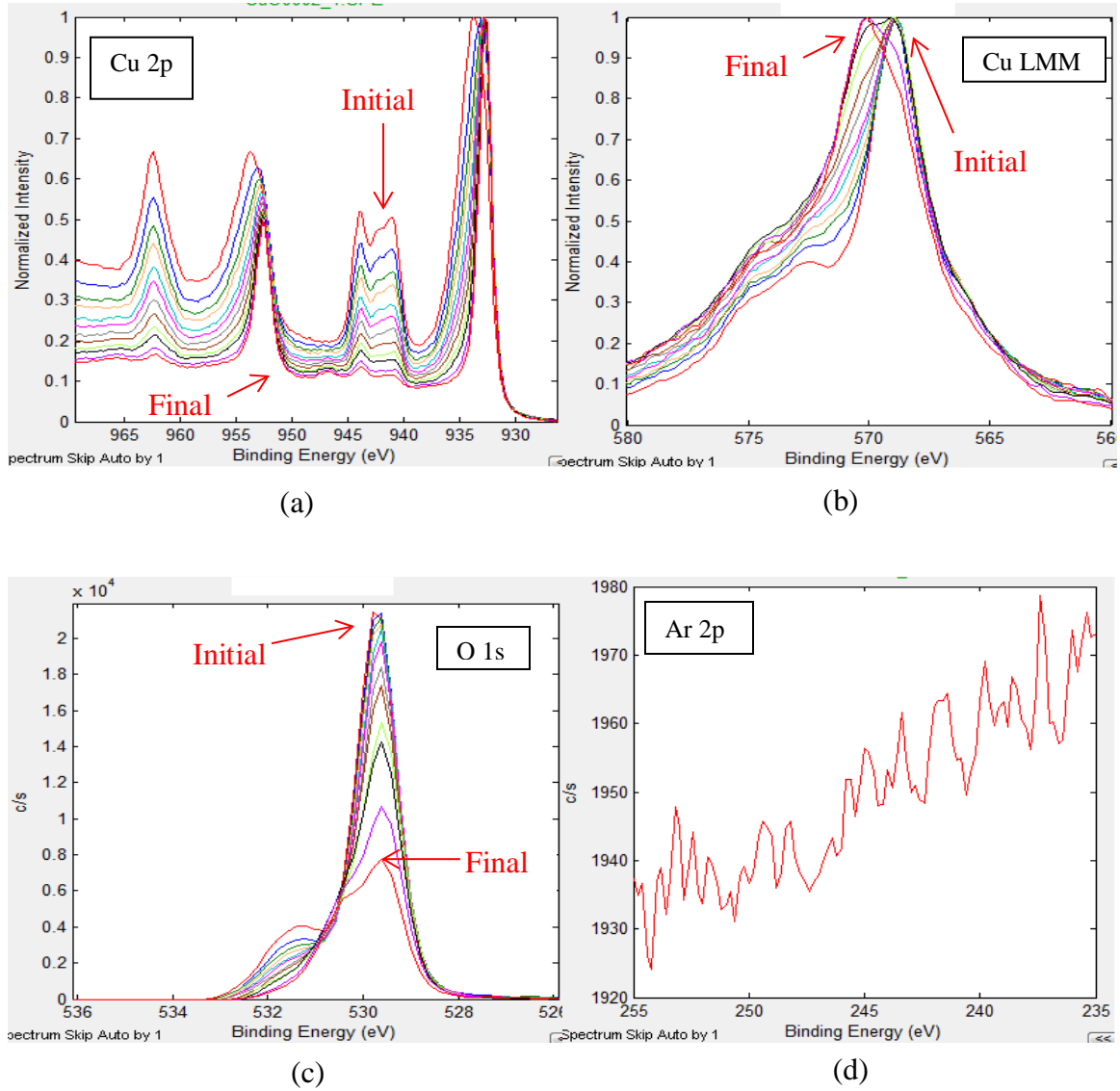


Fig. AI.3: Comparison of (a) Cu 2p (b) Cu L<sub>3</sub>M<sub>4,5</sub>M<sub>4,5</sub> (c) O 1s (d) Ar 2p peaks acquired on CuO specimen with increasing neutralization time.

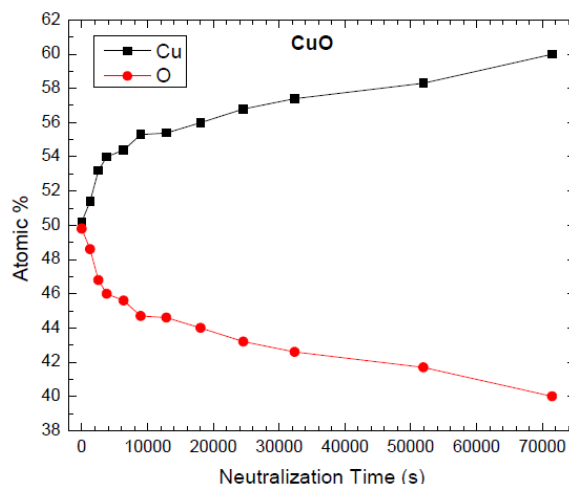


Fig. AI.4: Comparison of relative fractions of Cu and O at. % acquired on CuO specimen with increasing neutralization time.

A similar experiment was repeated on the native oxide of Cu formed upon exposure of pristine Cu surface to the atmosphere for 5 days. This sample was characterized to have Cu<sub>2</sub>O on the surface to begin with, although as revealed by the O 1s peak, the top-most layer was found to bear some form of hydroxide/water bearing compound. This sample also showed an extensive shift in the chemical nature of the Cu on continued neutralization. The normalized Cu L<sub>3</sub>M<sub>4,5</sub>M<sub>4,5</sub> peaks and the O 1s peaks are shown in Fig. AI.5 (a), and (b), respectively. Initially, the peak at 570.0 eV corresponding to Cu<sup>+</sup> in Cu<sub>2</sub>O was the predominant Cu L<sub>3</sub>M<sub>4,5</sub>M<sub>4,5</sub> peak. However, with increasing neutralization time, the predominant peak shifted to 568.0 eV, corresponding to metallic Cu. Correspondingly, the intensity of the O 1s peak reduced with increasing neutralization time. The BE position of the O 1s peak complied well to Cu<sub>2</sub>O, except for the first data set which revealed the presence of hydroxide/water as the major component. The Cu, and O atomic % variation plots with neutralization time are shown in Fig. AI.6. The surface atomic concentration of Cu increased from 43 %, in the initial condition, to 84 % on

neutralizing for 24300 s (6.8 h). This suggested that the surface had some adventitious O bearing compounds to begin with, which disappeared upon neutralization. Note, for all the three samples, the surface had some adventitious C as well, which also disappeared upon neutralization. The rapid removal of the adventitious compounds from the surface followed by substantial Cu enrichment of the surface upon continued neutralization, in all the three cases, clearly indicated towards differential sputtering of lighter elements – O, and C at a faster rate as compared to that of Cu. Hence, it was concluded that even low-energy neutralizer beams lead to differential sputtering assisted chemical reduction of the Cu surface.

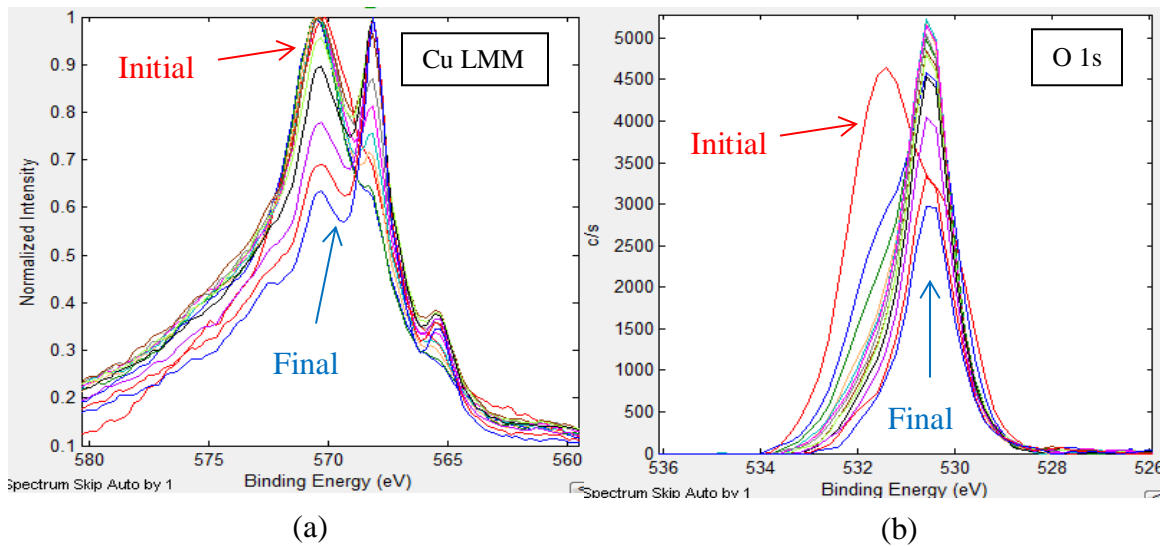


Fig. AI.5: Comparison of (a) Cu  $L_{3}M_{4,5}M_{4,5}$  (b) O 1s peaks acquired on native oxide of Cu with increasing neutralization time.

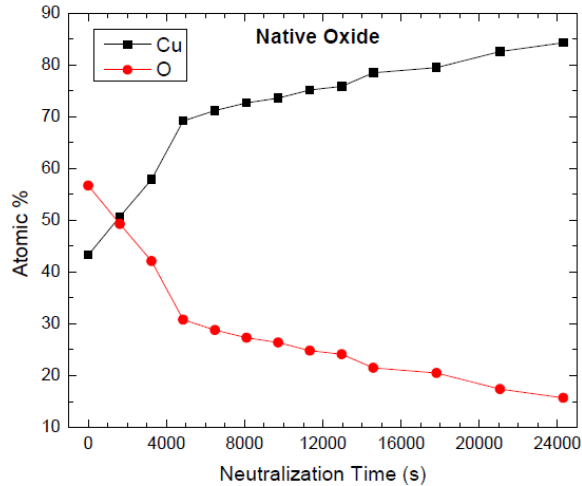


Fig. AI.6: Comparison of relative fractions of Cu and O at. % acquired on native oxide of Cu with increasing neutralization time.

In each case, the observed surface-reduction was confirmed to be an effect of the neutralizer beams as this phenomenon was not limited to the area over which data was acquired repeatedly. The neutralizer beams were projected over an area of 3 mm x 4 mm, essentially covering the entire sample face. At any instance of time, comparable degree of Cu reduction was observed in all regions of the sample surface. Thus, to avoid such surface-reduction artifact, neutralizer beams were disengaged while obtaining all the experimental results that are presented in chapter 4 of this PhD thesis.

## Bibliography

- [All07] Allam N.K., Hegazy H.S., Ashour E.A., "Inhibition of the sulfide induced pitting of copper nickel alloy using benzotriazole", International Journal of Electrochemical Science, Vol. 2, 2007, pp. 549-562
- [Alo06] Alov N.V., Kutsko D.M., Bordo K.V., Journal of Surface Investigation: X-Ray, Vol. 2, 2008, pp. 184-188
- [Ash06] El-Ashry E.-S.H., El-Rafey M.E., El-Nagdi M.H., Abou-Elnaga H.H., Bakry W.M.A., Boghdady Y.M., Lub.Sci., Vol. 18, 2006, pp. 109
- [ASMxx] ASM Handbook, Vol. 13
- [ASTxx] ASTM D 5968-96, "Standard test method for evaluation of corrosiveness of diesel engine oil"
- [Bas06] Bastidas D.M., "Adsorption of benzotriazole on copper surfaces in a hydrochloric acid solution", Surface and Interface Analysis, Vol. 38, 2006, pp. 1146-1152
- [Bas97] Bastidas J.M., Damborenea JJ, Vazquez A.J., Journal of Applied Electrochemistry, Vol. 27, 1997, pp. 345
- [Bel59] Belousov B.P., "Periodically acting reaction and its mechanism", Collection of Abstracts on Radiation Medicine, Vol. 147, 1959, pp. 145
- [Blu72] Blundy R.J., Pryor M.J., Corrosion Science, Vol. 12, 1972, pp. 65
- [Bre98] Breslin C.B., McDonald D.D., Electrochimica Acta., Vol. 44, 1998, pp. 643
- [Bri73] Briggs T.S., Rauscher W.C., "An oscillating iodine clock", Journal of Chemical Education, Vol. 50, 1973, pp. 496
- [Bri86] Briggs D., Hearn M. J., Vacuum, 1986, pp. 36.
- [Bru91] Brusic V., Frisch M.A., Eldridge B.N., Novak F.P., Kaufman F.B., Rush B.M., Frankel G.S., "Copper corrosion with and without inhibitors", Journal of Electrochemical Society, Vol. 138 (8), 1991, pp. 2253-2259
- [Bru92] Brunoro G., Parmigiani F., Perboni G., Rocchini G., Trabanelli G., Br. Corrosion J., Vol. 27, 1992, pp. 75
- [Cha99] Chan H.Y.H., Weaver M.J., Langmuir, Vol. 15, 1999, pp. 3348

- [Cli66] Clifton J.R., Yoke J.T., *Inorganic Chemistry*, Vol. 5, 1966, pp. 1630
- [Coh90] Cohen S.L., Brusica V.A., Kaufman F.B., Frankel G.S., Motakef S., Rush B., *Journal of Vacuum Science and Technology A*, Vol. 8, 1990, pp. 2417
- [Cus94] Cusano C.M., Wang J.C., "Corrosion of copper and lead containing materials by diesel lubricants", *Lub. Engg.*, Vol. 51 (1), 1994, pp. 89-95
- [Dam71] Damaskin W., Pietrij A., Batrakov W., *Adsorption of Organic Compounds on Electrode*, Plenum Press, New York, 1971
- [Edw94] Edwards A., Osborne C., Webster S., Klenerman D., Joseph M., Ostovar P., Doyle M., *Corrosion Science*, Vol. 36, 1994, pp. 315
- [Eis83] Eiselstein L.E., Syrett B.C., Wang S.S., Caligiuri R.D., *Corrosion Science*, Vol. 23, 1983, pp. 223
- [Fan86] Fang B.S., Olson C.G., Lynch D.W., *Surface Science*, Vol. 176, 1986, pp. 476
- [Fie07] Field R.J., <http://www.scholarpedia.org/article/Oregonator>, 2007
- [Fin08] Finšgar M., Lesar A., Kokalj A., Milošev I., *Electrochimica Acta.*, Vol. 53, 2008, pp. 8287-8297
- [Fin10] Finšgar M., Kovač J., Milošev I., "Surface analysis of 1-hydroxybenzotriazole and benzotriazole adsorbed on Cu by X-ray photoelectron spectroscopy", *Journal of The Electrochemical Society*, Vol. 157 (2), 2010, pp. C52-C60
- [Gao02] Gao P.G., Yao J.L., Zheng W., Gu R.A., Tian Z.Q., *Langmuir*, Vol. 18, 2002, pp. 100
- [Ham90] Hamblin P.C., Kristen U., Chasan D., *Lub.Sci.*, Vol. 2, 1990, pp. 287
- [Has88] Hashemi T., Hogarth C.A., *Electrochimica Acta*, Vol. 33, 1988, pp. 1123
- [Hay04] Hayez V., Franquet A., Hubin A., Terryn H., *Surface and Interface Analysis*, Vol. 36, 2004, pp. 876
- [Hod09] Hodgson A., Haq S., *Surface Science Reports*, Vol. 64, 2009, pp. 381-451
- [Hol85] Hollander O., May R.C., *Corrosion*, Vol. 41, 1985, pp. 39
- [Hol94] Holm R., Over J., Wittig M., Minnich R., Berg D., Eickmans J., Holtkamp D., Meyer K., Benninghoven A., "Chlorine's effects on triazole inhibitor layers on copper", *Materials Performance*, Vol. 33(5), 1994, pp. 49-53

- [Hux03] Hu X., Castro-Rodriguez I., Meyer K., "Copper complexes of nitrogen-anchored tripodal N-heterocyclic carbene ligands", *Journal of American Chemical Society*, Vol. 125(40), 2003, pp. 12237-45
- [Jay02] Jayne D.T., Shanklin J.R., Stachew C.F., "Controlling the corrosion of copper alloys in engine oil formulations: antiwear, friction modifier, dispersant synergy", *Society of Automotive Engineers*, 2002
- [Jia03] Jiang Y., Adams J. B., *Surface Science*, Vol. 529, 2003, pp. 428-442
- [Kha08] Khaled K.F., *Electrochimica Acta.*, Vol. 53, 2008, pp. 3484
- [Kha09] Khaled K.F., "Experimental and atomistic simulation studies of corrosion inhibition of copper by a new benzotriazole derivative in acid medium", *Electrochimica Acta.*, Vol. 54, 2009, pp. 4345-4352
- [Kha10] Khadom A.A., Yaro A.S., Khadum A.A.H., "Adsorption mechanism of benzotriazole for corrosion inhibition of copper-nickel alloy in hydrochloric acid", *J. Chil. Chem. Soc.*, Vol. 55 (1), 2010, pp. 150-152
- [Koe98] Koetter F., Benninghoven A., *Applied Surfaces*, Vol. 113, 1998, pp. 47
- [Kok04] Kokalj A., Dal Corso A., de Gironcoli S., Baroni S., *Surface Science*, 2004, 566-568, 1018-1023
- [Kok10] Kokalj A., Peljhan S., "Density functional theory study of ata, btah, and btaoh as copper corrosion inhibitors: adsorption onto Cu(111) from gas phase", *Langmuir*, Vol. 26(18), 2010, pp. 14582-14593
- [Kol05] Kollmer F., *Applied Surface Science*, Vol. 231, 2005, 153
- [Kwo06] Kwon K.Y., Lin X., Pawin G., Wong K., Bartels L., "Oxadiazole-metal interface: from isolated molecules to  $\pi$ -stacking", *Langmuir*, Vol. 22 (3), 2006, pp. 857-859
- [Lah99] Lahaye J., Nanse G., Bagreev A., Strelko V., *Carbon*, Vo. 37, 1999, pp. 585
- [Lei71] Leidheiser H. Jr., "Corrosion of Copper, Tin, and Their Alloys", NY John Wiley, 1971, pp.3
- [Lev07] Levin M., Wiklund P., Arwin H., "Adsorption and film growth of N-methylamino substituted triazoles on copper surfaces in hydrocarbon media", *Applied Surface Science*, Vol. 254, 2007, pp.1528-1533

- [Lev58] Levy M., "Corrosion inhibitors in automotive coolant media", *Industrial and Engineering Chemistry*, Vol. 50 (4), 1958, pp. 657-662
- [Lot25] Lotka A.J., *Elements of Physical Biology*, Williams and Wilkins, 1925
- [Luf94] Lu F., Rao N.M., Yang B., Hoots J.E., Budrys R. S., "Effect of halogenation on yellow metal corrosion: inhibition by triazoles", *Corrosion*, Houston, TX, USA, Vol.50(6), 1994, pp. 422-431
- [Mac08] Maciel J.M., Jaimes R.F., "The characterization of the protective film formed by benzotriazole on the 90/10 copper–nickel alloy surface in H<sub>2</sub>SO<sub>4</sub> media", *Corrosion Science*, Vol. 50, 2008, pp. 879-886
- [Man06] Mansikkamäki K., Haapanen U., Johans C., Kontturi K., Valden M., "Adsorption of Benzotriazole on the Surface of Copper Alloys Studied by SECM and XPS", *Journal of The Electrochemical Society*, Vol. 153 (8), 2006, pp. B311-B318
- [Man06'] Mansikkamäki K., Johans C., Kontturi K., *Journal of The Electrochemical Society*, Vol. 153, 2006, pp. B22
- [Man73] Mansfield F., Smith T., *Corrosion*, Vol. 29, 1973, pp. 105
- [Mcg85] McGeehan J.A., Yamaguchi E.S., Adams J.Q., "Some effects of zinc dithiophosphates and detergents on controlling engine wear", *SAE Tech. Paper* 852133, 1985
- [Mci81] McIntyre N.S., Sunder S., Shoesmith D.W., Stanchell F.W., *Journal of Vacuum Science and Technology*, Vol. 18, 1981, pp. 714
- [Met00] Metikos-Huckovic M., Babic R., Paic I., *Journal of Applied Electrochemistry*, Vol. 30, 2000, pp. 617
- [Mic04] Michaelides A., Alavi A., King D.A., *Physical Review B*, Vol.69, 2004, pp. 113404
- [Mor04] Morales-Gil P., Negron-Silva G., Romero-Romo M., Angeles-Chavez C., Palomar-Pardave M., *Electrochimica Acta*, Vol. 49, 2004, pp. 4733
- [Mou92] Moulder J.F., Stickle W.F., Sobol P.E., Bomben K.D., *Handbook of X-Ray Photoelectron Spectroscopy*, Perkin-Elmer Corporation, Eden Prairie, MN, 1992

- [Nis03] Nishi A., Sado M., Miki T., Fukui Y., "Evaluation of the Cu-CMP process by ToF-SIMS and XPS: time dependence of Cu surface adsorbents and oxidation states", *Applied Surface Science*, Vol. 203-204, 2003, pp. 270-272
- [Nor70] North R.F., Pryor M.J., *Corrosion Science*, Vol. 10, 1970, pp. 297
- [One76] O'Neal C. Jr., Borger R.N., "Corrosion inhibiting synergism by triazoles in aqueous multi-metal systems", *Materials Performance*, Vol. 15(2), 1976, pp. 9-13
- [Pap98] Papapanayiotou D., Deligianni H., Alkaine R.C., *Journal of Electrochemical Society*, Vol. 145, 1998, pp. 3016
- [Pol70] Poling G.W., *Corrosion Science*, Vol. 10, 1970, pp. 359
- [Pra86] Prabhakaran K., Sen P., Rao C.N., *Surface Science*, Vol. 177, 1986, L971
- [Pri10] Prigogine I., "IDEA - Internet Differential Equations Activities", <http://www.idea.wsu.edu/OscilChem/#Brusselator%20Model>, Washington State University, Retrieved 2010
- [Pro47] Procter and Gamble Ltd., British Pat. 652339, 1947
- [Qaf02] Quafsoui W., Blanc C., Pebere N., Srhiri A., Mankowski G., *Electrochimica Acta*, Vol. 47, 2002, pp. 4339
- [Qu05] Qu J.E., Guo X., Chen Z., "Adsorption behavior of dodecylamine on copper–nickel alloy surface in NaCl solutions studied by electrochemical methods and AFM", *Materials Chemistry and Physics*, Vol. 93, 2005, pp. 388-394
- [Rab04] Rabelo Neto R.C., Lima D.O., Pinheiro T.D.S., Almeida R.F., Castro Dantas T.N., Dantas M.S.G., Araujo M.A.S., Cavalcante Jr. C.L., Azevedo D.C.S., *Ind. Eng. Chem. Res.*, Vol. 43, 2004, pp.7428
- [Ram85] Ramnarayanan T., Alonzo J., *Oxid. Met.*, Vo. 24, 1985, pp. 17
- [Rav05] Ravera S.B., Chavez M.A., *Journal of the Chilean Chemical Society*, Vol. 50, 2005, pp. 739
- [Rou05] Roudgar A., Gross A., *Chemical Physics Letters*, Vol. 409, 2005, pp. 157-162
- [Rub83] Rubin J., Gutz I. G. R., Sala O., Orville-Thomas W.J., *Journal of Molecular Structure*, Vol. 100, 1983, pp. 571

- [Rud03] Rudnick L.R., *Lubricant Additives: Chemistry and Applications*, CRC Press, 2003
- [San84] Sanad S.H., Taman A.R., "Corrosion of copper and carbon steel in white petroleum oil", *Surface Technology*, Vol. 23, 1984, pp. 159-166
- [Sas01] Sastri S., *Corrosion Inhibitors Principles and Applications*, Johan Wiley and Sons publisher, USA, 2001
- [Sch00] Schreiber F., *Progress in Surface Science*, Vol. 65, 2000, pp. 151-257
- [Sch84] Schmitt G., *Br. Corros. J.*, London, Vol. 19, 1984, pp. 165
- [She06] Sherif M., Park S., *Electrochimica Acta.*, Vol. 51, 2006, pp. 4665
- [Sil06] Silversmit G., Depla D., Poelman H., Marin G.B., Gryse R.D., *Surface Science*, Vol. 600, 2006, pp. 3512-3517
- [Sut93] Sutter E.M.M, Fiaud C., Lincot D., "Electrochemical and photoelectrochemical characterization of naturally grown oxide layers on copper in sodium acetate solutions with and without benzotriazole", *Electrochimica Acta.*, Vol. 38(10), 1993, pp. 1471-1479
- [Swi95] Swift A.J., "Surface analysis of corrosion inhibitor films by XPS and ToF-SIMS", *Mikrochimica Acta.*, Vol. 120, 1995, pp. 149-158
- [Tom83] Tompkins H., Allara D., Pasteur G., *Surface and Interface Analysis*, Vol. 5, 1983, pp. 101
- [Tom89] Tomkvist C., Thierry D., Bergman J., Liedberg B., Leygraf C., *Journal of Electrochemical Society*, Vol. 136, 1989, pp. 58
- [Tom97] Tommesani L., Brunoro G., Frignani A., Monticelli C., Dal Colle M., *Corrosion Science*, Vol. 39, 1997, pp. 1221
- [Tor89] Tornkvist C., Thierry D., Bergman J., Liedberg B., Leygraf C., *Journal of Electrochemical Society*, Vol. 136, 1989, pp. 58
- [Tou96] Tougaard S., *Journal of Vacuum Science Technology A*, Vol. 14, 1996, pp. 1415
- [Tou03] Tougaard S., *Surface Analysis by Auger and X-Ray Photoelectron Spectroscopy*, Editors, Briggs D., Grant J.T., pp. 295 – 343, IM Publications, Manchester, UK, 2003

- [Tro08] Trouiller C., Petitdidier S., Ravanel X., Broussous L., Juhel M., Kwakman L.M.T., Wyon C., "Copper surface analysis with ToF-SIMS: spectra interpretation and stability issues", *Solid State Phenomena*, Vol. 134, 2008, pp. 371-374
- [Tro98] Tromans D., *Journal of Electrochemical Society*, Vo. 145, 1998, pp. L42
- [Uhl63] Uhlig H.H., *Corrosion and Corrosion Control*, John Wiley, N.Y., 1963, pp. 284
- [Umo08] Umoren A., Obot B., Ebenso E., *E-journal of Chemsitry*, Vol. 5, 2008, pp. 2008
- [Vog97] Vogt M. R., Polewska W., Magnussen O. M., Behm R.J., *Journal of Electrochemical Society*, Vol. 144, 1997, L113
- [Vol31] Volterra V., "Variations and fluctuations of the number of individuals in animal species living together in *Animal Ecology*", Chapman R.N. (ed), McGraw-Hill, 1931
- [Way01] Waynick J.A., *Energy Fuels* Vol. 15, 2001, p. 1325
- [Xie12] Xie F.Y., Gong L., *Journal of Electron Spectroscopy and Related Phenomena*, Vol. 185, 2012, pp. 112-118
- [Xue91] Xue G., Ding J., Lu P., Dong J., "SERS, XPS, and electroanalytical studies of the chemisorption of benzotriazole on a freshly etched surface and an oxidized surface of copper", *The Journal of Physical Chemistry*, Vol. 95 (19), 1991, pp. 7380-7384
- [Yao04] Yao J.L., Yuan Y.X., Gu R.A., *Journal of Electro-analytical Chemistry*, Vol. 573, 2004, pp. 255
- [You90] Youda R., Nishihara H., Aramaki K., *Electrochimica.Acta*, Vol. 35, 1990, pp. 1011
- [Yup03] Yu P., Liao D.M., Luo Y.B., Chen Z.G., *Corrosion (Houston)*, 59, 2003, pp. 314
- [Zha64] Zhabotinskii A. M., "Periodic oxidation reactions in liquid phase", *Doklady Akademii Nauk SSSR (in Russian)*, Vol. 157 (2), 1964, pp. 392-393
- [Zhu06] Zhu Y., Mimura K., Lim J. W., Isshiki M., Jiang Q., "Brief Review of Oxidation Kinetics of Copper at 350 °C to 1050 °C", *Metallurgical and Materials Transactions A*, Vol. 37A, 2006, pp. 1231

[Zuk82] Zucker J., "Prevention of corrosion failures in electrical equipment",  
Proceedings of the Technical Association of the Pulp and Paper Industry,  
1982, pp. 457-470